Origin versus context

Origin versus Context

Defining Key Determinants of Human Macrophage Function in Health and Disease

Adele Veronika Ruder

Cover design: Pia Schmutz
Layout: Adele Ruder
Printed by: Gildeprint
ISBN: 978-94-6419-843-0

Origin versus Context

Defining Key Determinants of Human Macrophage Function in Health and Disease

DISSERTATION

to obtain the degree of Doctor at Maastricht University,
on the authority of the Rector Magnificus, Prof. Dr. Pamela Habibović,

in accordance with the decision of the Board of Deans,
to be defended in public on

Tuesday, 31 October 2023, at 13:00 hours

by

Adele Veronika Ruder

Supervisors

Prof. Dr. Erik A.L. Biessen
Prof. Dr. Judith C. Sluimer

Co-supervisor

Dr. Lieve Temmerman

Assessment Committee

Prof. Dr. Monika Stoll (Chair)
Prof. Dr. Sabine Steffens (Ludwig-Maximilians-Universität München)
Dr. Marit Westerterp (Rijksuniversiteit Groningen)
Dr. Kristiaan Wouters

Financial support by the Dutch Heart Foundation for the publication of this thesis is gratefully acknowledged.

Contents


1

Chapter 1

General introduction

Cardiovascular disease

Cardiovascular disease (CVD) poses a heavy burden on global health (1). Despite ambitious efforts to decrease CVD mortality by the World Health Organisation (2), it remains the leading cause of death worldwide (3). The persistent burden of CVD on global health today is mainly attributable to the increased incidence in low- and middle-income countries (4), where more than 80% of CVD deaths occur (5).

Traditional risk factors for CVD include high cholesterol, high blood pressure, age, sex, diabetes, smoking, and obesity (6). However, as the prevalence of CVD among subjects who do not suffer from these risk factors is increasing, emerging non-traditional risk factors are being considered (7). These encompass lifestyle factors such as alcohol consumption, diet, and insufficient physical activity as well as environmental factors like air and noise pollution (7, 8). Despite the high availability of effective treatment options for the main traditional risk factors, hypercholesterolemia and hypertension, in high-income countries, CVD persists, indicating a need for additional interventions, especially targeting non-traditional risk factors (7, 8).

CVD comprises several disorders of the heart and blood vessels (8), including ischemic heart disease, stroke, and heart failure (2). CVD is most commonly caused by atherosclerosis (9), a slow-progressing inflammatory disease of medium and large arteries that leads to the formation of atherosclerotic plaques in the artery wall (10, 11). Atherosclerotic plaques can rupture, causing the formation of blood clots leading to myocardial infarction or stroke (12).

Atherosclerosis

Atherosclerosis begins early in life and progresses slowly (13). Whereas initial lesions and fatty streaks which may already occur in childhood and adolescence usually remain unnoticed, and may even regress, risk factor exposure later in life causes progression to atheromatous plaques and complicated lesions that may cause symptoms (14).

In healthy arteries, the endothelium maintains vascular homeostasis, regulating vascular tone and coagulation (15). In early stages of atherosclerosis, the endothelium becomes increasingly dysfunctional which leads to vasoconstriction, oxidative stress, chemotactic recruitment of monocytes, and increased permeability for low-density lipoprotein (LDL) (12). This allows plasma LDL particles to cross the endothelial layer whereupon they accumulate in the subendothelial space (16). LDL is oxidised through the reaction with free radicals or enzymatic activity, in turn activating endothelial cells (EC) (12). Activation of the endothelium leads to the expression of adhesion molecules which interact with selectins and integrins on monocytes, enabling their migration through the endothelial layer via rolling adhesion and diapedesis (17). In the intima, the recruited monocytes differentiate into macrophages (MΦ) in response to local differentiation factors (12). MΦs contribute to the ongoing inflammation by secreting

inflammatory cytokines, and ingest oxidised LDL (oxLDL) in an attempt to clear it from the intimal space (18). However, the increased uptake and decreased efflux of oxLDL leads to its accumulation within MΦ, turning them into foam cells (19). Foam cells also arise from vascular smooth muscle cells (SMC) which migrate to the intima and accumulate lipids, similarly to MΦ (20). Eventually, excessive intracellular oxLDL deposition induces foam cell apoptosis (12). Whilst these dead cells are removed through efferocytosis in early-stage atherosclerosis, clearance of apoptotic cells is impaired at later stages, leading to the formation of a lipid-rich necrotic core (21). Vascular SMC synthesise fibrillar collagens that form a fibrous cap, surrounding and stabilising the necrotic core (12, 22). The fibrous cap may be degraded by matrix metalloproteinases (MMPs) which decreases plaque stability and increases its susceptibility to rupture (23). Plaque rupture exposes the plaque core to the blood, initiating coagulation and thrombus formation (24).

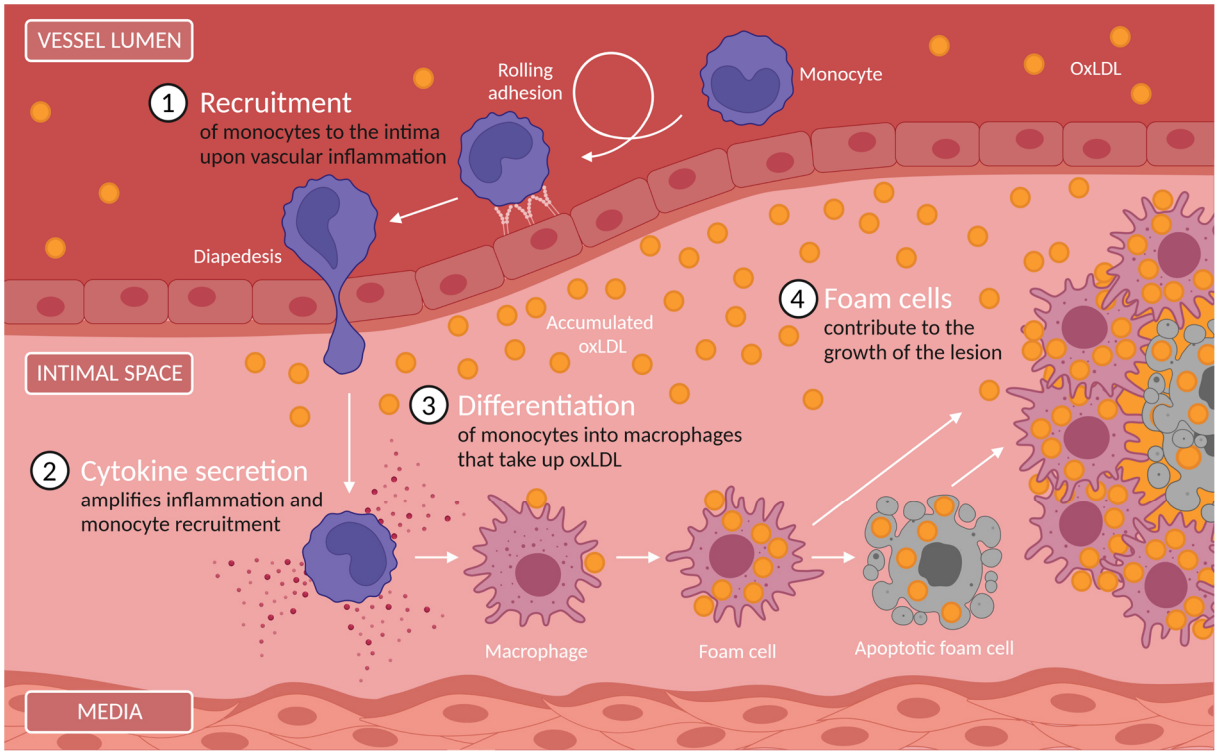

Figure 1: The role of monocytes and MΦ in atherogenesis
After recruitment, rolling adhesion, and diapedesis through the endothelial layer, monocytes secrete inflammatory cytokines and chemokines, sustaining the ongoing inflammation and recruiting other immune cells. Moreover, monocytes differentiate into MΦ which take up oxLDL in the intimal space. The intracellular accumulation of oxLDL makes MΦ turn into foam cells and eventually induces their apoptosis. Created with BioRender.com.

Inflammation in atherosclerosis

As implied by the pathogenesis of atherosclerosis, inflammation is of particular importance as it drives the recruitment of immune cells to the arterial wall and affects the resident cells already present (25). Inflammation in atherosclerosis already gained attention in the nineteenth century, although it was still a topic of discussion at that time (26). Meanwhile, there is ample evidence that atherosclerosis is an inflammatory disease (27, 28). As such, targeting inflammation as a therapeutic modality emerged, substantiated by the Canakinumab Anti-inflammatory Thrombosis Outcomes Study (CANTOS), among others (29).

The CANTOS trial demonstrated that reducing inflammation with canakinumab, a monoclonal antibody for interleukin (IL) -1β, reduced secondary cardiovascular events in patients with myocardial infarction who responded to LDL-lowering therapy but sustained high C-reactive protein (CRP) levels, indicative of systemic inflammation (30). Likewise, anti-inflammatory therapy with colchicine reduced the risk of cardiovascular events after myocardial infarction, as shown in the Colchicine Cardiovascular Outcomes Trial (COLCOT) (31). However, general immunosuppression with methotrexate failed to reduce cardiovascular events in the Cardiovascular Inflammation Reduction Trial (CIRT) (32), indicating that a careful selection of patients and further investigation of the inflammatory course of action in atherosclerosis are essential for effective immunomodulatory therapy (33).

Many immune cells participate in atherosclerosis, orchestrating a complex immune response involving the innate and adaptive immune system. (27). Neutrophils infiltrate lesion sites upon endothelial dysfunction where they secrete granule proteins, promoting recruitment and adhesion of monocytes (34). In turn, neutrophil extracellular traps (NET) released by dying neutrophils enforce the endothelial dysfunction, and stimulate MΦ to secrete IL-1β (35). Despite their short lifespan and limited presence in plaque (34), neutrophils contribute to early atherogenesis and influence plaque stability (36). Natural killer (NK) cells can enter lesions where they activate SMC and MΦ by the release of interferon-gamma (IFN-γ) upon interaction with dendritic cells (DC) (37). DC accumulation has been linked to increased plaque vulnerability (38). Although the underlying mechanisms and implications of these findings are still largely unknown, DC can give rise to foam cells and regulate T cells, bridging the innate to the adaptive immune response (38, 39).

The adaptive immune response in the atherosclerotic plaque is initiated shortly after the innate immune response, starting with infiltration by T lymphocytes (40). Depending on their phenotype and polarisation, T cells can exert both pro- and anti-atherogenic functions (41). On the one hand, cytotoxic T cells are activated after recognising lipoprotein-derived antigens presented by DC, subsequently inducing apoptosis in SMC and EC as well as the differentiation of monocytes to MΦ (42). On the other hand, regulatory T cells can protect against atherogenesis by secreting anti-inflammatory IL-10, but shift to an atherogenic phenotype in

advanced lesions (40, 42). Moreover, T helper (T_H) cells can polarise to functionally distinct subsets that can enhance or dampen inflammation and thereby influence other immune cells and plaque stability (41, 42). Overall, an imbalance of T lymphocytes in favour of pro-inflammatory as opposed to inflammation-resolving phenotypes will drive atherosclerosis (41). Similarly, different subsets of B lymphocytes can promote or protect from atherogenesis (43). While B cells producing immunoglobulin (Ig) M antibodies can decrease EC activation and foam cell formation by binding oxLDL, IgE antibodies can enhance the inflammatory response by activating MΦs (44).

The contribution of MΦ to atherosclerosis is substantial and multifaceted, as they adapt their phenotype in response to the stimuli they encounter in the atherosclerotic microenvironment (45). The next section will discuss monocyte-to-MΦ differentiation, MΦ plasticity, and MΦ phenotype.

MΦ phenotype in atherosclerosis

In atherogenesis, plaque MΦ are believed to arise from the expansion of resident macrophages, or from circulating monocytes that are recruited to lesion sites (46, 47), although this notion has been under debate in recent years. Monocytes are immune cells in the blood and the precursors of MΦ and DC (48). They extravasate to sites of inflammation where they exert effector functions, recruit other immune cells by secreting pro-inflammatory cytokines and chemokines (49, 50), and eventually differentiate into MΦ to replenish the depleted tissue-resident MΦ pool (51). Monocytes display large heterogeneity, for example in their expression of surface markers cluster of differentiation (CD) 14 and CD16 which is the basis for the current nomenclature distinguishing three human monocyte subsets (52). Monocytes of different subsets have been proposed to exert distinct functions (52). However, their functional characterisation is lacking, and recent advances suggest monocyte heterogeneity to extend beyond CD14/CD16 expression. Monocyte heterogeneity and the impact of monocytic origin on the phenotype of derived MΦ are extensively discussed in Chapter 2.

The most important growth factors to drive monocyte-to-MΦ differentiation are macrophage colony-stimulating factor (M-CSF) and granulocyte-macrophage colony-stimulating factor (GM-CSF). These are produced by various cell types present in the plaque, mainly EC and SMC (53, 54). M-CSF and GM-CSF not only induce MΦ differentiation and survival but also may prime the derived MΦ towards an anti-inflammatory or pro-inflammatory phenotype, respectively (55).

MΦ carry a repertoire of functions that is far from limited to immune functions. At steady-state, monocyte-derived MΦ replenish tissue-resident MΦ which can be found in every tissue of the body, although their phenotype and origin differ per organ (48). Whereas microglia, the tissue-resident MΦ population of the brain, are already seeded during embryonic development,

intestinal macrophages are replaced by monocyte-derived MΦ throughout life (49). Upon injury or trauma, MΦ sense tissue damage and contribute to the sterile inflammation and promote tissue repair, by phagocytosis of cell debris, efferocytosis of apoptotic cells, and induction of proliferation in other cell types (56). Upon infection, MΦ phagocytose pathogens and infected cells, display pathogen-derived antigens to T cells, and secrete pro-inflammatory cytokines and chemokines to attract other immune cells (57).

MΦ are highly plastic cells which modulate their functional phenotype in response to microenvironmental stimuli (57). Tissue MΦ are exposed to local niche-specific stimuli, instructing them to adopt a particular tissue-specific resident MΦ phenotype and to carry out tissue-specific functions (58). In contrast, strong cytokine signals of tissue injury or microbial stimuli elicit transcriptional programming, or polarisation, to an inflammation-upholding or inflammation-resolving phenotype (59, 60). *In vitro* activation of MΦ with (a limited number of) stimuli constitutes the M1/M2 paradigm of MΦ polarisation (61). A combination of IFN-γ and a toll-like receptor (TLR) agonist such as lipopolysaccharide (LPS) polarises MΦ to a phenotype which has been termed pro-inflammatory, or M1-like (62). The phenotype MΦ adopt after activation with IL-4 or IL-13 is referred to as alternatively activated, or M2-like (62). *In vivo*, IFN-γ is produced by T_H1 cells, and IL-4 or IL-13 by T_H2 cells (62). M1 MΦ uphold the inflammatory response against microbial infection by secreting inflammatory cytokines, whereas M2 MΦ secrete anti-inflammatory cytokines and are associated with the resolution of inflammation and wound healing (63). However, considering the complex combination of numerous stimuli MΦ encounter *in vivo*, the phenotypes of M1 and M2 MΦ should be considered as the two extremes of the polarisation spectrum (63). The atherosclerotic plaque constitutes a particularly diverse and complex microenvironment, and the phenotype of MΦ in the plaque is most likely a dynamic reflection of it (60). Indeed, this continuum of phenotypes and the heterogeneity of MΦ have been elucidated by single-cell RNA sequencing (scRNA-Seq) analysis of murine and human plaque immune cells. At least five MΦ subtypes can be distinguished in murine plaque, including resident-like MΦ, pro-inflammatory MΦ, foamy MΦ, and smaller populations of IFN-inducible MΦ and cavity MΦ (64). A pro-inflammatory and a foamy MΦ subset have also been identified in human plaque, next to a reparative M2-like MΦ subset, and M2 MΦ specialised in iron clearance (65). This illustrates the importance of assessing an integrated functional profile instead of single isolated functions.

Modulation of MΦ function

MΦ are highly plastic cells that play a central role in atherogenesis and plaque progression. Thus, modulating their function is an interesting and promising therapeutic strategy (66). Several MΦ-related processes can be targeted, such as monocyte recruitment, monocyte-to-MΦ differentiation, MΦ proliferation, restoring efferocytosis and cholesterol efflux to counteract foam cell formation, decreasing oxidative stress, and reinstructing MΦ to adopt

favourable functions dependent on plaque stage (66, 67). MΦ adapt their functional phenotype to their microenvironment, responding to local stimuli in the plaque on the one hand, and systemic changes due to their proximity to the bloodstream on the other (68).

With inflammation being one of the hallmarks of atherogenesis and MΦ secreting many cytokines, several monoclonal antibodies inhibiting cytokine secretion have been developed (69). However, although the CANTOS trial showed systemic IL-1β inhibition to reduce inflammation and secondary cardiovascular events, it also increased the incidence of infections (70). Thus, interventions targeting the atherosclerotic plaque might generally be favourable over systemic drug delivery.

One of the main obstacles of plaque-targeted drug delivery is premature clearance by spleen, liver, and lung (if particles size is in the micrometre range), which can be evaded by using drug carriers like nanoparticles (71). Nanoparticles are already commonly used in clinical practice as contrast agents to improve spatiotemporal resolution when imaging atherosclerotic plaques (72). To reach the atherosclerotic plaque, nanoparticles are often coated with (stealth) polymers or biomimetic membranes to circumvent clearance by spleen and liver (66). However, diffusion into the plaque requires a long circulation half-life of the particles (73), and as they enter the lesion likewise through the dysfunctional leaky endothelium, nanoparticles have been found to accumulate around endothelial openings instead of distributing homogeneously in the plaque (66). Moreover, nanoparticles can principally be taken up by all other cell types in the plaque. To target MΦ specifically, nanoparticles can be coated with ligands to receptors overexpressed on MΦ to increase uptake and accumulation in MΦ (66). However, establishing specificity for plaque MΦ over other tissue MΦ in light of their heterogeneity remains challenging.

Nanoparticles can be loaded with small-molecule drugs, microRNA (miR), or small interfering RNA (siRNA), improving their stability and pharmacokinetics (66). Lipid nanoparticles loaded with siRNA targeting CCR2, a key chemokine receptor for monocyte recruitment, were shown to prevent monocyte accumulation in murine models of atherosclerosis (74). Moreover, delivery of a Src homology region 2 domain-containing phosphatase 1 (SHP-1) inhibitor in carbon nanotubes interrupted CD47-signal regulatory protein α (SIRPα) signalling and led to enhanced efferocytosis in atherosclerotic mice, attenuating expansion of the necrotic core (70).

Another therapeutic strategy is MΦ-targeted gene therapy using viral vectors. Treatment of apolipoprotein E-knockout ($ApoE^{-/-}$) mice with an adenoviral vector encoding ApoE depleted plaque MΦ, leading to a decrease in plaque area and foam cell content (75). In another study, adenovirus-induced overexpression of peroxisome proliferator-activated receptor-γ1 (PPARγ1) reduced the accumulation of lipids and MΦ in the plaque leading to more stable plaques,

although the systemic modulation of PPARγ1 in this study may have contributed to this effect on atherosclerosis (76).

Overall, targeted MΦ reprogramming is a recent approach to modulate MΦ phenotype which is challenging regarding MΦ heterogeneity and their continuous microenvironmental sensing (77). For the development of safe and effective MΦ reprogramming therapies, a deeper understanding of factors and pathways influencing the functional phenotype of monocytes and MΦ is needed.

Overall aim and hypotheses

In conclusion, inflammation is a major driver of atherosclerosis, the main underlying cause of CVD. Monocytes and MΦ play an important role in atherosclerosis and are involved in all stages of its pathogenesis. MΦ are highly plastic cells that adapt their phenotype in response to microenvironmental stimuli and exert various functions in the plaque which can be pro- or anti-atherogenic. Thus, modulating the phenotype of MΦ for therapeutic benefit is a promising treatment strategy. However, it is still largely unknown how the functional phenotype of MΦ is constituted. Due to their high plasticity and responsiveness to their environment, MΦ phenotype can be altered at many levels. Nevertheless, previous studies often investigated only differentiated MΦ, missing phenotypic priming that may have occurred during differentiation into MΦ or that has been imprinted already at the monocytic precursor stage. Moreover, most *in vitro* studies on MΦ phenotype have only looked at individual functions or only used single polarisation stimuli which do not adequately represent the complex disease environment MΦ are exposed to *in vivo*.

In this thesis, we aim to investigate how MΦ phenotype is shaped by monocytic origin, growth factors during monocyte-to-MΦ differentiation, and sensing of the microenvironment. We hypothesise that:

1) MΦ originating from different monocyte subsets are functionally and transcriptionally different (Chapter 3).
2) MΦ phenotype *in vitro* is influenced by culture density (Chapter 4).
3) MΦ phenotype is primed during monocyte-to-MΦ differentiation by growth factors (Chapter 5).
4) MΦ respond to uptake of superparamagnetic iron oxide nanoparticles (Chapter 6).
5) MΦ respond to the systemic coronavirus disease 2019 (COVID-19) disease environment reflected in the serum of COVID-19 patients (Chapter 7).

Outline of this thesis

Human monocytes present in three phenotypes: classical $CD14^{++}CD16^{-}$, intermediate $CD14^{++}CD16^{+}$, and non-classical $CD14^{+}CD16^{++}$ monocytes. Their relative distribution and absolute counts have been reported to associate with CVD incidence, and to exert different functions. However, there is insufficient evidence of the subsets' causative role in CVD. Moreover, recent advances in scRNA-Seq and cytometry by time-of-flight (CyTOF) have revealed an even greater heterogeneity of the monocyte lineage, extending beyond the current CD14/CD16-based nomenclature. In Chapter 2, we discuss the implications of these findings for the prevailing view on monocyte heterogeneity and demonstrate the need to refine the current nomenclature of monocyte subsets. Moreover, we highlight associations of monocyte subsets, particularly intermediate monocytes, with CVD and CVD risk assessment. Finally, we summarise the current understanding of the influence of monocytic origin on the phenotype and functions of derived MΦ, a largely understudied topic in the field of cardiovascular inflammation. In Chapter 3, we study experimentally whether MΦ derived from monocytes of different subsets retain the functional identity of their monocyte precursors, leading to functional differences in the differentiated MΦ.

MΦ sense cues from neighbouring cells and respond by functional adaptations. This "quorum sensing" has recently been demonstrated to depend on cell density. However, the density of MΦ cultured *in vitro* as a model of MΦ in (inflamed) tissue is often disregarded. In Chapter 4, we comprehensively investigate the effects of culture density on many functions of human MΦ, using MΦ derived from the THP-1 cell line as well as primary human monocyte-derived MΦ. Moreover, we study the hypothesis that a colony-forming growth pattern contributes to functional adaptations in THP-1 MΦ, and that substantial inter-donor variability leads to functional differences in primary MΦ.

Monocyte-to-MΦ differentiation in atherosclerosis is primarily mediated by M-CSF and GM-CSF. However, quantitative measurement of M-CSF and GM-CSF as well as a comprehensive study of the differentiation dynamics they induce are lacking. Chapter 5 investigates the phenotypic changes during M-CSF- or GM-CSF-driven differentiation at functional and transcriptional level. We map similarities and differences in the trajectories induced by M-CSF or GM-CSF at four timepoints during monocyte-to-MΦ differentiation. Moreover, we measure M-CSF and GM-CSF in human atherosclerotic plaque and investigate the enrichment of M-CSF- and GM-CSF-associated gene signatures in plaque MΦ populations.

Small and ultrasmall superparamagnetic iron oxide nanoparticles, (U)SPIO, are commonly used as contrast agents for magnetic resonance imaging (MRI) to identify high-risk plaques and are assumed to be safe for clinical applications in CVD. However, safety tests were largely based on normolipidemic models, not fully representative of the clinical setting. In Chapter 6, we investigate the effect of (U)SPIO on disease-relevant endpoints in hyperlipidemic models of

atherosclerosis. Moreover, we consider coating formulation and particle size as possible determinants of cytotoxicity of (U)SPIO.

In Chapter 7, we use serum of COVID-19 patients to elucidate the functional response of MΦ to the COVID-19 disease environment. We investigate associations between the functional measurements and clinical parameters as well as their predictive value in terms of disease progression reflected in respiratory failure and the need for intensive care unit (ICU) treatment.

Chapter 8 considers the findings of this thesis and the implications for future research in a general discussion. Chapter 9 summarises the main findings presented in this thesis. Finally, Chapter 10 discusses the scientific and societal impact of this thesis.

References

1. Tsao CW, Aday AW, Almarzooq ZI, Alonso A, Beaton AZ, Bittencourt MS, et al. Heart Disease and Stroke Statistics—2022 Update: A Report From the American Heart Association. Circulation. 2022;145(8):e153-e639.
2. Joseph P, Leong D, McKee M, Anand SS, Schwalm J-D, Teo K, et al. Reducing the Global Burden of Cardiovascular Disease, Part 1. Circ Res. 2017;121(6):677-94.
3. Roth GA, Mensah GA, Johnson CO, Addolorato G, Ammirati E, Baddour LM, et al. Global Burden of Cardiovascular Diseases and Risk Factors, 1990–2019: Update From the GBD 2019 Study. J Am Coll Cardiol. 2020;76(25):2982-3021.
4. Bansilal S, Castellano JM, Fuster V. Global burden of CVD: focus on secondary prevention of cardiovascular disease. Int J Cardiol. 2015;201:S1-S7.
5. Gheorghe A, Griffiths U, Murphy A, Legido-Quigley H, Lamptey P, Perel P. The economic burden of cardiovascular disease and hypertension in low- and middle-income countries: a systematic review. BMC Public Health. 2018;18(1):975.
6. deGoma EM, Knowles JW, Angeli F, Budoff MJ, Rader DJ. The evolution and refinement of traditional risk factors for cardiovascular disease. Cardiol Rev. 2012;20(3):118-29.
7. Libby P. The changing landscape of atherosclerosis. Nature. 2021;592(7855):524-33.
8. Timmis A, Vardas P, Townsend N, Torbica A, Katus H, De Smedt D, et al. European Society of Cardiology: cardiovascular disease statistics 2021. Eur Heart J. 2022;43(8):716-99.
9. Björkegren JLM, Lusis AJ. Atherosclerosis: Recent developments. Cell. 2022;185(10):1630-45.
10. Libby P, Buring JE, Badimon L, Hansson GK, Deanfield J, Bittencourt MS, et al. Atherosclerosis. Nat Rev Dis Primers. 2019;5(1):56.
11. Libby P, Ridker PM, Maseri A. Inflammation and Atherosclerosis. Circulation. 2002;105(9):1135-43.
12. Jebari-Benslaiman S, Galicia-García U, Larrea-Sebal A, Olaetxea JR, Alloza I, Vandenbroeck K, et al. Pathophysiology of Atherosclerosis. Int J Mol Sci. 2022;23(6):3346.
13. Gidding SS. Assembling Evidence to Justify Prevention of Atherosclerosis Beginning in Youth. Circulation. 2010;122(24):2493-4.
14. Melaku L, Dabi A. The cellular biology of atherosclerosis with atherosclerotic lesion classification and biomarkers. Bull Natl Res Cent. 2021;45(1):225.
15. Davignon J, Ganz P. Role of Endothelial Dysfunction in Atherosclerosis. Circulation. 2004;109(23 Suppl 1): III27-32.
16. Zhang X, Sessa WC, Fernández-Hernando C. Endothelial Transcytosis of Lipoproteins in Atherosclerosis. Front Cardiovasc Med. 2018;5:130.
17. Gerhardt T, Ley K. Monocyte trafficking across the vessel wall. Cardiovasc Res. 2015;107(3):321-30.
18. Barrett TJ. Macrophages in Atherosclerosis Regression. Arterioscler Thromb Vasc Biol. 2020;40(1):20-33.
19. Chistiakov DA, Bobryshev YV, Orekhov AN. Macrophage-mediated cholesterol handling in atherosclerosis. J Cell Mol Med. 2016;20(1):17-28.
20. Allahverdian S, Chehroudi AC, McManus BM, Abraham T, Francis GA. Contribution of Intimal Smooth Muscle Cells to Cholesterol Accumulation and Macrophage-Like Cells in Human Atherosclerosis. Circulation. 2014;129(15):1551-9.
21. Kathryn M, Tabas J. Macrophages in the Pathogenesis of Atherosclerosis. Cell. 2011;145(3):341-55.
22. Watson MG, Byrne HM, Macaskill C, Myerscough MR. A two-phase model of early fibrous cap formation in atherosclerosis. J Theor Biol. 2018;456:123-36.
23. Olejarz W, Łacheta D, Kubiak-Tomaszewska G. Matrix Metalloproteinases as Biomarkers of Atherosclerotic Plaque Instability. Int J Mol Sci. 2020;21(11):3946.
24. Bentzon JF, Otsuka F, Virmani R, Falk E. Mechanisms of Plaque Formation and Rupture. Circ Res. 2014;114(12):1852-66.
25. Libby P, Ridker PM, Hansson GK. Progress and challenges in translating the biology of atherosclerosis. Nature. 2011;473(7347):317-25.
26. Nieto FJ. Infections and Atherosclerosis: New Clues from an Old Hypothesis? Am J Epidemiol. 1998;148(10):937-48.
27. Taleb S. Inflammation in atherosclerosis. Arch Cardiovasc Dis. 2016;109(12):708-15.
28. Wolf D, Ley K. Immunity and Inflammation in Atherosclerosis. Circ Res. 2019;124(2):315-27.

29. Soehnlein O, Libby P. Targeting inflammation in atherosclerosis — from experimental insights to the clinic. Nat Rev Drug Discov. 2021;20(8):589-610.
30. Ridker PM, Everett BM, Thuren T, MacFadyen JG, Chang WH, Ballantyne C, et al. Antiinflammatory Therapy with Canakinumab for Atherosclerotic Disease. N Engl J Med. 2017;377(12):1119-31.
31. Tardif J-C, Kouz S, Waters DD, Bertrand OF, Diaz R, Maggioni AP, et al. Efficacy and Safety of Low-Dose Colchicine after Myocardial Infarction. N Engl J Med. 2019;381(26):2497-505.
32. Ridker PM, Everett BM, Pradhan A, MacFadyen JG, Solomon DH, Zaharris E, et al. Low-Dose Methotrexate for the Prevention of Atherosclerotic Events. N Engl J Med. 2019;380(8):752-62.
33. Ruparelia N, Choudhury R. Inflammation and atherosclerosis: what is on the horizon? Heart. 2020;106(1):80-5.
34. Soehnlein O. Multiple Roles for Neutrophils in Atherosclerosis. Circ Res. 2012;110(6):875-88.
35. Döring Y, Soehnlein O, Weber C. Neutrophil Extracellular Traps in Atherosclerosis and Atherothrombosis. Circ Res. 2017;120(4):736-43.
36. Döring Y, Drechsler M, Soehnlein O, Weber C. Neutrophils in Atherosclerosis. Arterioscler Thromb Vasc Biol. 2015;35(2):288-95.
37. Palano MT, Cucchiara M, Gallazzi M, Riccio F, Mortara L, Gensini GF, et al. When a Friend Becomes Your Enemy: Natural Killer Cells in Atherosclerosis and Atherosclerosis-Associated Risk Factors. Front Immunol. 2022;12:798155.
38. Zernecke A. Dendritic Cells in Atherosclerosis. Arterioscler Thromb Vasc Biol. 2015;35(4):763-70.
39. Subramanian M, Tabas I. Dendritic cells in atherosclerosis. Semin Immunopathol. 2014;36(1):93-102.
40. Hansson GK, Hermansson A. The immune system in atherosclerosis. Nat Immunol. 2011;12(3):204-12.
41. Tabas I, Lichtman AH. Monocyte-Macrophages and T Cells in Atherosclerosis. Immunity. 2017;47(4):621-34.
42. Saigusa R, Winkels H, Ley K. T cell subsets and functions in atherosclerosis. Nat Rev Cardiol. 2020;17(7):387-401.
43. Ma SD, Mussbacher M, Galkina EV. Functional Role of B Cells in Atherosclerosis. Cells. 2021;10(2):270.
44. Sage AP, Tsiantoulas D, Binder CJ, Mallat Z. The role of B cells in atherosclerosis. Nat Rev Cardiol. 2019;16(3):180-96.
45. Colin S, Chinetti-Gbaguidi G, Staels B. Macrophage phenotypes in atherosclerosis. Immunol Rev. 2014;262(1):153-66.
46. Ley K, Miller YI, Hedrick CC. Monocyte and macrophage dynamics during atherogenesis. Arterioscler Thromb Vasc Biol. 2011;31(7):1506-16.
47. Swirski FK. The spatial and developmental relationships in the macrophage family. Arterioscler Thromb Vasc Biol. 2011;31(7):1517-22.
48. Yona S, Jung S. Monocytes: subsets, origins, fates and functions. Curr Opin Hematol. 2010;17(1):53-9.
49. Geissmann F, Manz MG, Jung S, Sieweke MH, Merad M, Ley K. Development of monocytes, macrophages, and dendritic cells. Science. 2010;327(5966):656-61.
50. Ginhoux F, Jung S. Monocytes and macrophages: developmental pathways and tissue homeostasis. Nat Rev Immunol. 2014;14(6):392-404.
51. Kratofil RM, Kubes P, Deniset JF. Monocyte Conversion During Inflammation and Injury. Arterioscler Thromb Vasc Biol. 2017;37(1):35-42.
52. Ziegler-Heitbrock L, Ancuta P, Crowe S, Dalod M, Grau V, Hart DN, et al. Nomenclature of monocytes and dendritic cells in blood. Blood. 2010;116(16):e74-80.
53. Ushach I, Zlotnik A. Biological role of granulocyte macrophage colony-stimulating factor (GM-CSF) and macrophage colony-stimulating factor (M-CSF) on cells of the myeloid lineage. J Leukoc Biol. 2016;100(3):481-9.
54. Sinha SK, Miikeda A, Fouladian Z, Mehrabian M, Edillor C, Shih D, et al. Local M-CSF (Macrophage Colony-Stimulating Factor) Expression Regulates Macrophage Proliferation and Apoptosis in Atherosclerosis. Arterioscler Thromb Vasc Biol. 2021;41(1):220-33.
55. Lacey DC, Achuthan A, Fleetwood AJ, Dinh H, Roiniotis J, Scholz GM, et al. Defining GM-CSF- and macrophage-CSF-dependent macrophage responses by in vitro models. J Immunol. 2012;188(11):5752-65.
56. Minutti CM, Knipper JA, Allen JE, Zaiss DMW. Tissue-specific contribution of macrophages to wound healing. Semin Cell Dev Biol. 2017;61:3-11.
57. Shapouri-Moghaddam A, Mohammadian S, Vazini H, Taghadosi M, Esmaeili S-A, Mardani F, et al. Macrophage plasticity, polarization, and function in health and disease. J Cell Physiol. 2018;233(9):6425-40.

58. Guilliams M, Thierry GR, Bonnardel J, Bajenoff M. Establishment and Maintenance of the Macrophage Niche. Immunity. 2020;52(3):434-51.
59. Sica A, Erreni M, Allavena P, Porta C. Macrophage polarization in pathology. Cell Mol Life Sci. 2015;72(21):4111-26.
60. Tabas I, Bornfeldt KE. Macrophage Phenotype and Function in Different Stages of Atherosclerosis. Circ Res. 2016;118(4):653-67.
61. Mills CD, Kincaid K, Alt JM, Heilman MJ, Hill AM. M-1/M-2 Macrophages and the Th1/Th2 Paradigm. J Immunol. 2000;164(12):6166-73.
62. Murray PJ. Macrophage Polarization. Annu Rev Physiol. 2017;79(1):541-66.
63. Nagenborg J, Goossens P, Biessen EAL, Donners MMPC. Heterogeneity of atherosclerotic plaque macrophage origin, phenotype and functions: Implications for treatment. Eur J Pharmacol. 2017;816:14-24.
64. Zernecke A, Winkels H, Cochain C, Williams JW, Wolf D, Soehnlein O, et al. Meta-Analysis of Leukocyte Diversity in Atherosclerotic Mouse Aortas. Circ Res. 2020;127(3):402-26.
65. Fernandez DM, Rahman AH, Fernandez NF, Chudnovskiy A, Amir E-AD, Amadori L, et al. Single-cell immune landscape of human atherosclerotic plaques. Nat Med. 2019;25(10):1576-88.
66. Chen W, Schilperoort M, Cao Y, Shi J, Tabas I, Tao W. Macrophage-targeted nanomedicine for the diagnosis and treatment of atherosclerosis. Nat Rev Cardiol. 2022;19(4):228-49.
67. Saha P, Modarai B, Humphries J, Mattock K, Waltham M, Burnand KG, et al. The monocyte/macrophage as a therapeutic target in atherosclerosis. Curr Opin Pharmacol. 2009;9(2):109-18.
68. Biessen EAL, Wouters K. Macrophage complexity in human atherosclerosis: opportunities for treatment? Curr Opin Lipidol. 2017;28(5):419-26.
69. Ji E, Lee S. Antibody-Based Therapeutics for Atherosclerosis and Cardiovascular Diseases. Int J Mol Sci. 2021;22(11):5770.
70. Flores AM, Hosseini-Nassab N, Jarr K-U, Ye J, Zhu X, Wirka R, et al. Pro-efferocytic nanoparticles are specifically taken up by lesional macrophages and prevent atherosclerosis. Nat Nanotechnol. 2020;15(2):154-61.
71. Peng R, Ji H, Jin L, Lin S, Huang Y, Xu K, et al. Macrophage-Based Therapies for Atherosclerosis Management. J Immunol Res. 2020;2020:8131754.
72. Palekar RU, Jallouk AP, Lanza GM, Pan H, Wickline SA. Molecular imaging of atherosclerosis with nanoparticle-based fluorinated MRI contrast agents. Nanomedicine (Lond). 2015;10(11):1817-32.
73. Forouzandehmehr M, Ghoytasi I, Shamloo A, Ghosi S. Particles in coronary circulation: A review on modelling for drug carrier design. Mater Des. 2022;216:110511.
74. Leuschner F, Dutta P, Gorbatov R, Novobrantseva TI, Donahoe JS, Courties G, et al. Therapeutic siRNA silencing in inflammatory monocytes in mice. Nat Biotechnol. 2011;29(11):1005-10.
75. Potteaux S, Gautier EL, Hutchison SB, van Rooijen N, Rader DJ, Thomas MJ, et al. Suppressed monocyte recruitment drives macrophage removal from atherosclerotic plaques of Apoe–/– mice during disease regression. J Clin Invest. 2011;121(5):2025-36.
76. Peroxisome Proliferator-Activated Receptor-γ1 Gene Therapy Attenuates Atherosclerosis and Stabilizes Plaques in Apolipoprotein E-Deficient Mice. Hum Gene Ther. 2008;19(3):287-299.
77. Bart VMT, Pickering RJ, Taylor PR, Ipseiz N. Macrophage reprogramming for therapy. Immunology. 2021;163(2):128-44.


2

Chapter 2

Monocyte heterogeneity in cardiovascular disease

AV Ruder, SMW Wetzels, L Temmerman, EAL Biessen* and P Goossens*

* Authors contributed equally

Adapted from *Cardiovascular Research. 2023;cvad069*

Abstract

Monocytes circulate the vasculature at steady state and are recruited to sites of inflammation where they differentiate into macrophages (MΦ) to replenish tissue-resident MΦ populations and engage in the development of cardiovascular disease (CVD). Monocytes display considerable heterogeneity, currently reflected by a nomenclature based on their expression of cluster of differentiation (CD) 14 and CD16, distinguishing $CD14^{++}CD16^{-}$ classical (cMo), $CD14^{++}CD16^{+}$ intermediate (intMo) and $CD14^{+}CD16^{++}$ non-classical (ncMo) monocytes. Several reports point to shifted subset distributions in the context of CVD, with significant association of intMo numbers with atherosclerosis, myocardial infarction, and heart failure. However, clear indications of their causal involvement as well as their predictive value for CVD are lacking.

As recent high-parameter cytometry and single-cell RNA sequencing (scRNA-Seq) studies suggest an even higher degree of heterogeneity, better understanding of the functionalities of these subsets is pivotal. Considering their high heterogeneity, surprisingly little is known about functional differences between MΦ originating from monocytes belonging to different subsets, and implications thereof for CVD pathogenesis. This chapter provides an overview of recent findings on monocyte heterogeneity in the context of homeostasis and disease as well as functional differences between the subsets and their potential to differentiate into MΦ, focusing on their role in vessels and the heart. The emerging paradigm of monocyte heterogeneity transcending the current tripartite subset division argues for an updated nomenclature and functional studies to substantiate marker-based subdivision and to clarify subset-specific implications for CVD.

Graphical abstract

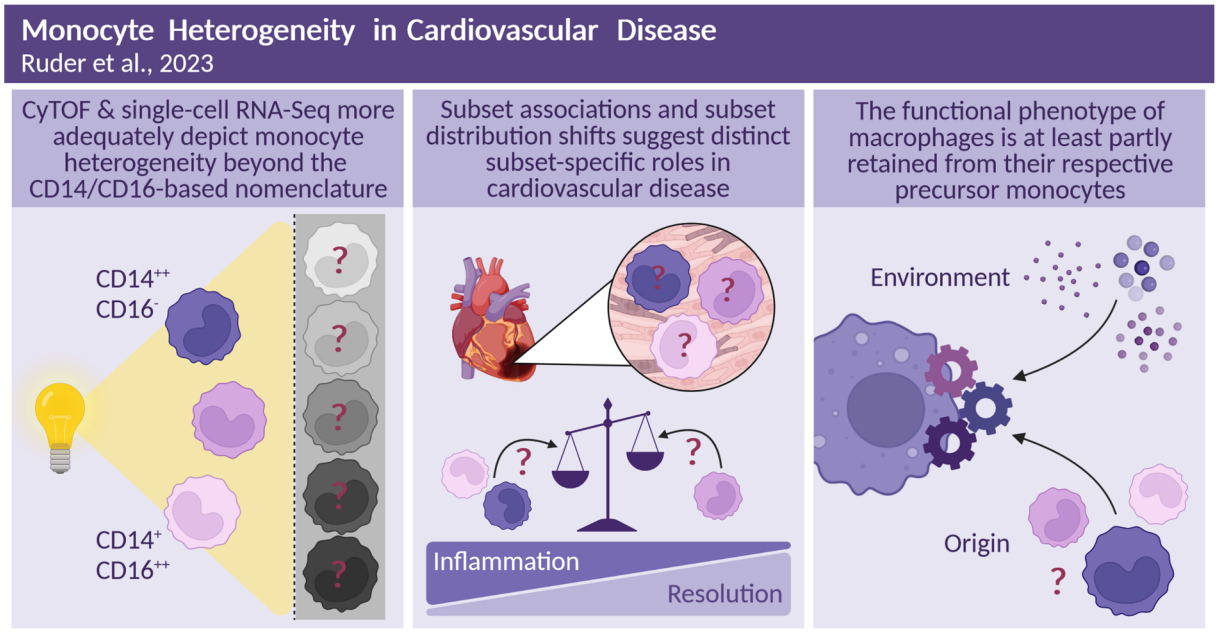

CyTOF: cytometry by time-of-flight; RNA-Seq: RNA sequencing. Created with BioRender.com.

Introduction

With their high functional diversity, monocytes and monocyte-derived macrophages (MΦ) play a key role in the pathogenesis and progression of cardiovascular disease (CVD) and atherosclerosis-related ischemic heart disease and heart failure (HF) (1). MΦ are abundant in every tissue in the body, including heart and vessel wall, where they regulate tissue homeostasis and monitor trauma and infection (2, 3). Recent evidence suggests that tissue-resident MΦ pools have mixed ontological origins arising both from embryonic progenitors and blood monocytes (4). The phenotype of tissue-resident MΦ is influenced by their microenvironment, resulting in high location-dependent heterogeneity (5, 6). Monocytes are haematopoietic cells that not only serve as MΦ precursors, complementing tissue-resident MΦ pools, but also play an important role in innate immunity. Upon inflammation, monocytes will locally extravasate towards the affected tissue where they differentiate into monocyte-derived MΦ and exert MΦ functions (7).

In humans, monocytes circulating in blood can be divided into three subsets: $CD14^{++}CD16^{-}$ "classical" monocytes (cMo), $CD14^{++}CD16^{+}$ "intermediate" monocytes (intMo) and $CD14^{+}CD16^{++}$ "non-classical" monocytes (ncMo) (8). Although many publications report functional differences between the three subsets, a delineating characterisation of their functions to assign distinct functional phenotypes is lacking (9). Advances in the study of the monocyte subsets, especially recent high-parameter cytometry studies (10, 11), have overhauled the prevailing view on monocyte heterogeneity and suggest the current classification scheme may be inadequate to cover the functional diversity of monocytes. In addition, despite studies describing the potential of all three monocyte subsets to differentiate into MΦ (12), it remains unclear whether they give rise to functionally distinct MΦ. In this review, we will present an overview of current insights on monocyte heterogeneity and implications for monocyte taxonomy. We will address subset-specific monocyte functions in health and CVD, as well as subset correlation to CVD. Moreover, we will outline the current knowledge on the impact of the subset of the monocytic progenitor on MΦ phenotype and activity in tissue, with particular focus on heart and vessel wall, and implications thereof for CVD progression.

Monocyte heterogeneity and consequences for monocyte taxonomy

First attempts to define monocyte heterogeneity were solely based on cell size and volume, distinguishing two major subpopulations referred to as large and small monocytes (13, 14). These featured differences in antibody-dependent cellular cytotoxicity (14) and chemotaxis towards zymosan-activated human serum (13), providing first evidence for functional differences between monocyte subpopulations. Flow cytometry and fluorescence-activated cell sorting (FACS) enabled a more granular analysis, leading to the identification and isolation of a monocyte subset smaller in size, characterised by low expression of cluster of

differentiation (CD) 14, a lipopolysaccharide (LPS) receptor (15), and co-expression of CD16, an FcγIII receptor (16, 17). These differences in expression of CD14 and CD16 serve as the basis for the nomenclature introduced in 2010 which is predominantly used today, classifying three human monocyte subsets: $CD14^{++}CD16^{-}$ cMo, $CD14^{++}CD16^{+}$ intMo and $CD14^{+}CD16^{++}$ ncMo (8). Accordingly, the terms cMo, intMo, an ncMo will be used to refer to the monocyte subsets in this review, and CD14/CD16 expression patterns will be included if subset definitions used in previously published studies deviate from the 2010 nomenclature.

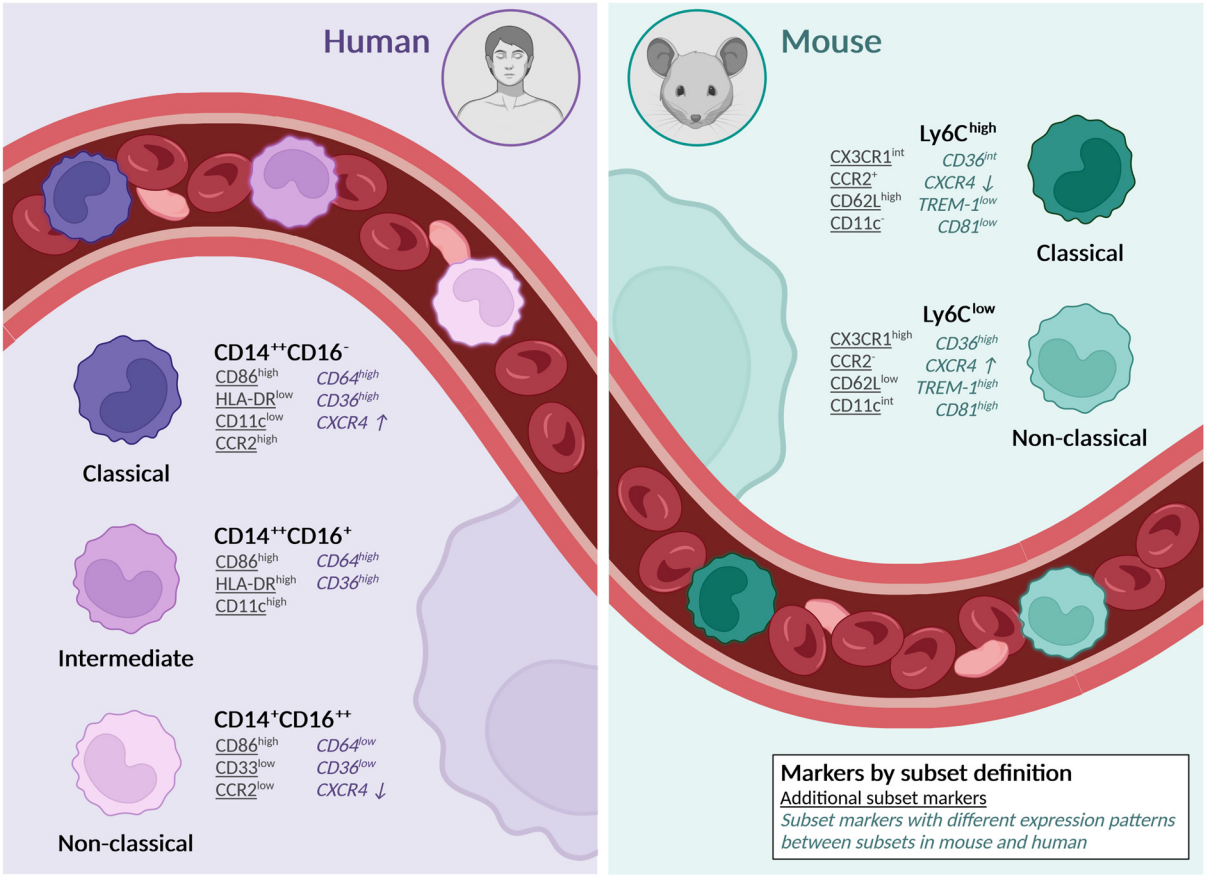

Figure 1: Monocyte subset markers in human and mouse
Overview of markers by definition of the current monocyte subset nomenclature (bold) and additional markers to distinguish between monocyte subset in human and mouse (underlined). Although human classical $CD14^{++}CD16^{-}$ and murine $Ly6C^{high}$, likewise non-classical $CD14^{+}CD16^{++}$ and $Ly6C^{low}$ are considered counterparts, markers that identify a subset in one species are not necessarily transferable to the same subset in the other species. For example, while CD36 expression is lower on classical $Ly6C^{high}$ than in non-classical $Ly6C^{low}$ monocytes, classical $CD14^{++}CD16^{-}$ express high levels and non-classical $CD14^{+}CD16^{++}$ low levels of CD36. Markers with different expression patterns when comparing corresponding subsets in mouse and human are contained in this overview (cursive). Expression of TREM-1 and CD81 in intermediate $CD14^{++}CD16^{+}$ and non-classical $CD14^{+}CD16^{++}$ was not included as published studies did not distinguish between the two subsets. CD64 expression is similar between $Ly6C^{high}$ and $Ly6C^{low}$ monocyte subsets and thus not mentioned for the murine subsets. CXCR4 expression levels are not clearly definable as high or low but show a higher (↑) or lower (↓) expression between subsets, indicated by arrows. All expression levels depicted refer to protein-based expression and were gathered from Ingersoll et al. (2010), Mildner et al. (2016), Thomas et al. (2017), Ong et al. (2019), and Mueller et al. (2019). Created with BioRender.com.

In mice, two main monocyte subsets have been described: Ly6C^{high} monocytes which resemble CD14^{++}CD16^{-} cMo and Ly6C^{low} monocytes which represent the murine counterpart to CD14^{+}CD16^{++} ncMo (18, 19). Although considered counterparts, CD14/CD16 and Ly6C are not inert in the other species, respectively, and may modulate subset function differently. Moreover, the proportions of circulating monocyte subsets in mice and humans differ substantially (approximately 95% CD14^{++}CD16^{-} cMo versus 50% Ly6C^{high}) (19), a note that should be considered for the interpretation of data from mouse studies (**Figure 1**). In addition, monocyte heterogeneity varies between mice of different sexes and strains, including the widely used BALB/c strain as well as C57Bl/6, the background strain of apolipoprotein E-knockout (ApoE$^{-/-}$) and low-density lipoprotein receptor-knockout (LDLR$^{-/-}$) mice, models commonly used in CVD research (20, 21).

The CD14/CD16-based definition of monocyte subsets provided clear terminology for monocyte subsets but might not be sufficient for unambiguous identification. CD14 and CD16 expression depend on activation status and disease context (11, 22), making a gating strategy relying solely on these markers insufficiently robust. More worrisome, natural killer (NK) cells, like ncMo, also express CD16 and are CD14-negative, potentially giving rise to contamination of ncMo by these CD56 (NCAM)^{dim} cells. Inclusion of human leukocyte antigen (HLA)-DR in the FACS panel allows more selective discrimination of ncMo (**Figure 2**) (23, 24). Consequently, a separation of monocyte subsets solely based on CD14 and CD16 may be insufficient to unequivocally distinguish monocyte subsets.

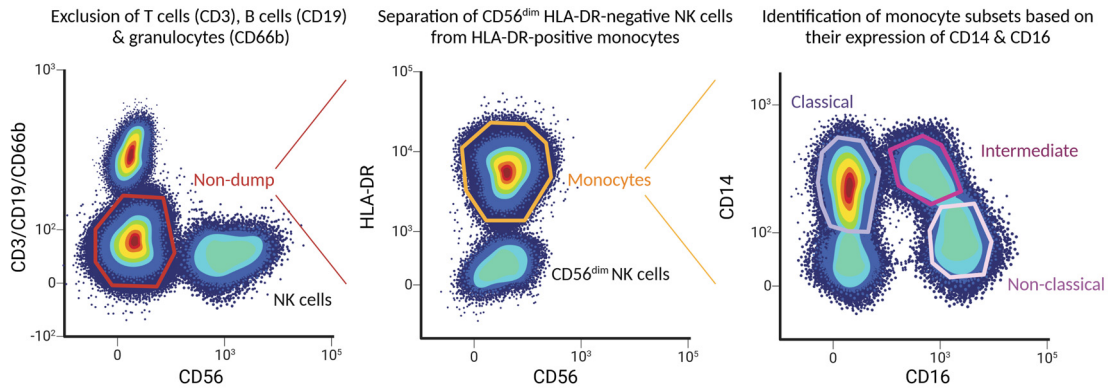

Figure 2: Schematic gating strategy to discriminate human monocyte subsets
The plots depicted serve as an illustration of a gating strategy to identify human subset populations from peripheral blood mononuclear cells and to allow fluorescence-activated cell sorting at high purity. After gating of live and single cells, CD3-positive T cells, CD19-positive B cells, CD66b-positive granulocytes, and CD56^{high} NK cells are excluded by dump gating. Next, monocytes are selected based on HLA-DR expression, and HLA-DR-negative NK56^{dim} cells which may not have been excluded in the previous gating step are separated from HLA-DR-positive monocytes. Finally, the three human monocyte subsets as defined by the current nomenclature are distinguished based on their expression of CD14 and CD16, with classical CD14^{++}CD16^{-}, intermediate CD14^{++}CD16^{+} and non-classical CD14^{+}CD16^{++} monocytes. Although the ratio of the subsets, especially of non-classical and intermediate monocytes, varies greatly between donors, the proportion of classical monocytes consistently predominates over the two other subsets. Created with BioRender.com.

Recent high-parameter cytometry and single-cell RNA sequencing (scRNA-Seq) studies have revolutionised our view on monocyte heterogeneity and led to an improved resolution of the aforementioned monocyte subsets, especially of intMo and ncMo (10). Previously, 6-sulfo LacNAc (slan) expression had been shown to more reliably distinguish slan-negative $CD14^{++}CD16^{+}$ intMo from slan-positive $CD14^{+}CD16^{++}$ ncMo using FACS and massive analysis of complimentary DNA ends (MACE) (22). To complicate matters, a high-resolution approach using cytometry by time-of-flight (CyTOF) to profile monocyte heterogeneity by Roussel et al. revealed that slan expression may also mark separate subsets within the ncMo population (25). Although slan-positive monocytes show similar cytokine production patterns (26) and transcriptional profiles (27) as ncMo, they seem to differ in their expression of CXCR6 (28, 29). As a study by Cros et al. failed to confirm the slan-based sub-differentiation within the ncMo (18), the jury is still out on the added value of slan as a monocyte subset marker. In parallel, Villani et al. aimed at improving monocyte subset identification using scRNA-Seq of human monocytes which were FACS-sorted with a CD14/CD16-based gating strategy (30). Their study revealed four monocyte clusters of which two were located within the intMo subset. However, as one of the subsets within intMo was typified by established NK markers such as KLRC4, CTSW and PRF1, the true monocyte nature of this subset remains to be addressed. Conversely, Mildner et al. describe a newly-identified $Ly6C^{int}$ intMo subset in mice showing transcriptional as well as phenotypic overlap to both $Ly6C^{high}$ cMo and $Ly6C^{low}$ ncMo (31). Similarly, Thomas et al. found human intMo to cluster with both cMo and ncMo using CyTOF (32). Addition of CD11c (integrin α-X), HLA-DR, CD36 (GP4, GP3B, SCARB3), and CCR2 (CD192) to their CD14/CD16-based gating strategy allowed clear separation of the three conventional monocyte subsets. Although the introduction of additional subset markers improved differentiation between intMo and ncMo, the latter still relies on prior subset identification using CD14 and CD16. However, as Ong et al. showed, a CD64 (FCGR1)-, CD86 (B7.2)-, CD33 (SIGLEC3)-, CCR2-, and HLA-DR-based marker panel performs equally well to reliably identify $CD16^{-}$ cMo, $CD16^{+}CD14^{high}$ intMo, and $CD16^{+}CD14^{low}$ ncMo (11), suggesting a CD14/CD16-independent separation is possible.

Next to enabling improved identification of the conventional three subsets, high-parameter cytometry and scRNA-Seq technology combined with high-dimensional analyses advanced the identification of new subsets within the three monocyte populations (11, 25, 30, 32, 33). In human, Hamers et al. identified eight monocyte subsets using CyTOF, with three subsets falling within ncMo and four within cMo (29). Merah-Mourah et al., using 17-colour FACS, identified a set of large and a set of small monocytes that could be further divided by their expression of CD16, resulting in a total of six monocyte subsets. Large and small monocyte sets showed differences in the production of tumour necrosis factor (TNF) and interleukin (IL) -1β in response to toll-like receptor (TLR) agonists, as well as in their expression of adhesion molecules, suggesting distinct functions (33). However, the conventional tripartite differentiation of monocytes was underpinned by Dutertre et al. who applied a machine

learning algorithm for subset discrimination in scRNA-Seq and CyTOF including 14 backbone lineage markers plus one of 332 variable markers each (34). These partly conflicting findings could be caused by minor differences in the source sample but most likely by differences in strategy of and settings for data analysis. Notably, the cMo and intMo populations identified by Dutertre et al. each embedded two marginally different subsets, such as CD35 $(CR1)^+$/CD89 $(FCAR)^+$ cMo and CD55 $(DAF)^+$/$Mac2^+$ cMo (34).

In conclusion, by both the use of new surface markers or the inclusion of additional markers to the conventional CD14- and CD16-based panel, greater heterogeneity within the human monocyte population than the current trinomial terminology suggests was revealed, and new monocyte subpopulations were identified. Although recent findings mostly agree on heterogeneity within the original cMo and ncMo subsets, a lack of a clear consensus is evident by differences in the number of subpopulations reported. This may be attributable to differences in number and combination of markers as well as (unsupervised) clustering methods used. The reproducibility and comparability may be further impacted by substantial differences in the identification and annotation of cell clusters. Whether or not these new subpopulations represent truly separate phenotypes or reflect the stochastic diversity within the mother populations remains to be established by lineage tracing and differentiation studies. It is not unlikely that some studies have considerably over-clustered this cell species. Moreover, standardised cluster annotation approaches such as the reference mapping included in Seurat v4 (35) are needed to consistently define monocyte subpopulations.

In 2016, an update to the 2010 nomenclature was proposed, suggesting the numerical labels “Mon1” for cMo, “Mon2” for intMo, and “Mon3” for ncMo (36). Despite resemblance to the M1/M2 terminology for MΦ polarisation states, these labels were not chosen to express a predisposition of MΦ to adopt a M1 or M2 polarisation state depending on the monocyte subset they originate from, but to simplify monocyte subset terminology (36). A numerical nomenclature does not only allow detachment from a marker-based subset definition which may change with the discovery of additional or alternative subset markers, it could also facilitate the coherent naming of newly-identified monocyte subsets. However, it appears that the ambiguity observed in literature to date may at least partly be attributed to an incomplete subset definition, exclusively based on surface marker expression, which should be complemented with distinctive functions and differentiation potential of monocyte subsets. Thus, a taxonomy putting newly-identified monocyte subsets into context, as suggested by Bassler et al. (37) will still be necessary to adequately describe monocyte heterogeneity. Moreover, functional differences of established original and newly-identified monocyte subsets remain to be assessed and related to their role as precursors of tissue-resident MΦ and to pathogen and endogenous trauma responses.

Monocyte subset distribution in CVD

Monocytes are major players in the development of CVD, illustrated by the observation that the number of circulating monocytes has a predictive value for cardiovascular risk and mortality (38-40). However, most studies did not stratify for monocyte subsets. Moreover, the interpretation of findings reported in studies that did discriminate between monocyte subsets is complicated by differences in subset definition, in staining and gating protocols as well as the number and combination of markers used to identify subsets. In a prospective study using flow cytometry to determine monocyte subset counts, Rogacev et al. showed that intMo were the only subset to independently predict cardiovascular disease risk in elective coronary angiography patients in 3 years of follow-up (41). These findings are in contrast with a study by Berg et al., showing elevated cMo counts to predict cardiovascular events, defined as fatal or non-fatal myocardial infarction (MI), ischemic stroke or coronary heart disease-related death. The use of frozen leukocyte samples and the smaller study population (n=700) in the study by Berg et al. compared to fresh samples in Rogacev et al. (n=951) might account for the different observations between the two studies (41, 42). Wildgruber et al. found increased intMo and decreased ncMo numbers in patients with progression of peripheral artery occlusive disease, the number of cMo remaining unchanged (43). Similarly, while CD106 (VCAM-1) expression on cMo was reported to be increased in coronary artery disease (CAD) patients, these patients also featured elevated intMo counts, possibly due to a shift from cMo to ncMo at levels that were predictive of adverse cardiovascular disease outcome (44). Interestingly, CAD patients with elevated levels of lipoprotein (a) [Lp(a)], a pro-atherogenic lipoprotein and independent risk factor for CVD (45), had increased intMo compared to patients with normal Lp(a) levels, whereas ncMo and cMo proportions remained unchanged in both patient groups (46). As compared to cMo, telomere length of intMo was shorter which might indicate senescence, although comparisons of telomere length [reviewed in (47)] between different cell types/subsets should be taken with caution. Moreover, intMo expression of chemokine receptors like CCR2, CCR5 (CD195), CCR7 (CD197) and CX3CR1 was higher than in the other subsets (48), suggesting they are more responsive to chemotactic cues in CVD.

Several studies also investigated correlations between monocyte subset counts and atherosclerotic plaque composition and/or stability, with inconsistent outcomes (**Table 1**). Interrogating the AtheroExpress plaque cohort, none of the monocyte subsets was found to be associated with critical plaque characteristics such as fat deposition, collagen deposition, calcification, intraplaque haemorrhage, intraplaque vessel and smooth muscle cell density (49). However, in a cohort of 588 individuals that underwent coronary computed tomography (CT) angiography for routine health check-up, intMo levels correlated with mixed and calcified plaque types, whereas cMo counts correlated with non-calcified plaques (50). In a smaller cohort (n=51) in which asymptomatic coronary artery plaques were analysed by virtual histology based on intravascular ultrasound, intMo were significantly correlated with plaque

vulnerability traits such as burden of fibrous components, necrotic core size and calcification (51).

These findings were confirmed by Yamamoto et al. in a small prospective optical coherence tomography and coronary angiography study of coronary artery patients (52). Although findings are not completely consistent, the overall picture emerging from these studies is that intMo numbers seem most predictive of CVD and strongest associated with plaque vulnerability. Whether intMo are causally involved in CVD or whether the CVD context leads to aberrant cMo-to-ncMo conversion or increased expression of intMo markers remains subject to further studies.

Table 1: Reported shifts in monocyte subsets distributions in atherosclerosis

Source	Cohort size	Outcome
Meeuwsen et al. 2019 (49), The Netherlands	175 undergoing CEA (63.4% male)	No association of any monocyte subset with vulnerable plaque traits
Lo et al. 2017 (50), Taiwan	588 undergoing general health check with coronary CT (68.7% male)	Correlation of intMo with mixed and calcified plaque types Correlation of cMo with non-calcified plaque type
Yoshida et al. 2017 (51), Japan	51 asymptomatic CAD (75% male)	Correlation of intMo with vulnerable plaque traits
Yamamoto et al. 2018 (52), Japan	50 CAD (80% male)	Counts of intMo associated with vulnerable plaque traits

CEA: carotid endarterectomy; CAD: coronary artery disease; CT: computed tomography; cMo: classical monocytes; intMo: intermediate monocytes; ncMo: non-classical monocytes.

Plaque destabilisation and rupture can eventually lead to an ischemic event causing myocardial necrosis. Recruited monocytes and cardiac resident MΦ are instrumental in the trauma repair response to infarct [reviewed in (53)]. According to Tsujioka et al., $CD14^{++}CD16^{-}$ cMo are the monocyte subset recruited first, peaking 2.6 days after infarct onset, while CD16-positive intMo and ncMo are recruited in a later phase to peak around day 5 after onset (54). This timely sequence might reflect the developmental trajectory of cMo to ncMo (as discussed below) after monocytosis in response to trauma. Interestingly, peak recruitment of cMo, but not CD16-positive intMo and ncMo was inversely correlated with myocardial salvage and left ventricular ejection fraction 6 months after onset (54) (Table 2). As shown by Tapp et al., circulating cMo and intMo counts were increased in the first day after ST-elevation myocardial infarction (STEMI), upon which intMo levels were significantly correlated with plasma cytokine and cardiac troponin levels, and recovery of left ventricular function (55), suggesting this subset to play a key role in cardiac healing. Histopathological examination of myocardial tissue collected from autopsy indicated cMo accumulation at the border of the infarct zone surrounding the necrotic area during the inflammatory phase at 12 hours to 5 days after acute myocardial infarction (AMI). In the following proliferative phase at 5 to 14 days after AMI, infiltration of the infarct zone by CD16-positive monocytes was observed, though these were not further

classified into $CD14^{++}CD16^{+}$ intMo or $CD14^{+}CD16^{++}$ ncMo (56). Apparently, apart from $CD14^{++}$ $CD16^{-}$ cMo, CD16-positive monocytes (probably ncMo) are also needed for proper AMI repair, likely because they serve different functions. As described above, the AMI-associated expansion of intMo was predictive of adverse cardiovascular events within 2 years after the primary event (57), suggesting a detrimental role of intMo in AMI repair or in atherosclerosis. According to Zeng et al., particularly STEMI patients with persistent elevations of circulating intMo after infarct were at risk of a major adverse cardiovascular event during 2.5-year follow-up (58), suggesting that not only the subset profile but also subset dynamics upon infarct can impact the outcome of cardiovascular events. This may support the finding of Dutta et al. in mice where increased monocyte recruitment in the aftermath of an infarct was not limited to the infarct zone itself but also implicated distal sites of chronic atherosclerosis, resulting in recurrent events (59).

Table 2: Reported shifts in monocyte subsets distributions in myocardial infarction

Source	Cohort size	Outcome
Shantsila et al. 2019 (62), UK	245 STEMI (78% male)	Increased absolute number of intMo
Tapp et al. 2012 (55), UK	50 STEMI, 40 CAD and 40 healthy controls (80-86% male)	Counts of circulating cMo and intMo increased on first day after STEMI IntMo levels correlated with cytokine and troponin levels as well as recovery of left ventricular function
Zhou et al. 2016 (57), China	100 STEMI, 60 CAD and 35 healthy controls (68-78% male)	Expansion of intMo predictive of adverse cardiovascular events within 2-year follow-up
Zeng et al. 2018 (58), China	96 STEMI (78% male)	Persisting elevation of intMo after STEMI associated with risk for major adverse cardiovascular events within 2.5-year follow-up
Tsuijoka et al. 2009 (54), Japan	36 AMI (75% male)	Peak levels of cMo inversely correlated with myocardial salvage and LVEF after infarct onset
Van der Laan et al. 2014 (56), The Netherlands	28 AMI and 12 other causes (67% male)	Accumulation of cMo at border of infarct zone 12 hours to 5 days after AMI, followed by infiltration of intMo/ncMo

STEMI: ST-elevated myocardial infarction; AMI: acute myocardial infarction; CAD: coronary artery disease; LVEF: left ventricular ejection fraction; cMo: classical monocytes; intMo: intermediate monocytes; ncMo: non-classical monocytes.

AMI-associated loss of cardiac function can develop into HF, the major cause of morbidity and mortality after AMI (60). HF patients had an increased percentage of $CD14^{++}CD16^{+}$ intMo compared to healthy subjects at increased cardiovascular risk which correlated with disease severity (61), a finding that was confirmed by Shantsila et al. for absolute subset numbers (62) (Table 3). Moreover, intMo had higher expression of the cell adhesion molecules ICAM-1 (CD54) and VCAM-1, of which the latter was associated with adverse clinical outcome for acute HF (63). In keeping with this, significant increases in intMo counts in (acute) HF were reported by Wrigley et al. (cross-sectional study) (64) and by Elchinova et al. (65). Interestingly, while the

former also noted elevated cMo levels, the latter, larger study found reduced cMo levels. In this study, also the number of intMo (cells/µl) in HF patients was independently associated with all-cause death (65). Finally, a study by Amir et al. failed to reproduce these findings, reporting an unchanged intMo proportion in HF patients, but reduced percentages of cMo and increased percentages of ncMo (66). Moreover, the percentage of ncMo, but not cMo or intMo, was inversely correlated with severe HF. Discrepancies between these study outcomes may be attributable to differences in the study populations' risk and environmental factor profile. Indeed, the secretome of adipose tissue of obese HF patients was able to induce a shift towards ncMo differentiation, in contrast to that of non-obese HF patients (67). Oxysterol-mediated activation of NR4A1, a nuclear receptor critically involved in ncMo differentiation, could explain this finding (68, 69). It remains unclear whether this obesity-associated ncMo increase is a protective response or merely a consequence of larger disease characteristics. MΦ origin in the heart was also shown to change with ageing, resulting in increased monocyte recruitment and a shift towards M1-like cardiac MΦ (70), suggesting increased susceptibility for and worse outcome of CVD in aged individuals. Thus, the increased presence of monocyte-derived MΦ in the heart and arteries may have disease-relevant repercussions for MΦ phenotype in these organs.

Table 3: Reported shifts in monocyte subsets distributions in heart failure

Source	Cohort size	Outcome
Barisione et al. 2010 (61), Italy	30 congestive HF and 26 healthy controls (all male)	Increased percentage of intMo in HF correlating with disease severity
Wrigley et al. 2013 (64), UK	51 acute HF, 42 stable HF, 44 CAD and 40 healthy controls (58-83% male)	Increased intMo count in acute HF compared to stable HF and CAD Increased intMo count in stable HF compared to CAD Elevated cMo levels in acute HF compared to stable HF, CAD, and healthy controls No difference in ncMo counts
Wrigley et al. 2013 (63), UK	51 acute HF, 42 stable HF and 44 CAD (68-83% male)	Higher expression of ICAM-1 on intMo of acute HF compared to stable HF & CAD VCAM-1 expression on intMo of acute HF associated with death or hospitalisation
Elchinova et al. 2018 (65), Spain	400 HF (72.8% male)	Increased intMo count Absolute number of intMo per µl blood associated with all-cause death Reduced cMo levels
Amir et al. 2012 (66), Israel	59 systolic HF and 29 controls without heart disease (53-76% male)	Reduced percentage of cMo in HF Increased percentage of ncMo in HF Percentage of ncMo inversely correlated with severe HF No difference in intMo percentage

HF: heart failure; CAD: coronary artery disease; cMo: classical monocytes; intMo: intermediate monocytes; ncMo: non-classical monocytes.

Overall, most studies agree that monocyte subset distribution shifts in cardiovascular disease, although cause and direction of this shift still need to be further investigated. A shift towards

ncMo is also observed with ageing which may reflect accelerated immune ageing and increased susceptibility to CVD. Several studies suggest an association of the intMo subset with CVD, atherosclerosis, AMI, and HF, although not all studies agree on their predictiveness of prognosis.

Functional diversity of monocyte subsets in health and disease

Today, monocytes are no longer viewed as mere precursors of MΦ, as this dogma has been challenged by several studies showing clear functional specialisations of cMo and ncMo subsets (Figure 3) (71, 72). The recently reported high heterogeneity of this lineage may have further eroded this view. Monocytes functionally adapt to inflammatory stimuli and carry out effector functions in innate immune responses to pathogens in circulation and in trauma monitoring of the endothelium (72-74). However, assigning functional phenotypes to monocyte subsets has been impeded by conflicting results, differences in methodology and readout, and functions being assigned to multiple subsets (75, 76). The official CD14/CD16-based nomenclature intentionally avoids terms like “inflammatory” and “anti-inflammatory” to allow broader function-based categorisation. Further investigation of functional differences between the subsets is still necessary (8, 77), taking into account the potential heterogeneity of the monocyte subsets as suggested by the aforementioned single-cell studies.

CMo sense cues from sites of injury and inflammation, are released into circulation via CCL2-CCR2 signalling, and extravasate into affected tissues (78-80). They are highly active in phagocytosis and production of reactive oxygen species (ROS) (75, 81). In response to bacterial signals, cMo secrete inflammatory cytokines such as IL-6, IL-8 and IL-1β (12, 18). Although they are able to clear debris (79), this capacity is less developed than in ncMo (82), a difference that has been used for selective bead-based tracking of ncMo *in vivo* (83). Moreover, cMo were found to differentiate into intMo which in turn differentiate into ncMo, following a sequential ontogeny scenario as shown by Patel et al. (84) using a humanised mouse model, the MISTRG mouse (85). In humans, after endotoxin-induced depletion of blood monocytes, re-population followed a sequential pattern of cMo appearing first, followed by intMo and finally ncMo (84). In a smaller study (n=12), Thaler et al. observe cMo to be the first subset to appear after LPS challenge and cMo counts to recover within 6 hours (86). Moreover, they report a reduction in cMo counts and considerable shift towards intMo in the next 18 hours, suggesting enhanced differentiation of cMo into intMo in response to inflammatory cues. The time needed for cell trafficking from bone marrow to circulation seems to be decreased under inflammatory conditions, which might be caused by the release of cMo retained in the bone marrow and spleen as an “emergency pool” (84). Most evidence on this emergency release and the contribution of bone marrow-derived monocytes was obtained from mouse experiments, where two main monocyte subsets are distinguished based on their expression of Ly6C (87). The circulating pool of Ly6C^{high} cMo is rapidly replenished by egress of CXCR4^{high} Ly6C^{high} bone marrow monocytes (88), which may have alternative phenotypes and functional adaptations,

similar to neutrophil-like Ly6C^{high} cMo or segregated nucleus-containing atypical Ly6C^{low} ncMo [reviewed in (89)]. The control of this emergency release of monocytes is associated with microRNA (miR)-146a, leading to expansion and trafficking of Ly6C^{high} cMo and resulting in an increased inflammatory response against bacteria [reviewed in (90)]. Circulating Ly6C^{high} cMo may also convert into Ly6C^{low} ncMo, as proposed by Yona et al. regarding the rapid appearance of BrdU-labelled Ly6C^{high} cMo in circulation, whereas BrdU-positive Ly6C^{low} ncMo became detectable after 5 days (91).

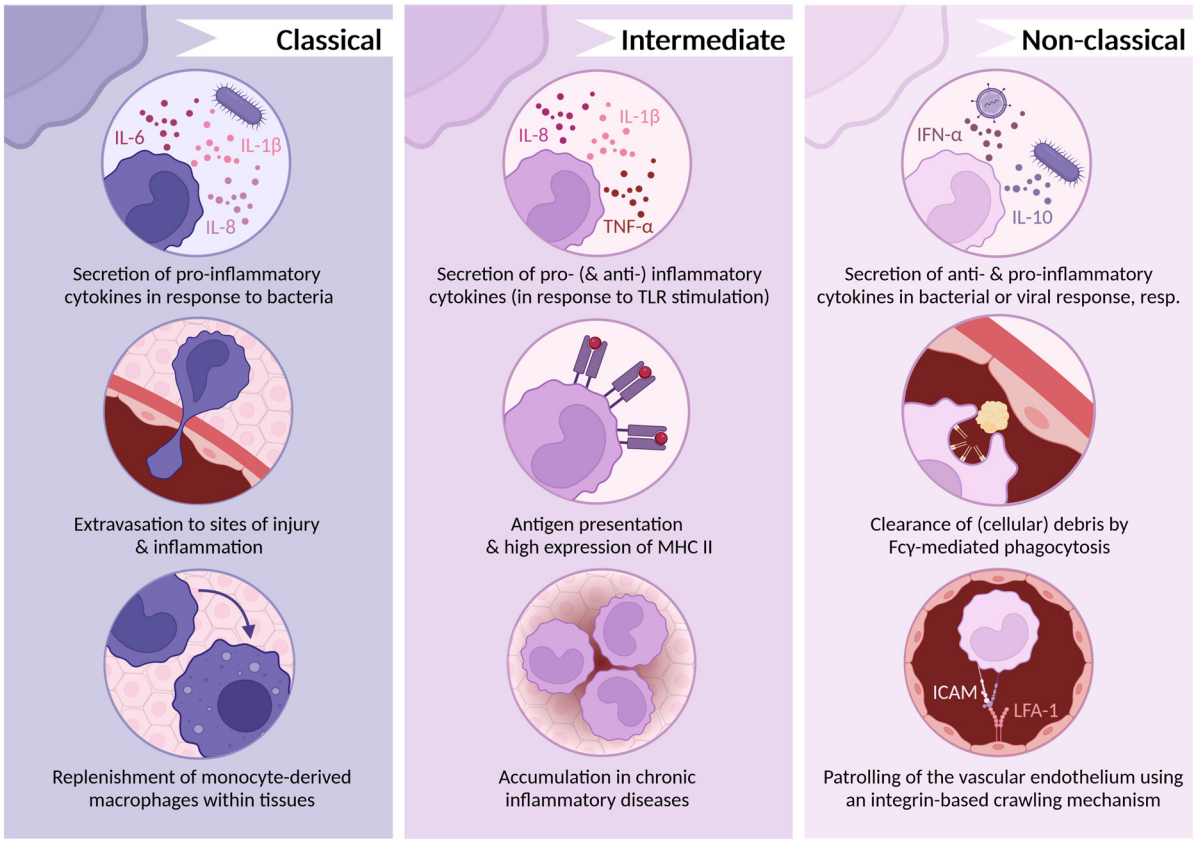

Figure 3: Functions of classical, intermediate, and non-classical monocytes
Monocytes of different subsets exert different functions, illustrated in this figure. The current nomenclature purposefully avoids the terms "pro-inflammatory" and "anti-inflammatory" to describe monocyte subsets. Considering their functions, especially cytokine secretion by the different monocyte subsets, the importance of a nomenclature independent of single functions becomes apparent, as non-classical monocytes produce pro-inflammatory cytokines in response to viruses but are often termed "anti-inflammatory". MHC: major histocompatibility complex; TLR: toll-like receptor. Created with BioRender.com.

The conversion to Ly6C^{low} ncMo was found to be dependent on CCR2 (91) which is expressed exclusively by Ly6C^{high} cMo (18). The mechanism underlying the conversion of Ly6C^{high} cMo to Ly6C^{low} ncMo was elucidated by Thomas et al. who studied the regulation of the Nr4a1 gene which encodes transcription factor Nur77 (69) In line with previous results, Ly6C^{low} ncMo showed higher expression of Nr4a1 than Ly6C^{high} cMo (68, 69). Nr4a1 knockout led to partial depletion of the Ly6C^{low} ncMo pool, indicating its crucial role for the generation of Ly6C^{low} monocytes (68). Thomas et al. found Nr4a1 to be regulated by the interaction of Klf2 with the

Nr4a1 super-enhancer domain E2 (69). In line with this finding, Patel et al. addressed the kinetics of human monocyte subsets by isotopic 6,6-$^{2}H_2$-glucose labelling in healthy volunteers, showing turnover rates of 1 day for cMo, 4.3 days for intMo and 7.4 days for ncMo (84), corresponding to the observations in mice. These data could be partly confirmed by Tak et al. (n=14) who also observed consecutive isotopic labelling of the three monocyte subsets, pointing to a linear differentiation model. Only few cMo were differentiating into intMo, while almost all intMo were on their way to become ncMo, suggesting that the first step is rate limiting. Blood residence times for cMo and ncMo were approximately 2.5 days; however, intMo were seen to have much shorter blood residence time in this study (<1 day) (92). Additional studies will be needed to fully clarify this. Taken together, under steady state conditions, cMo can either differentiate into MΦ to replace tissue-resident MΦ or develop into ncMo with involvement of Nr4a1.

In contrast to cMo, ncMo produce anti-inflammatory cytokines like IL-10 in response to bacterial stimuli (18). However, this does not render ncMo the anti-inflammatory counterpart of cMo, as they produce high levels of inflammatory cytokines in a TLR7-mediated response to viruses and nucleic acids (18, 80, 90). NcMo were shown to initiate recruitment and activation of other innate immune cells, such as NK cells and neutrophils through TNF-α-induced upregulation of E-selectin on endothelial cells (89, 93). The main function of ncMo seems to be patrolling of the vascular endothelium and removal of cell debris via Fcγ-mediated phagocytosis (79, 80, 89). Their patrolling behaviour rests on a crawling mechanism slower than the rolling adhesion preceding classical monocyte extravasation and is dependent on LFA-1/ICAM interaction (75, 80, 89). NcMo showed high expression of genes associated with adhesion and cytoskeleton arrangement, which may serve to facilitate motility for patrolling (91, 94). As reported by Chimen et al., pooled ncMo and intMo transmigrate through unstimulated endothelial cell monolayers faster *in vitro*, although fewer ncMo/intMo adhere compared to cMo (93). Moreover, the former did not re-enter the blood stream, whereas cMo did, in line with findings on the regress of Ly6C^{high} cMo but not Ly6C^{low} ncMo to the bone marrow in mice (91, 95). Apparently, ncMo are either not equipped to respond to signals for reverse transmigration or more firmly retained in the subendothelial space (93). NcMo are also believed to play a role in the resolution of inflammation, as they were shown to differentiate into wound-healing MΦ (83) and have increased expression of miR-150 and miR-21, although substantial and tissue-specific evidence is still missing (80, 83, 90). It has been reported that CD16-positive monocytes have higher antigen presentation capacity (96) as well as decreased lipid accumulation and migration towards complement component C5a (97), but a sufficient delimitation between ncMo and intMo is still outstanding. Whether ncMo produce ROS is still unclear, as studies have shown both high levels of ROS production at baseline (11) as well as low ROS levels in response to immunoglobulin (Ig) G-opsonised bovine serum albumin (BSA) (18). Altogether, ncMo patrol the vasculature at steady state and contribute to the maintenance of vascular integrity.

Compared to ncMo and cMo, little is known about the functions of intMo in both homeostasis and inflammation, partly due to the low and variable numbers of this subset in circulation. Moreover, due their low abundance, intMo were often examined after pooling with ncMo, complicating the interpretation of findings. The question whether intMo merely represent an intermediate step in the conversion of cMo to ncMo or a separate population exerting a distinct functional role is legitimate. However, several studies do report an increase of intMo in the context of chronic inflammatory diseases such as CVD. For example, the Prospective Halle Monocyte Study (PHAMOS) showed a shift from cMo to intMo in patients with CAD (98). IntMo express high levels of major histocompatibility complex (MHC) II and have high antigen presentation capacity (79, 99). Like cMo, they show phagocytic activity and basal production of ROS (75, 94). IntMo were found to produce both pro- and anti-inflammatory cytokines upon TLR stimulation (79). Cros et al. report highest secretion of TNF-α and IL-1β by intMo compared to cMo and cMo. Moreover, they found intMo to secrete IL-8, although at lower levels than cMo (18). In contrast, Wong et al. report ncMo to secrete the highest levels of TNF-α and IL-1β and similar levels of IL-8 secreted by all subsets (99). Thorough functional mapping of intMo and its differentiation kinetics is needed to clarify their role in homeostasis and disease, and more specifically, to address whether the observed association with disease reflects adverse functions or is a bystander effect of a failure to mature into ncMo.

In conclusion, ncMo and cMo exert specialised functions in the innate host defence to pathogens and injury, with prominent viral response and injury monitoring activity for the former and pro-inflammatory activity for the latter. Although the functions exerted by intMo are less clear, they seem to be associated with inflammatory diseases. The sequential development of monocyte subsets seems to follow the course of inflammation and its resolution. Additional studies, in particular functional assays are needed to complement already existing knowledge from transcriptional studies. Generally, further research considering monocyte heterogeneity beyond the conventional nomenclature is needed to understand the role of monocyte subpopulations in homeostasis and inflammation.

Role of monocytes as MΦ precursors in health and disease

The foundation for our current model of the mononuclear phagocyte system was laid by a concept proposed by van Furth et al. in 1972, postulating that monocytes arising from (bone marrow) myeloid precursors extravasate to differentiate into MΦ and repopulate the tissue-resident MΦ pool (7). However, over the last years, lineage tracing studies in mice have revealed that tissue-resident MΦ originate from the yolk sac and foetal liver and have self-renewal capacity, ensuring homeostatic MΦ levels in the tissue (100). The tissue-resident MΦ pools in the skin (Langerhans cells) and brain (microglia) are maintained by self-renewal throughout life without contribution of bone marrow-derived monocytes (101-103). Yet, the MΦ pools in heart (104, 105), dermis (106) and gut (107-109) were shown to contain both embryo- and bone marrow-derived MΦ in steady state, with a ratio that gradually shifts

towards the latter during life. Although it was long unclear whether this also held for humans, Bajpai et al. were able to unravel the contribution of bone marrow-derived monocytes to the tissue MΦ pool in the human heart with gender mismatched heart transplantation (110). Their data revealed that, similar to mice, maintenance of the heart-resident MΦ pool partly relies on the self-renewal capacity of donor heart MΦ and partly on the influx of recipient bone marrow-derived MΦ. Moreover, Bigley et al. showed that in subjects with autosomal dominant and sporadic monocytopenia, Langerhans cells and skin-resident MΦ levels were unaffected and preserved (111). This suggests that not only in mice but also in human, tissue-resident MΦ pools are gradually replaced by monocyte influx in some organs like heart, but not all. Which of the monocyte subsets is responsible for replenishment of the cardiac and vascular MΦ pool at steady state is an outstanding question. Under pathogen-induced or sterile inflammatory conditions, the pool of tissue-resident MΦ will be partly depleted during a first-response wave, and tissue compartments will open for monocytes to enter which re-populate the tissue and assist in defence and repair (112). After MI, circulating monocytes are recruited to the heart via CCL2 where they differentiate into MΦ [reviewed in (70)]. In atherosclerosis-susceptible apolipoprotein E-deficient mice, combined inhibition of CCR2, CCR5 and CXC3R1 led to an almost complete absence of lesions and was found to be more effective in reducing atherosclerosis than individual inhibition of these chemokine receptors (113). Considering their differential expression on monocyte subsets, with higher CX3CR1 expression levels on ncMo in both mice and humans (114), these findings indicate different pathways of infiltration and subsequent MΦ accumulation (113). Indeed, in human atherosclerosis, more cMo were found to enter lesions than ncMo, although ncMo were shown to bind and become loaded with oxidised low-density lipoprotein (LDL) (115), suggesting differential roles of the monocyte subsets in atherosclerosis [reviewed in (116)].

Recently, the MΦ niche concept has been coined [reviewed in (117)], in which the niche ensures maintenance of the tissue-resident MΦ pool by the production of trophic factors that induce proliferation of tissue MΦ. MΦ consume these factors and self-regulate the proliferation rate in this tissue niche. MΦ death will result in increased availability of trophic factors, thereby inducing MΦ proliferation. In parallel, MΦ death, especially in secondary necrosis or necroptosis, will induce chemokine release, leading to the recruitment of circulatory monocytes. In health, the former route will prevail (proliferation being faster than recruitment), but in disease the latter pathway may dominate, (temporarily) tipping the balance in tissue towards monocyte-derived MΦ.

CMo exit the circulation at steady state and differentiate into MΦ in tissues that require monocyte influx to replace tissue-resident MΦ and fill available niches, as discussed above. CMo that are not recruited and remain in circulation develop into ncMo, following a sequential ontogeny scenario (84, 89, 118). Transcriptome profiling of cMo and ncMo revealed several differentially expressed genes that hint towards subset-specific functions (119). CMo were

found to express more CD11b (integrin α-M), CCR2 and TLR4 (CD284), suggesting an important role in bacterial infection and inflammation. Lack of CCR2 which prevents cMo stromal egress leads to a reduction of the tissue MΦ pool in the intestine and dermis compartments, known to be replenished by monocytes in steady state (100, 107, 120, 121), suggesting that cMo are the main source contributing to the tissue MΦ pool. In the same study, ncMo were seen to express low levels of CD11b and CCR2, but high levels of CX3CR1, LFA-1 (CD11a), HLA-DR and genes necessary for cytoskeletal dynamics (119). This confirms earlier work by Geissmann et al. (73) and others showing that ncMo patrol the vessels to maintain vessel integrity and can be viewed as luminal end stage differentiated "MΦ" (91, 122, 123). Whether or not ncMo are able to differentiate into full-fledged tissue MΦ remains subject to debate. However, blocking LFA-1 or ICAM-1 resulted in a reduced patrolling phenotype and concomitantly increased circulatory ncMo numbers (124), suggesting that the ncMo pool may partly reside in the sub-endothelium. Moreover, as shown by Schyns et al., a subset of lung interstitial MΦ was derived from intravascular ncMo in steady state (125), collectively suggesting that also ncMo are able to populate tissue during steady state, although in this setting they appear to be vessel-confined as well.

Impact of monocyte subset origin on MΦ phenotype or function

MΦ display immense phenotypic diversity (37, 126) with subsets displaying specialised organ- and condition-specific functions (127, 128) and were previously described to differentially affect CVD (129, 130). As discussed earlier, this heterogeneity results from the plastic adaptation to their microenvironment, but also to differences in origin (embryonic versus monocyte-derived). Hence, the functional specialisation of the MΦ pool in heart and arteries is likely to be impacted by monocyte heterogeneity (and age/disease-dependent shifts therein) (131). This legitimates the question whether cardiac and arterial MΦ partly retain the functional phenotype of the monocyte they were derived from (89).
Colony-stimulating factors (CSF) such as macrophage (M-) CSF and granulocyte-macrophage (GM-) CSF which control monocyte survival and differentiation may act differentially on cMo, intMo, and ncMo. GM-CSF receptor CD116 (CSF2R) was found to be expressed on all monocyte subsets, with highest expression in cMo (132). In contrast, expression of M-CSF receptor CD115 (CSF1R) was high on ncMo (133), and blocking M-CSF receptor signalling reduced ncMo but not cMo numbers (134).

In vivo support for monocyte subset-specific MΦ differentiation was provided by Menezes et al., showing that MHCII^{-} Ly6C^{high} cMo differentiate into iNOS-positive MΦ upon microbial challenge, a process regulated by the myeloid lineage commitment factor PU.1 (128). As Olingy et al. demonstrated, Ly6C^{low} ncMo preferentially develop into CD206 (MRC1)-positive wound-healing MΦ in peri-implant tissue as compared to Ly6C^{high} cMo (83). These observations underpin the notion that ncMo are primarily involved in tissue repair and suggest that the phenotype of monocyte-derived MΦ mirrors their precursors' phenotype to some extent. Both

studies support the concept that MΦ phenotypes are determined by their monocyte progenitor (37).

These murine finding however do not necessarily translate directly to human monocyte-to-MΦ differentiation, where the picture is less clear. Goudot et al.'s study showed that only CD14-positive cMo are capable of differentiating into bona fide MΦ, while CD16-positive monocytes had low survival in culture and did not contribute greatly (127). While committed to differentiate into MΦ, cMo need additional cues for dendritic cell (DC) differentiation, a process controlled by the aryl hydrocarbon receptor (AHR) (127). However, other groups have succeeded in differentiating MΦ from CD16-positive intMo and ncMo (12, 135). For instance, Frankenberger et al. reported both CD16-negative cMo and CD16-positive intMo/ncMo to develop into MΦ after differentiation with M-CSF. Interestingly, cMo-derived MΦ (cMo-MΦ) showed higher expression of CD14, CD163 (M130, SCARI1), and versican (VCAN) compared to MΦ from CD16-positive monocytes, a difference already present at the monocyte stage (135). Moreover, M-CSF-matured MΦ derived from CD16-positive monocytes showed higher phagocytic activity, similar to their precursor. Again, ncMo and intMo were pooled to CD16-positive monocytes, so intMo may be accountable for the observed effects. In contrast, Boyette et al. report an inherent commitment of ncMo to become MΦ even in the absence of growth factors, as they displayed signs of MΦ differentiation already after 2 days in culture. In fact, all monocyte subsets developed into MΦ and secreted increasing amounts of MΦ-associated cytokines with progressing differentiation and increasing phagocytic activity along the way (12). The highest phagocytic activity was observed in cMo-MΦ in comparison to intMo-MΦ and ncMo-MΦ (12). This seems opposite to the findings of Frankenberger et al., although it should be noted that the platforms (antibody-opsonised Escherichia coli bacteria versus polystyrene beads) and consequently scavenger receptors and mechanism involved were different. Collectively, findings on subset-dependent functional differences of monocyte-derived MΦ are conflicting, and a clear consensus is lacking. The general notion is that MΦ phenotype reflects the phenotypic characteristics of the precursor population at least to some extent, and suggest that the response of monocyte-derived MΦ to environmental stimuli may indeed be influenced by their origin. This may be especially relevant in the context of inflammation, in which monocyte-derived MΦ may respond differently to inflammatory signals than tissue-resident MΦ (131).

Conclusions and perspectives

Monocytes are a heterogeneous population that allows classification into subgroups based on characteristics like size, marker expression, or function, although the current terminology distinguishing three monocyte subsets is based on CD14 and CD16 expression. The main functions of cMo are phagocytosis and production of ROS in response to bacterial stimuli, and maturation into ncMo in the absence of inflammation. The ncMo subset responds to viral challenge with the secretion of pro-inflammatory cytokines and patrols the vasculature at steady state. The intMo subset seems to be associated strongest with CVD, as intMo were found to be predictive of CVD and secondary cardiovascular events and increase in acute HF.

Due to the low abundance of intMo and ncMo compared to cMo, they have commonly been studied as a pool of CD16-positive monocytes. This complicates the interpretation of the results and does not allow to assign specific functions to these two subsets. Especially the functional phenotype of intMo lacks a distinct characterisation to define its role in inflammation and steady state. Thus, more studies focusing on functional differences between intMo and ncMo are needed. The capacity of human monocytes of different subsets to extravasate and their fate after they have left the circulation are still unknown. Although all monocyte subsets have been shown to be able to differentiate into MΦ *in vitro*, it is not clear if and to what extent subsets contribute to the tissue-resident MΦ pool in the heart and vasculature. Considering the patrolling behaviour of ncMo, it is still an open question whether ncMo can be considered circulating MΦ with specialised sensing functions as such, bypassing their differentiation to bona fide tissue MΦ. In general, it is not clear to what extent MΦ function is influenced by environmental factors of the niche they have been recruited to or the retention of at least part of the functional phenotype of their precursor monocyte. Thus, differences between the phenotype of monocyte-derived and tissue-resident MΦ might be preserved.

The classification of monocytes into subgroups has become more sophisticated thanks to emerging technologies like high-parameter cytometry and scRNA-Seq, and transcends a taxonomy defined by merely two surface markers. Future studies, especially employing novel methods such as multiplex staining and multi-omics approaches that combine transcriptomics and surface marker information, will further expand our understanding of monocyte heterogeneity (136, 137). The reappraisal of monocyte heterogeneity demonstrates the importance of unequivocal subset definition and demands an updated terminology to account for the heterogeneity of the monocyte population. Moreover, subset-specific intervention studies are needed to assess functional diversity of monocyte subsets and monocyte subset-derived MΦ to dissect their individual role in CVD.

Authors contributions

A.V.R. and S.M.W.W. wrote and revised the manuscript. L.T., E.A.L.B., and P.G. revised the manuscript.

Funding

This work was supported by the Dutch Heart Foundation (Dekker 2020T042 to P.G.), the European Research Area Network Joint Transnational Call for Cardiovascular Disease (ERA-CVD; JTC2017 AtheroMacHete to E.A.L.B. and P.G.), the Netherlands Organisation for Scientific Research (NWO)/ São Paulo Research Foundation (FAPESP; DNAMoving to E.A.L.B. and S. M.W.W.), and NWO-STW (#13568 Barcoding the Obese to E.A.L.B.).

Conflict of interest

The authors declare the absence of any commercial or financial relationships that could be construed as a potential conflict of interest.

References

1. Oh ES, Na M, Rogers CJ. The Association Between Monocyte Subsets and Cardiometabolic Disorders/Cardiovascular Disease: A Systematic Review and Meta-Analysis. Front Cardiovasc Med. 2021;8:640124.
2. DeBerge M, Shah SJ, Wilsbacher L, Thorp EB. Macrophages in Heart Failure with Reduced versus Preserved Ejection Fraction. Trends Mol Med. 2019;25(4):328-40.
3. Watanabe S, Alexander M, Misharin AV, Budinger GRS. The role of macrophages in the resolution of inflammation. J Clin Invest. 2019;129(7):2619-28.
4. Epelman S, Lavine KJ, Randolph GJ. Origin and functions of tissue macrophages. Immunity. 2014;41(1):21-35.
5. Gosselin D, Link VM, Romanoski CE, Fonseca GJ, Eichenfield DZ, Spann NJ, et al. Environment drives selection and function of enhancers controlling tissue-specific macrophage identities. Cell. 2014;159(6):1327-40.
6. Lavin Y, Winter D, Blecher-Gonen R, David E, Keren-Shaul H, Merad M, et al. Tissue-resident macrophage enhancer landscapes are shaped by the local microenvironment. Cell. 2014;159(6):1312-26.
7. van Furth R, Cohn ZA, Hirsch JG, Humphrey JH, Spector WG, Langevoort HL. The mononuclear phagocyte system: a new classification of macrophages, monocytes, and their precursor cells. Bull World Health Organ. 1972;46(6):845-52.
8. Ziegler-Heitbrock L, Ancuta P, Crowe S, Dalod M, Grau V, Hart DN, et al. Nomenclature of monocytes and dendritic cells in blood. Blood. 2010;116(16):e74-e80.
9. Cormican S, Griffin MD. Human Monocyte Subset Distinctions and Function: Insights From Gene Expression Analysis. Front Immunol. 2020;11:1070.
10. Loke P, Niewold TB. By CyTOF: Heterogeneity of Human Monocytes. Arterioscler Thromb Vasc Biol. 2017;37(8):1423-4.
11. Ong S-M, Teng K, Newell E, Chen H, Chen J, Loy T, et al. A Novel, Five-Marker Alternative to CD16–CD14 Gating to Identify the Three Human Monocyte Subsets. Front Immunol. 2019;10:1761.
12. Boyette LB, Macedo C, Hadi K, Elinoff BD, Walters JT, Ramaswami B, et al. Phenotype, function, and differentiation potential of human monocyte subsets. PLoS One. 2017;12(4):e0176460.
13. Arenson EB Jr, Epstein MB, Seeger RC. Volumetric and functional heterogeneity of human monocytes. J Clin Invest. 1980;65(3):613-8.
14. Norris DA, Morris RM, Sanderson RJ, Kohler PF. Isolation of Functional Subsets of Human Peripheral Blood Monocytes. J Immunology. 1979;123(1):166-72.
15. Devitt A, Moffatt OD, Raykundalia C, Capra JD, Simmons DL, Gregory CD. Human CD14 mediates recognition and phagocytosis of apoptotic cells. Nature. 1998;392(6675):505-9.
16. Kruger M, Coorevits L, De Wit TP, Casteels-Van Daele M, Van De Winkel JG, Ceuppens JL. Granulocyte-macrophage colony-stimulating factor antagonizes the transforming growth factor-beta-induced expression of Fc gamma RIII (CD16) on human monocytes. Immunology. 1996;87(1):162-7.
17. Passlick B, Flieger D, Ziegler-Heitbrock L. Identification and Characterization of a Novel Monocyte Subpopulation in Human Peripheral Blood. Blood. 1989;74(7):2527-34.
18. Cros J, Cagnard N, Woollard K, Patey N, Zhang SY, Senechal B, et al. Human CD14dim monocytes patrol and sense nucleic acids and viruses via TLR7 and TLR8 receptors. Immunity. 2010;33(3):375-86.
19. Ingersoll MA, Spanbroek R, Lottaz C, Gautier EL, Frankenberger M, Hoffmann R, et al. Comparison of gene expression profiles between human and mouse monocyte subsets. Blood. 2010;115(3):e10-9.
20. Elderman M, van Beek A, Brandsma E, de Haan B, Savelkoul H, de Vos P, et al. Sex impacts Th1 cells, Tregs, and DCs in both intestinal and systemic immunity in a mouse strain and location-dependent manner. Biol Sex Differ. 2016;7(1):21.
21. Petkova SB, Yuan R, Tsaih S-W, Schott W, Roopenian DC, Paigen B. Genetic influence on immune phenotype revealed strain-specific variations in peripheral blood lineages. Physiol Genomics. 2008;34(3):304-14.
22. Hofer TP, Zawada AM, Frankenberger M, Skokann K, Satzl AA, Gesierich W, et al. slan-defined subsets of CD16-positive monocytes: impact of granulomatous inflammation and M-CSF receptor mutation. Blood. 2015;126(24):2601-10.
23. Abeles D, McPhail MJ, Sowter D, Antoniades CG, Vergis N, Vijay GKM, et al. CD14, CD16 and HLA-DR reliably identifies human monocytes and their subsets in the context of pathologically reduced HLA-DR expression by CD14hi/CD16neg monocytes: Expansion of CD14hi/CD16pos and contraction of CD14lo/CD16pos monocytes in acute liver failure. Cytometry Part A. 2012;81A(10):823-34.

24. Autissier P, Soulas C, Burdo TH, Williams KC. Evaluation of a 12-color flow cytometry panel to study lymphocyte, monocyte, and dendritic cell subsets in humans. Cytometry Part A. 2010;77A(5):410-9.
25. Roussel M, Ferrell PB Jr, Greenplate AR, Lhomme F, Le Gallou S, Diggins KE, et al. Mass cytometry deep phenotyping of human mononuclear phagocytes and myeloid-derived suppressor cells from human blood and bone marrow. J Leukoc Biol. 2017;102(2):437-47.
26. Hofer TP, van de Loosdrecht AA, Stahl-Hennig C, Cassatella MA, Ziegler-Heitbrock L. 6-Sulfo LacNAc (Slan) as a Marker for Non-classical Monocytes. Front Immunol. 2019;10:2052.
27. van Leeuwen-Kerkhoff N, Lundberg K, Westers TM, Kordasti S, Bontkes HJ, de Gruijl TD, et al. Transcriptional profiling reveals functional dichotomy between human slan+ non-classical monocytes and myeloid dendritic cells. J Leukoc Biol. 2017;102(4):1055-68.
28. Ahmad F, Döbel T, Schmitz M, Schäkel K. Current Concepts on 6-sulfo LacNAc Expressing Monocytes (slanMo). Front Immunol. 2019;10:948.
29. Hamers AAJ, Dinh HQ, Thomas GD, Marcovecchio P, Blatchley A, Nakao CS, et al. Human Monocyte Heterogeneity as Revealed by High-Dimensional Mass Cytometry. Arterioscler Thromb Vasc Biol. 2019;39(1):25-36.
30. Villani A-C, Satija R, Reynolds G, Sarkizova S, Shekhar K, Fletcher J, et al. Single-cell RNA-seq reveals new types of human blood dendritic cells, monocytes, and progenitors. Science. 2017;356(6335):eaah4573.
31. Mildner A, Schönheit J, Giladi A, David E, Lara-Astiaso D, Lorenzo-Vivas E, et al. Genomic Characterization of Murine Monocytes Reveals C/EBPβ Transcription Factor Dependence of Ly6C− Cells. Immunity. 2017;46(5):849-62.e7.
32. Thomas GD, Hamers AAJ, Nakao C, Marcovecchio P, Taylor AM, McSkimming C, et al. Human Blood Monocyte Subsets: A New Gating Strategy Defined Using Cell Surface Markers Identified by Mass Cytometry. Arterioscler Thromb Vasc Biol. 2017;37(8):1548-58.
33. Merah-Mourah F, Cohen SO, Charron D, Mooney N, Haziot A. Identification of Novel Human Monocyte Subsets and Evidence for Phenotypic Groups Defined by Interindividual Variations of Expression of Adhesion Molecules. Sci Rep. 2020;10(1):4397.
34. Dutertre C-A, Becht E, Irac SE, Khalilnezhad A, Narang V, Khalilnezhad S, et al. Single-Cell Analysis of Human Mononuclear Phagocytes Reveals Subset-Defining Markers and Identifies Circulating Inflammatory Dendritic Cells. Immunity. 2019;51(3):573-89.e8.
35. Hao Y, Hao S, Andersen-Nissen E, Mauck WM, Zheng S, Butler A, et al. Integrated analysis of multimodal single-cell data. Cell. 2021;184(13):3573-87.e29.
36. Weber C, Shantsila E, Hristov M, Caligiuri G, Guzik T, Heine GH, et al. Role and analysis of monocyte subsets in cardiovascular disease. Joint consensus document of the European Society of Cardiology (ESC) Working Groups "Atherosclerosis & Vascular Biology" and "Thrombosis". Thromb Haemost. 2016;116(4):626-37.
37. Bassler K, Schulte-Schrepping J, Warnat-Herresthal S, Aschenbrenner AC, Schultze JL. The Myeloid Cell Compartment—Cell by Cell. Annu Rev Immunol. 2019;37(1):269-93.
38. Choi SH, Kim JH, Lim S, Lim JY, Kim KW, Park KS, et al. Monocyte count as a predictor of cardiovascular mortality in older Korean people. Age Ageing. 2017;46(3):433-8.
39. Kim J-H, Lee Y-J, Park B. Higher monocyte count with normal white blood cell count is positively associated with 10-year cardiovascular disease risk determined by Framingham risk score among community-dwelling Korean individuals. Medicine (Baltimore). 2019;98(17):e15340.
40. Waterhouse DF, Cahill RA, Sheehan F, McCreery C. Prediction of calculated future cardiovascular disease by monocyte count in an asymptomatic population. Vasc Health Risk Manag. 2008;4(1):177-87.
41. Rogacev KS, Cremers B, Zawada AM, Seiler S, Binder N, Ege P, et al. CD14++CD16+ monocytes independently predict cardiovascular events: a cohort study of 951 patients referred for elective coronary angiography. J Am Coll Cardiol. 2012;60(16):1512-20.
42. Berg KE, Ljungcrantz I, Andersson L, Bryngelsson C, Hedblad B, Fredrikson GN, et al. Elevated CD14++CD16- monocytes predict cardiovascular events. Circ Cardiovasc Genet. 2012;5(1):122-31.
43. Wildgruber M, Aschenbrenner T, Wendorff H, Czubba M, Glinzer A, Haller B, et al. The "Intermediate" CD14(++)CD16(+) monocyte subset increases in severe peripheral artery disease in humans. Sci Rep. 2016;6:39483.
44. Cappellari R, D'Anna M, Bonora BM, Rigato M, Cignarella A, Avogaro A, et al. Shift of monocyte subsets along their continuum predicts cardiovascular outcomes. Atherosclerosis. 2017;266:95-102.
45. Nordestgaard BG, Chapman MJ, Ray K, Boren J, Andreotti F, Watts GF, et al. Lipoprotein(a) as a cardiovascular risk factor: current status. Eur Heart J. 2010;31(23):2844-53.

46. Krychtiuk KA, Kastl SP, Hofbauer SL, Wonnerth A, Goliasch G, Ozsvar-Kozma M, et al. Monocyte subset distribution in patients with stable atherosclerosis and elevated levels of lipoprotein(a). J Clin Lipidol. 2015;9(4):533-41.
47. Vaiserman A, Krasnienkov D. Telomere Length as a Marker of Biological Age: State-of-the-Art, Open Issues, and Future Perspectives. Front Genet. 2021;11:630186.
48. Merino A, Buendia P, Martin-Malo A, Aljama P, Ramirez R, Carracedo J. Senescent CD14+CD16+ monocytes exhibit proinflammatory and proatherosclerotic activity. J Immunol. 2011;186(3):1809-15.
49. Meeuwsen JAL, de Vries JJ, van Duijvenvoorde A, van der Velden S, van der Laan SW, van Koeverden ID, et al. Circulating CD14(+)CD16(-) classical monocytes do not associate with a vulnerable plaque phenotype, and do not predict secondary events in severe atherosclerotic patients. J Mol Cell Cardiol. 2019;127:260-9.
50. Lo SC, Lee WJ, Chen CY, Lee BC. Intermediate CD14(++)CD16(+) monocyte predicts severe coronary stenosis and extensive plaque involvement in asymptomatic individuals. Int J Cardiovasc Imaging. 2017;33(8):1223-36.
51. Yoshida N, Yamamoto H, Shinke T, Otake H, Kuroda M, Terashita D, et al. Impact of CD14(++)CD16(+) monocytes on plaque vulnerability in diabetic and non-diabetic patients with asymptomatic coronary artery disease: a cross-sectional study. Cardiovasc Diabetol. 2017;16(1):96.
52. Yamamoto H, Yoshida N, Shinke T, Otake H, Kuroda M, Sakaguchi K, et al. Impact of CD14(++)CD16(+) monocytes on coronary plaque vulnerability assessed by optical coherence tomography in coronary artery disease patients. Atherosclerosis. 2018;269:245-51.
53. Frantz S, Nahrendorf M. Cardiac macrophages and their role in ischaemic heart disease. Cardiovasc Res. 2014;102(2):240-8.
54. Tsujioka H, Imanishi T, Ikejima H, Kuroi A, Takarada S, Tanimoto T, et al. Impact of heterogeneity of human peripheral blood monocyte subsets on myocardial salvage in patients with primary acute myocardial infarction. J Am Coll Cardiol. 2009;54(2):130-8.
55. Tapp LD, Shantsila E, Wrigley BJ, Pamukcu B, Lip GY. The CD14++CD16+ monocyte subset and monocyte-platelet interactions in patients with ST-elevation myocardial infarction. J Thromb Haemost. 2012;10(7):1231-41.
56. van der Laan AM, Ter Horst EN, Delewi R, Begieneman MP, Krijnen PA, Hirsch A, et al. Monocyte subset accumulation in the human heart following acute myocardial infarction and the role of the spleen as monocyte reservoir. Eur Heart J. 2014;35(6):376-85.
57. Zhou X, Liu XL, Ji WJ, Liu JX, Guo ZZ, Ren D, et al. The Kinetics of Circulating Monocyte Subsets and Monocyte-Platelet Aggregates in the Acute Phase of ST-Elevation Myocardial Infarction: Associations with 2-Year Cardiovascular Events. Medicine (Baltimore). 2016;95(18):e3466.
58. Zeng S, Yan LF, Luo YW, Liu XL, Liu JX, Guo ZZ, et al. Trajectories of Circulating Monocyte Subsets After ST-Elevation Myocardial Infarction During Hospitalization: Latent Class Growth Modeling for High-Risk Patient Identification. J Cardiovasc Transl Res. 2018;11(1):22-32.
59. Dutta P, Courties G, Wei Y, Leuschner F, Gorbatov R, Robbins CS, et al. Myocardial infarction accelerates atherosclerosis. Nature. 2012;487(7407):325-9.
60. Cahill TJ, Kharbanda RK. Heart failure after myocardial infarction in the era of primary percutaneous coronary intervention: Mechanisms, incidence and identification of patients at risk. World J Cardiol. 2017;9(5):407-15.
61. Barisione C, Garibaldi S, Ghigliotti G, Fabbi P, Altieri P, Casale MC, et al. CD14CD16 monocyte subset levels in heart failure patients. Dis Markers. 2010;28(2):115-24.
62. Shantsila E, Ghattas A, Griffiths HR, Lip GYH. Mon2 predicts poor outcome in ST-elevation myocardial infarction. J Intern Med. 2019;285(3):301-16.
63. Wrigley BJ, Shantsila E, Tapp LD, Lip GYH. Increased expression of cell adhesion molecule receptors on monocyte subsets in ischaemic heart failure. Thromb Haemost. 2013;110(1):92-100.
64. Wrigley BJ, Shantsila E, Tapp LD, Lip GYH. CD14++CD16+ monocytes in patients with acute ischaemic heart failure. Eur J Clin Invest. 2013;43(2):121-30.
65. Elchinova E, Teubel I, Roura S, Fernandez MA, Lupon J, Galvez-Monton C, et al. Circulating monocyte subsets and heart failure prognosis. PLoS One. 2018;13(9):e0204074.
66. Amir O, Spivak I, Lavi I, Rahat MA. Changes in the monocytic subsets CD14(dim)CD16(+) and CD14(++)CD16(-) in chronic systolic heart failure patients. Mediators Inflamm. 2012;2012:616384.
67. Eiras S, Varela-Roman A, Andrade MC, Castro A, Gonzalez-Ferreiro R, Vinuela JE, et al. Non classical Monocytes Levels, Increased by Subcutaneous Fat-Secretome, Are Associated with Less Rehospitalization after Heart Failure Admission. J Cardiovasc Transl Res. 2017;10(1):16-26.

68. Hanna RN, Carlin LM, Hubbeling HG, Nackiewicz D, Green AM, Punt JA, et al. The transcription factor NR4A1 (Nur77) controls bone marrow differentiation and the survival of Ly6C- monocytes. Nat Immunol. 2011;12(8):778-85.
69. Thomas GD, Hanna RN, Vasudevan NT, Hamers AA, Romanoski CE, McArdle S, et al. Deleting an Nr4a1 Super-Enhancer Subdomain Ablates Ly6Clow Monocytes while Preserving Macrophage Gene Function. Immunity. 2016;45(5):975-87.
70. Ma Y, Mouton AJ, Lindsey ML. Cardiac macrophage biology in the steady-state heart, the aging heart, and following myocardial infarction. Transl Res. 2018;191:15-28.
71. Jakubzick CV, Randolph GJ, Henson PM. Monocyte differentiation and antigen-presenting functions. Nat Rev Immunol. 2017;17(6):349-62.
72. Wacleche VS, Tremblay CL, Routy J-P, Ancuta P. The Biology of Monocytes and Dendritic Cells: Contribution to HIV Pathogenesis. Viruses. 2018;10(2):65.
73. Geissmann F, Manz MG, Jung S, Sieweke MH, Merad M, Ley K. Development of monocytes, macrophages, and dendritic cells. Science. 2010;327(5966):656-61.
74. Ginhoux F, Jung S. Monocytes and macrophages: developmental pathways and tissue homeostasis. Nat Rev Immunol. 2014;14(6):392-404.
75. Sampath P, Moideen K, Ranganathan UD, Bethunaickan R. Monocyte Subsets: Phenotypes and Function in Tuberculosis Infection. Front Immunol. 2018;9:1726.
76. Wong KL, Yeap WH, Tai JJY, Ong SM, Dang TM, Wong SC. The three human monocyte subsets: implications for health and disease. Immunol Res. 2012;53(1-3):41-57.
77. van de Veerdonk FL, Netea MG. Diversity: A Hallmark of Monocyte Society. Immunity. 2010;33(3):289-91.
78. França CN, Izar MCO, Hortêncio MNS, do Amaral JB, Ferreira CES, Tuleta ID, et al. Monocyte subtypes and the CCR2 chemokine receptor in cardiovascular disease. Clin Sci. 2017;131(12):1215-24.
79. Kapellos TS, Bonaguro L, Gemünd I, Reusch N, Saglam A, Hinkley ER, et al. Human Monocyte Subsets and Phenotypes in Major Chronic Inflammatory Diseases. Front Immunol. 2019;10:2035.
80. Thomas G, Tacke R, Hedrick CC, Hanna RN. Nonclassical Patrolling Monocyte Function in the Vasculature. Arterioscler Thromb Vasc Biol. 2015;35(6):1306-16.
81. Sprangers S, de Vries TJ, Everts V. Monocyte Heterogeneity: Consequences for Monocyte-Derived Immune Cells. J Immunol Res. 2016;2016:1475435.
82. Carlin LM, Stamatiades EG, Auffray C, Hanna RN, Glover L, Vizcay-Barrena G, et al. Nr4a1-Dependent Ly6Clow Monocytes Monitor Endothelial Cells and Orchestrate Their Disposal. Cell. 2013;153(2):362-75.
83. Olingy CE, San Emeterio CL, Ogle ME, Krieger JR, Bruce AC, Pfau DD, et al. Non-classical monocytes are biased progenitors of wound healing macrophages during soft tissue injury. Sci Rep. 2017;7(1):447.
84. Patel AA, Zhang Y, Fullerton JN, Boelen L, Rongvaux A, Maini AA, et al. The fate and lifespan of human monocyte subsets in steady state and systemic inflammation. J Exp Med. 2017;214(7):1913-23.
85. Rongvaux A, Willinger T, Martinek J, Strowig T, Gearty SV, Teichmann LL, et al. Development and function of human innate immune cells in a humanized mouse model. Nat Biotechnol. 2014;32(4):364-72.
86. Thaler B, Hohensinner PJ, Krychtiuk KA, Matzneller P, Koller L, Brekalo M, et al. Differential in vivo activation of monocyte subsets during low-grade inflammation through experimental endotoxemia in humans. Sci Rep. 2016;6(1):30162.
87. Mildner A, Marinkovic G, Jung S, Gordon S. Murine Monocytes: Origins, Subsets, Fates, and Functions. Microbiol Spectr. 2016;4(5).
88. Chong SZ, Evrard M, Devi S, Chen J, Lim JY, See P, et al. CXCR4 identifies transitional bone marrow premonocytes that replenish the mature monocyte pool for peripheral responses. J Exp Med. 2016;213(11):2293-314.
89. Guilliams M, Mildner A, Yona S. Developmental and Functional Heterogeneity of Monocytes. Immunity. 2018;49(4):595-613.
90. Duroux-Richard I, Robin M, Peillex C, Apparailly F. MicroRNAs: Fine Tuners of Monocyte Heterogeneity. Front Immunol. 2019;10:2145.
91. Yona S, Kim K-W, Wolf Y, Mildner A, Varol D, Breker M, et al. Fate mapping reveals origins and dynamics of monocytes and tissue macrophages under homeostasis. Immunity. 2013;38(1):79-91.
92. Tak T, Drylewicz J, Conemans L, de Boer RJ, Koenderman L, Borghans JAM, et al. Circulatory and maturation kinetics of human monocyte subsets in vivo. Blood. 2017;130(12):1474-7.

93. Chimen M, Yates CM, McGettrick HM, Ward LSC, Harrison MJ, Apta B, et al. Monocyte Subsets Coregulate Inflammatory Responses by Integrated Signaling through TNF and IL-6 at the Endothelial Cell Interface. J Immunol. 2017;198(7):2834-43.
94. Zawada AM, Rogacev KS, Rotter B, Winter P, Marell R-R, Fliser D, et al. SuperSAGE evidence for CD14++CD16+ monocytes as a third monocyte subset. Blood. 2011;118(12):e50-e61.
95. Varol C, Landsman L, Fogg DK, Greenshtein L, Gildor B, Margalit R, et al. Monocytes give rise to mucosal, but not splenic, conventional dendritic cells. J Exp Med. 2007;204(1):171-80.
96. Ziegler-Heitbrock L. The CD14+ CD16+ blood monocytes: their role in infection and inflammation. J Leukoc Biol. 2007;81(3):584-92.
97. Jackson WD, Weinrich TW, Woollard KJ. Very-low and low-density lipoproteins induce neutral lipid accumulation and impair migration in monocyte subsets. Sci Rep. 2016;6(1):20038.
98. Höpfner F, Jacob M, Ulrich C, Russ M, Simm A, Silber RE, et al. Subgroups of monocytes predict cardiovascular events in patients with coronary heart disease. The PHAMOS trial (Prospective Halle Monocytes Study). Hellenic J Cardiol. 2019;60(5):311-21.
99. Wong KL, Tai JJ-Y, Wong W-C, Han H, Sem X, Yeap W-H, et al. Gene expression profiling reveals the defining features of the classical, intermediate, and nonclassical human monocyte subsets. Blood. 2011;118(5):e16-e31.
100. Ginhoux F, Guilliams M. Tissue-Resident Macrophage Ontogeny and Homeostasis. Immunity. 2016;44(3):439-49.
101. Ajami B, Bennett JL, Krieger C, Tetzlaff W, Rossi FMV. Local self-renewal can sustain CNS microglia maintenance and function throughout adult life. Nat Neurosci. 2007;10(12):1538-43.
102. Ginhoux F, Greter M, Leboeuf M, Nandi S, See P, Gokhan S, et al. Fate mapping analysis reveals that adult microglia derive from primitive macrophages. Science. 2010;330(6005):841-5.
103. Merad M, Manz MG, Karsunky H, Wagers A, Peters W, Charo I, et al. Langerhans cells renew in the skin throughout life under steady-state conditions. Nat Immunol. 2002;3(12):1135-41.
104. Epelman S, Lavine KJ, Beaudin AE, Sojka DK, Carrero JA, Calderon B, et al. Embryonic and adult-derived resident cardiac macrophages are maintained through distinct mechanisms at steady state and during inflammation. Immunity. 2014;40(1):91-104.
105. Molawi K, Wolf Y, Kandalla PK, Favret J, Hagemeyer N, Frenzel K, et al. Progressive replacement of embryo-derived cardiac macrophages with age. J Exp Med. 2014;211(11):2151-8.
106. Tamoutounour S, Guilliams M, Montanana Sanchis F, Liu H, Terhorst D, Malosse C, et al. Origins and functional specialization of macrophages and of conventional and monocyte-derived dendritic cells in mouse skin. Immunity. 2013;39(5):925-38.
107. Bain CC, Bravo-Blas A, Scott CL, Perdiguero EG, Geissmann F, Henri S, et al. Constant replenishment from circulating monocytes maintains the macrophage pool in the intestine of adult mice. Nat Immunol. 2014;15(10):929-37.
108. De Schepper S, Verheijden S, Aguilera-Lizarraga J, Viola MF, Boesmans W, Stakenborg N, et al. Self-Maintaining Gut Macrophages Are Essential for Intestinal Homeostasis. Cell. 2018;175(2):400-15.
109. Shaw TN, Houston SA, Wemyss K, Bridgeman HM, Barbera TA, Zangerle-Murray T, et al. Tissue-resident macrophages in the intestine are long lived and defined by Tim-4 and CD4 expression. J Exp Med. 2018;215(6):1507-18.
110. Bajpai G, Schneider C, Wong N, Bredemeyer A, Hulsmans M, Nahrendorf M, et al. The human heart contains distinct macrophage subsets with divergent origins and functions. Nat Med. 2018;24(8):1234-45.
111. Bigley V, Haniffa M, Doulatov S, Wang X-N, Dickinson R, McGovern N, et al. The human syndrome of dendritic cell, monocyte, B and NK lymphoid deficiency. J Exp Med. 2011;208(2):227-34.
112. Teh YC, Ding JL, Ng LG, Chong SZ. Capturing the Fantastic Voyage of Monocytes Through Time and Space. Front Immunol. 2019;10:834.
113. Combadière C, Potteaux S, Rodero M, Simon T, Pezard A, Esposito B, et al. Combined Inhibition of CCL2, CX3CR1, and CCR5 Abrogates Ly6Chi and Ly6Clo Monocytosis and Almost Abolishes Atherosclerosis in Hypercholesterolemic Mice. Circulation. 2008;117(13):1649-57.
114. Tacke F, Alvarez D, Kaplan TJ, Jakubzick C, Spanbroek R, Llodra J, et al. Monocyte subsets differentially employ CCR2, CCR5, and CX3CR1 to accumulate within atherosclerotic plaques. J Clin Invest. 2007;117(1):185-94.
115. Mosig S, Rennert K, Krause S, Kzhyshkowska J, Neunübel K, Heller R, et al. Different functions of monocyte subsets in familial hypercholesterolemia: potential function of CD14+CD16+ monocytes in detoxification of oxidized LDL. The FASEB Journal. 2009;23(3):866-74.

116. Gautier EL, Jakubzick C, Randolph GJ. Regulation of the Migration and Survival of Monocyte Subsets by Chemokine Receptors and Its Relevance to Atherosclerosis. Arterioscler Thromb Vasc Biol. 2009;29(10):1412-8.
117. Guilliams M, Thierry GR, Bonnardel J, Bajenoff M. Establishment and Maintenance of the Macrophage Niche. Immunity. 2020;52(3):434-51.
118. Poller WC, Nahrendorf M, Swirski FK. Hematopoiesis and Cardiovascular Disease. Circ Res. 2020;126(8):1061-85.
119. Anbazhagan K, Duroux-Richard I, Jorgensen C, Apparailly F. Transcriptomic network support distinct roles of classical and non-classical monocytes in human. Int Rev Immunol. 2014;33(6):470-89.
120. Platt AM, Bain CC, Bordon Y, Sester DP, Mowat AM. An independent subset of TLR expressing CCR2-dependent macrophages promotes colonic inflammation. J Immunol. 2010;184(12):6843-54.
121. Zigmond E, Varol C, Farache J, Elmaliah E, Satpathy AT, Friedlander G, et al. Ly6C hi monocytes in the inflamed colon give rise to proinflammatory effector cells and migratory antigen-presenting cells. Immunity. 2012;37(6):1076-90.
122. Auffray C, Sieweke MH, Geissmann F. Blood monocytes: development, heterogeneity, and relationship with dendritic cells. Annu Rev Immunol. 2009;27(1):669-92.
123. Williams JW, Randolph GJ, Zinselmeyer BH. A Polecat's View of Patrolling Monocytes. Circ Res. 2017;120(11):1699-701.
124. Buscher K, Marcovecchio P, Hedrick CC, Ley K. Patrolling Mechanics of Non-Classical Monocytes in Vascular Inflammation. Front Cardiovasc Med. 2017;4:80.
125. Schyns J, Bai Q, Ruscitti C, Radermecker C, De Schepper S, Chakarov S, et al. Non-classical tissue monocytes and two functionally distinct populations of interstitial macrophages populate the mouse lung. Nat Commun. 2019;10(1):3964.
126. Wynn TA, Chawla A, Pollard JW. Macrophage biology in development, homeostasis and disease. Nature. 2013;496(7446):445-55.
127. Goudot C, Coillard A, Villani AC, Gueguen P, Cros A, Sarkizova S, et al. Aryl Hydrocarbon Receptor Controls Monocyte Differentiation into Dendritic Cells versus Macrophages. Immunity. 2017;47(3):582-96.e6.
128. Menezes S, Melandri D, Anselmi G, Perchet T, Loschko J, Dubrot J, et al. The Heterogeneity of Ly6Chi Monocytes Controls Their Differentiation into iNOS+ Macrophages or Monocyte-Derived Dendritic Cells. Immunity. 2016;45(6):1205-18.
129. Nagenborg J, Goossens P, Biessen EAL, Donners M. Heterogeneity of atherosclerotic plaque macrophage origin, phenotype and functions: Implications for treatment. Eur J Pharmacol. 2017;816:14-24.
130. Stremmel C, Stark K, Schulz C. Heterogeneity of Macrophages in Atherosclerosis. Thromb Haemost. 2019;119(8):1237-46.
131. Bonnardel J, Guilliams M. Developmental control of macrophage function. Curr Opin Immunol. 2018;50:64-74.
132. Evren E, Ringqvist E, Tripathi KP, Sleiers N, Rives IC, Alisjahbana A, et al. Distinct developmental pathways from blood monocytes generate human lung macrophage diversity. Immunity. 2021;54(2):259-75.e7.
133. Ożańska A, Szymczak D, Rybka J. Pattern of human monocyte subpopulations in health and disease. Scand J Immunol. 2020;92(1):e12883.
134. Kerkhofs D, van Hagen BT, Milanova IV, Schell KJ, van Essen H, Wijnands E, et al. Pharmacological depletion of microglia and perivascular macrophages prevents Vascular Cognitive Impairment in Ang II-induced hypertension. Theranostics. 2020;10(21):9512-27.
135. Frankenberger M, Hofer TPJ, Marei A, Dayyani F, Schewe S, Strasser C, et al. Transcript profiling of CD16-positive monocytes reveals a unique molecular fingerprint. Eur J Immunol. 2012;42(4):957-74.
136. Lawlor N, Nehar-Belaid D, Grassmann JDS, Stoeckius M, Smibert P, Stitzel ML, et al. Single Cell Analysis of Blood Mononuclear Cells Stimulated Through Either LPS or Anti-CD3 and Anti-CD28. Front Immunol. 2021;12:636720.
137. Rogers BM, Smith L, Dezso Z, Shi X, DiGiammarino E, Nguyen D, et al. VISTA is an activating receptor in human monocytes. J Exp Med. 2021;218(8):e20201601.
138. Mueller KAL, Hanna DB, Ehinger E, Xue X, Baas L, Gawaz MP, et al. Loss of CXCR4 on non-classical monocytes in participants of the Women's Interagency HIV Study (WIHS) with subclinical atherosclerosis. Cardiovasc Res. 2019;115(6):1029–40.


3

Chapter 3

Classical, intermediate, and non-classical monocytes give rise to functionally distinct macrophages

AV Ruder, GE Rizzi, L Wijnands, K Hoeft, CG Schalkwijk, JC Sluimer, L Temmerman, EAL Biessen

In preparation


4

Chapter 4

Culture density influences the functional phenotype of human macrophages

AV Ruder, L Temmerman, JMA van Dommelen, J Nagenborg, C Lu, JC Sluimer, P Goossens* and EAL Biessen*

* Authors contributed equally

Adapted from *Frontiers in Immunology. 2023;14:1078591*

Abstract

Macrophages (MΦ) are commonly cultured *in vitro* as a model of their biology and functions in tissues. Recent evidence suggests MΦ to engage in quorum sensing, adapting their functions in response to cues about the proximity of neighbouring cells. However, culture density is frequently overlooked in the standardisation of culture protocols as well as the interpretation of results obtained *in vitro*. In this study, we investigated how the functional phenotype of MΦ was influenced by culture density. We assessed 10 core functions of human MΦ derived from the THP-1 cell line as well as primary monocyte-derived MΦ. THP-1 MΦ showed increasing phagocytic activity and proliferation with increasing density but decreasing lipid uptake, inflammasome activation, mitochondrial stress, and secretion of cytokines interleukin (IL) -10, IL-6, IL-1β, IL-8, and tumour necrosis factor (TNF) -α. For THP-1 MΦ, the functional profile displayed a consistent trajectory with increasing density when exceeding a threshold (of 0.2 x 10^3 cells/mm^2), as visualised by principal component analysis. Culture density was also found to affect monocyte-derived MΦ, with functional implications that were distinct from those observed in THP-1 MΦ, suggesting particular relevance of density effects for cell lines. With increasing density, monocyte-derived MΦ exhibited progressively increased phagocytosis, increased inflammasome activation, and decreased mitochondrial stress, whereas lipid uptake was unaffected. These different findings in THP-1 MΦ and monocyte-derived MΦ could be attributed to the colony-forming growth pattern of THP-1 MΦ. At the lowest density, the distance to the closest neighbouring cells showed greater influence on THP-1 MΦ than monocyte-derived MΦ. In addition, functional differences between monocyte-derived MΦ from different donors could at least partly be attributed to differences in culture density. Our findings demonstrate the importance of culture density for MΦ function and demand for awareness of culture density when conducting and interpreting *in vitro* experiments.

Introduction

Macrophages (MΦ) have attracted growing interest as a therapeutic target due to their dynamic role in various pathologies, including inflammatory diseases and cancer (1-3). Cell lines like THP-1, J774 or RAW264.7, or primary MΦ derived from bone marrow cells or blood monocytes are commonly used as models of human MΦ in biological assays or screening tools *in vitro* (1). To ensure reproducibility and comparability of results obtained from MΦ cultured *in vitro*, standardised cultivation protocols optimised for each cell type and assay are essential (4, 5). However, culture density at point of observation is an often-overlooked factor and either not specified at all or insufficiently substantiated by experimental data. Even though seeding density is usually mentioned and cells are often seeded at similar densities, differences in growing protocols, experimenters, and experimental conditions may result in density differences during experimentation. This is particularly worrisome in view of the reported importance of local contact and context for MΦ viability (6) and recent growing evidence of quorum sensing by MΦ (7).

Quorum sensing, a term adopted from bacteriology, refers to the modulation of gene expression by diffusible molecular cues (autoinducers) which convey information about density between cells (8-10). Quorum sensing had originally been established for biofilm formation of bacteria (8) but has recently also been observed in MΦ (7, 9, 11). In RAW264.7 MΦ, gelsolin was identified as autoinducer of programmed cell death 4 (PDCD4) expression which increased at higher cell density (11). Moreover, a quorum sensing mechanism has been observed in mice where the inflammation-resolving effect of nitric oxide (NO) was found to be dependent on the density of NO-producing MΦ (7).

Along with quorum sensing, cell density is vital for MΦ proliferation and viability. Indeed, MΦ were found to resume exponential growth faster (12), and to exhibit a more mature phenotype (13) and improved viability (12) at lower density. At higher density on the other hand, more MΦ adopted a high activation state (9). Moreover, culture density has been shown to influence several key functions of MΦ, including cytokine secretion (9, 13), polarisation (13), phagocytosis (14), accumulation of esterified cholesterol (15), formation of multinucleated giant cells (16), and inhibition of mycobacterial growth (17). However, previous studies mostly compared two densities ("high" versus "low") for only a single function, and either focused on murine MΦ cell lines or on bone marrow-derived MΦ (BMDM). So far, a comprehensive study of the functional implications of density in human MΦ models is lacking. Failure to account for density differences may introduce bias as it remains unclear whether observed effects of a treatment agent are merely attributable to its effect on culture density, either by promoting proliferation and cell survival, or by inducing cell death.

The aim of this study was to investigate the influence of culture density on human MΦ function. Using high-throughput measurement of 10 functional parameters, we studied the phenotype of THP-1 MΦ as well as human primary monocyte-derived MΦ (MDM). Moreover, we considered the colony-forming growth pattern of THP-1 cells, and donor-specific differences in MDM as additional modulators of culture density-related functional changes.

Methods

THP-1 cell culture and differentiation to MΦ

THP-1 cells were seeded at increasing densities in 96-well black clear-bottom imaging microplates (Corning #353219) in RPMI medium with HEPES and GlutaMAX (Gibco #72400-021) supplemented with 10% heat-inactivated (30 minutes at 56 °C) foetal bovine serum (FBS; SERANA #S-FBS-SA-015) and 1% penicillin-streptomycin (Gibco #15070-063). Seeding densities were 5,000, 12,000, 21,000, 37,000, 53,000, 69,000, or 87,000 cells/well, denoted as x 10^3 cells/mm^2 (0.16, 0.38, 0.66, 1.16, 1.66, 2.16, or 2.72 x 10^3 cells/mm^2, respectively) that were rounded to one decimal digit to improve readability (0.2, 0.4, 0.7, 1.2, 1.7, 2.2, or 2.7 x 10^3 cells/mm^2, respectively). THP-1 cells were differentiated into MΦ by exposure to 2000 nM phorbol 12-myristate 13-acetate (PMA; Sigma #P1585) for 48 hours at 37 °C, 5% CO_2 after which they were rested for 24 hours in fresh culture medium before performing the functional assays.

PBMC isolation, monocyte isolation, and differentiation to MΦ

Peripheral blood mononuclear cells (PBMCs) were isolated from leukocyte reduction system cones, a by-product of thrombopheresis of routine blood donations from healthy volunteers collected at the University Hospital RWTH Aachen, Germany, by density centrifugation with Lymphoprep™ (STEMCELL Technologies #07861). Isolated PBMCs were cryopreserved for later use in one-third freezing medium containing 75% FBS and 25% dimethyl sulfoxide (DMSO; Merck #102950). CD14 MicroBeads (Miltenyi #130-096-052) were used to positively select CD14-positive monocytes, following the manufacturer's protocol. Monocytes of 6 donors were pooled before seeding at the respective densities in 96-well black clear-bottom imaging microplates, or kept separate and seeded in 384-well plates (Greiner Bio-One #781866) in culture medium containing RPMI medium with HEPES and GlutaMAX supplemented with 10% heat-inactivated FBS and 1% penicillin-streptomycin. Seeding densities were 30,000, 64,000, 98,000, 132,000, 166,000, or 200,000 cells/well, denoted as x 10^3 cells/mm^2 (0.94, 2.0, 3.06, 4.13, 5.19, or 6.25 x 10^3 cells/mm^2, respectively) that were rounded to integers to improve readability (1, 2, 3, 4, 5, or 6 x 10^3 cells/mm^2, respectively). At 384-well format, cells were plated at 13,000 cells/well. Monocytes were differentiated into MΦ with 100 ng/ml recombinant human macrophage colony-stimulating factor (M-CSF) (ImmunoTools #11343113) for 7 days at 37 °C, 5% CO_2 with one medium change.

Functional high-throughput measurements

MΦ functions were assessed using the "MacroScreen" high-content analysis (HCA) platform developed in-house, a semi-automated microscale (96- to 384-well format) assay platform to perform an expanding range of fluorescence-based functional assays (18). All MacroScreen assays have been benchmarked against conventional mesoscale assays. Images were taken using the BD Pathway 855 automated fluorescent microscope (BD Biosciences) by taking 9

images per well with a 10x Olympus 0.40 NA objective (96-well format) or 20x Olympus 0.75 NA objective (384-well format). All experiments were performed in n=3-6 replicates. Images were analysed with CellProfiler software version 4.0.4 (19) by creating a digital segmentation mask for each cell based on its nuclear staining signal using the IdentifyPrimaryObjects module followed by the ExpandOrShrinkObject module. Percentage of positive cells was measured using the MeasureObjectIntensity module followed by the ClassifyObjects module, which determines the amount of positive cells relative to the total number of segmented objects in the image. Distance to the closest neighbouring cell was measured per image, for each cell, using the MeasureObjectNeighbors module in CellProfiler 4.0.4 (19).

Phagocytosis

Cells were incubated with 25 µl/ml pHrodo™ Red Zymosan Bioparticles™ (ThermoFisher Scientific #P35364) per well in culture medium for 1 hour at 37 °C, 5% CO_2. Zymosan particles taken up by cells are reflected by tetramethyl rhodamine isothicyanate (TRITC) fluorescence signal. Nuclei were stained with Hoechst 33342 (Sigma #B2261) in culture medium for 10 minutes at 37 °C, 5% CO_2 which was replaced by phosphate-buffered saline (PBS) before imaging.

Lipid uptake

Low-density lipoprotein (LDL) was isolated from serum of healthy volunteers via density centrifugation and oxidised using $CuSO_4$ as described previously (20). Cells were incubated with 8 µg/ml oxidised LDL (oxLDL) pre-mixed with 2 µg/ml TopFluor® Cholesterol (Avanti Polar Lipid #810255P) in culture medium for 3 hours at 37 °C, 5% CO_2, reflected by fluorescein isothiocyanate (FITC) fluorescence signal. Nuclei were stained with Hoechst 33342 in culture medium for 10 minutes at 37 °C, 5% CO_2 which was replaced by PBS before imaging.

Inflammasome

Cells were primed with 50 ng/ml lipopolysaccharide (LPS) from E. coli (Invivogen #tlrl-eblps) for 3 hours at 37 °C, 5% CO_2. 10 µM nigericin (Invivogen #tlrl-nig) for 1 hour at 37 °C, 5% CO_2 served as second signal for inflammasome activation. Fc receptor was blocked with Fc receptor binding inhibitor antibody (Invitrogen #14-9161-73) before cells were fixed using 2% paraformaldehyde (PFA) with 5 mM EDTA in PBS and permeabilised using 5% FBS and 0.5% Triton X-100 in PBS for 20 minutes on ice. Next, the intracellular adapter protein apoptosis-associated speck-like protein containing a CARD (ASC) was stained using PE-conjugated anti-ASC antibody (clone HASC-71; BioLegend #653904) overnight at 4 °C. Nuclei were stained with Hoechst 33342 in PBS for 10 minutes on ice, and cells were washed with and imaged in PBS afterwards.

Mitochondrial stress

Mitochondrial stress was induced using 1200 nM staurosporine (Sigma #S4400) for 1 hour at 37 °C, 5% CO_2. Mitochondria and nuclei were stained simultaneously with 250 nM MitoTracker™ Deep Red FM (ThermoFisher Scientific #M22426) and Hoechst 33342, respectively, in culture medium for 30 minutes at 37 °C, 5% CO_2 before imaging in PBS. Alexa 594 fluorescence signal reflects mitochondrial staining dependent on membrane potential.

Proliferation

Cells were incubated with 10 µM 5'ethynyl-2'-deoxyuridine (EdU; ThermoFisher Scientific #A10044) for 2 hours at 37 °C, 5% CO_2. Next, cells were fixated with 3.7% PFA in PBS for 15 minutes and washed twice with PBS before permeabilisation with 0.1% Triton X-100 in PBS for 15 minutes. After another wash with PBS, Click-iT reaction cocktail (ThermoFisher Scientific #C10269) including Alexa Fluor 594 azide (ThermoFisher Scientific, #A10270) prepared according to the manufacturer's instructions was added. After 30 minutes, cells were washed with PBS and nuclei stained with Hoechst 33342 for 15 minutes. Cells were imaged in 1:5 KI quencher (1M KI in 10 mM KH_2PO_4) in PBS.

Multiplex ELISA

THP-1-derived MΦ were stimulated with 50 ng/ml LPS from E. coli for 6 hours at 37 °C, 5% CO_2. Supernatant was collected and cytokine levels of interleukin (IL) -1β, IL-6, IL-8, IL-10, IL-12p70, and tumour necrosis factor (TNF) -α were measured in a custom V-plex human cytokine ELISA (MSD Meso Scale Diagnostics) according to the manufacturer's protocol. Measured levels of IL-12p70 were close to or below the standard curve (0.1169 pg/ml), thus these data are not presented here.

Dimensionality reduction and visualisation

We calculated the mean of the replicates for each feature of HCA functional data and cytokine data at the same density, resulting in a density-feature matrix with 7 rows (densities) and 10 columns (features/functions). The functional profile of THP-1 MΦ for the 7 different densities was analysed in an integrated manner by two-dimensional principal component analysis (PCA), where the relative contribution of each individual function to the first (PC1) and second principal component (PC2) axes was visualised outside the X and Y axes.

Statistical analysis

Data are expressed as mean ± SEM, unless stated otherwise. Normal distribution was assessed by Shapiro-Wilkes normality test, and equality of variances by Brown-Forsythe test. For normally distributed data with equal variance, significance was assessed by one-way ANOVA followed by Tukey's multiple comparisons test at a significance level of $p < 0.05$. For normally distributed data with unequal variance, significance was assessed by Brown-Forsythe ANOVA

and Dunnett's T3 multiple comparisons test, and Kruskal-Wallis test with Dunn's multiple comparisons test was used for not normally distributed data. All statistical analyses were performed using GraphPad Prism 8 software.

Results

Density influences the functional phenotype of MΦ

We assessed the functional phenotype of THP-1-derived MΦ seeded at 7 different densities ranging from 0.2 to 2.7 x 10^3 cells/mm^2 using the MacroScreen platform, an HCA platform based on several fluorescent imaging-based functional assays. For clarity's sake, we presented the p-values of all group comparisons for all assays in a significance matrix (**Supplementary Table 1**). As expected, the number of nuclei per fluorescent image increased with density in all high-content functional assays (**Supplementary Figure 1A-E**). No changes in the pH of the culture medium were observed. Whereas the phagocytic activity of THP-1 MΦ was found to increase with higher density (**Figure 1A**), uptake of oxLDL decreased (**Figure 1B**). MΦ seeded at 0.2 x 10^3 cells/mm^2, the lowest density in the tested density range, showed the highest inflammasome activation in response to LPS and nigericin (**Figure 1C**). Moreover, at lower densities, MΦ were found to be more resistant to staurosporine-induced mitochondrial stress (**Figure 1D**). Proliferation measured by EdU incorporation increased with density (**Figure 1E**). Secretion of the cytokines IL-10, IL-1β, IL-6, IL-8, and TNF-α in response to LPS stimulation was measured using multiplex ELISA, and was found to decrease with density, after an initial sharp increase between the two lowest densities included in the density range (0.2 and 0.4 x 10^3 cells/mm^2) (**Figure 1F-J**). PCA allowed separation of THP-1 MΦ seeded at different densities based on their functional profiles (**Figure 1K**). A large proportion of variation (61.27%) could be explained by PC1 which loadings included mitochondrial stress, lipid uptake, proliferation and phagocytosis, suggesting these functions to be mostly influenced by density. Variation along PC2 (largely attributable to inflammasome activation and cytokine secretion) almost exclusively manifested at the lowest density (0.2 x 10^3 cells/mm^2). Together, these data demonstrate the profound and variable impact of culture density on several THP-1 MΦ functions. Execution of certain functions may depend on exceeding a lower density threshold.

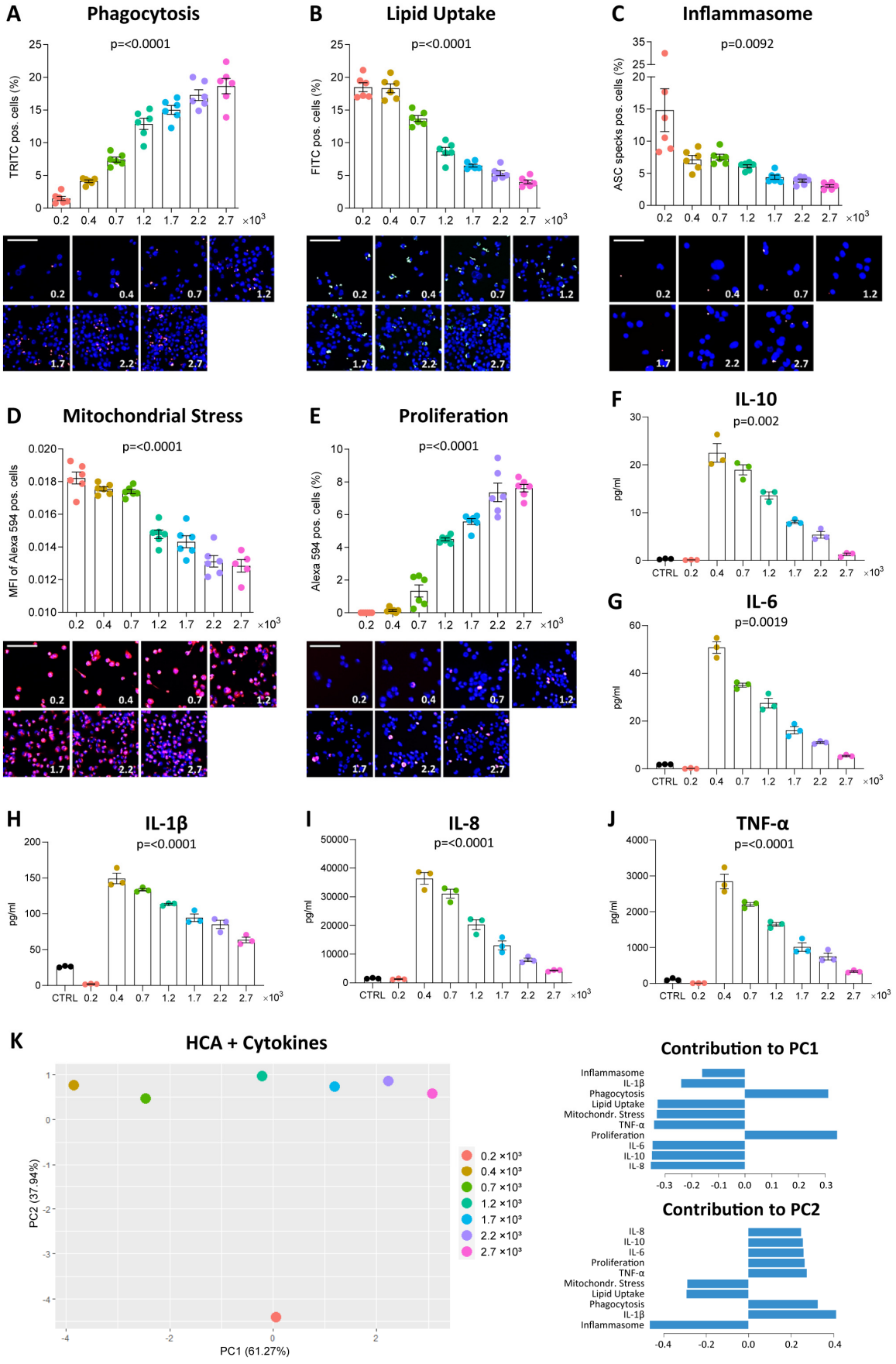
A
Phagocytosis
p=<0.0001
TRITC pos. cells (%)
B
Lipid Uptake
p=<0.0001
FITC pos. cells (%)
C
Inflammasome
p=0.0092
ASC specks pos. cells (%)
D
Mitochondrial Stress
p=<0.0001
MFI of Alexa 594 pos. cells
E
Proliferation
p=<0.0001
Alexa 594 pos. cells (%)
F
IL-10
p=0.002
G
IL-6
p=0.0019
H
IL-1β
p=<0.0001
I
IL-8
p=<0.0001
J
TNF-α
p=<0.0001
pg/ml
CTRL
×10³
K
HCA + Cytokines
PC1 (61.27%)
PC2 (37.94%)
0.2 ×10³
0.4 ×10³
0.7 ×10³
1.2 ×10³
1.7 ×10³
2.2 ×10³
2.7 ×10³
Contribution to PC1
Inflammasome
IL-1β
Phagocytosis
Lipid Uptake
Mitochondr. Stress
TNF-α
Proliferation
IL-6
IL-10
IL-8
Contribution to PC2

Figure 1: Density affects MΦ function

THP-1 cells were seeded at the respective densities (0.2-2.7 x 10^3 cells/mm²) and differentiated with 2000 nM PMA for 48 hours followed by a resting period of 24 hours. Phagocytosis of zymosan-coated beads (A, red), uptake of fluorescently-labelled oxLDL (B, green), inflammasome activation (C, red), mitochondrial stress in response to staurosporine (D, red) and EdU incorporation in proliferating cells (E, red) were assessed using the fluorescent imaging MacroScreen platform. Hoechst was used for nuclear labelling (blue). In the representative fluorescent images, the scale bar refers to 50 µM. In the representative images for the inflammasome assay, the scale bar refers to 25 µM. Secretion of IL-10 (F), IL-6 (G), IL-1β (H), IL-8 (I), and TNF-α (J) in response to 6-hour stimulation with 50 ng/ml LPS were measured by multiplex ELISA. Cells in the control (CTRL) condition were seeded at 1.7 x 10^3 cells/mm² and not stimulated with LPS. The indicated p-values refer to overall significance, p-values of all group comparisons can be found in **Supplementary Table 1**. (K) PCA plot of the high-content analysis (HCA) data and cytokine measurements with the factor loadings for PC1 and PC2. MFI: Mean fluorescence intensity.

Density influences the functional phenotype of primary MΦ

We also investigated whether culture density influences the functional phenotype of human MDM, pooled from 6 healthy donors. A significance matrix with the p-values of all group comparisons can be found in **Supplementary Table 2**. As seen in THP-1 MΦ, the number of detected nuclei increased with increasing seeding density (**Supplementary Figure 1F-I**). Phagocytic activity increased in the lower densities but decreased again at seeding densities exceeding 3 x 10^3 cells/mm^2, possibly reflecting limited substrate (**Figure 2A**). Using a constant substrate-to-cell ratio, increased phagocytosis also at higher densities could be observed (**Supplementary Figure 2**). OxLDL uptake between MDM seeded at different densities was similar, contrary to THP-1 MΦ (**Figure 2B**). With increasing density, MDM demonstrated more inflammasome activation (**Figure 2C**) and were more susceptible to mitochondrial stress (**Figure 2D**). Overall, our findings show that density also affects primary MΦ and leads to changes in several functions. In MDM, these changes were less pronounced and less consistent compared to THP-1 MΦ, suggesting that the observed impact of density on MΦ function may be particularly relevant for cell lines.

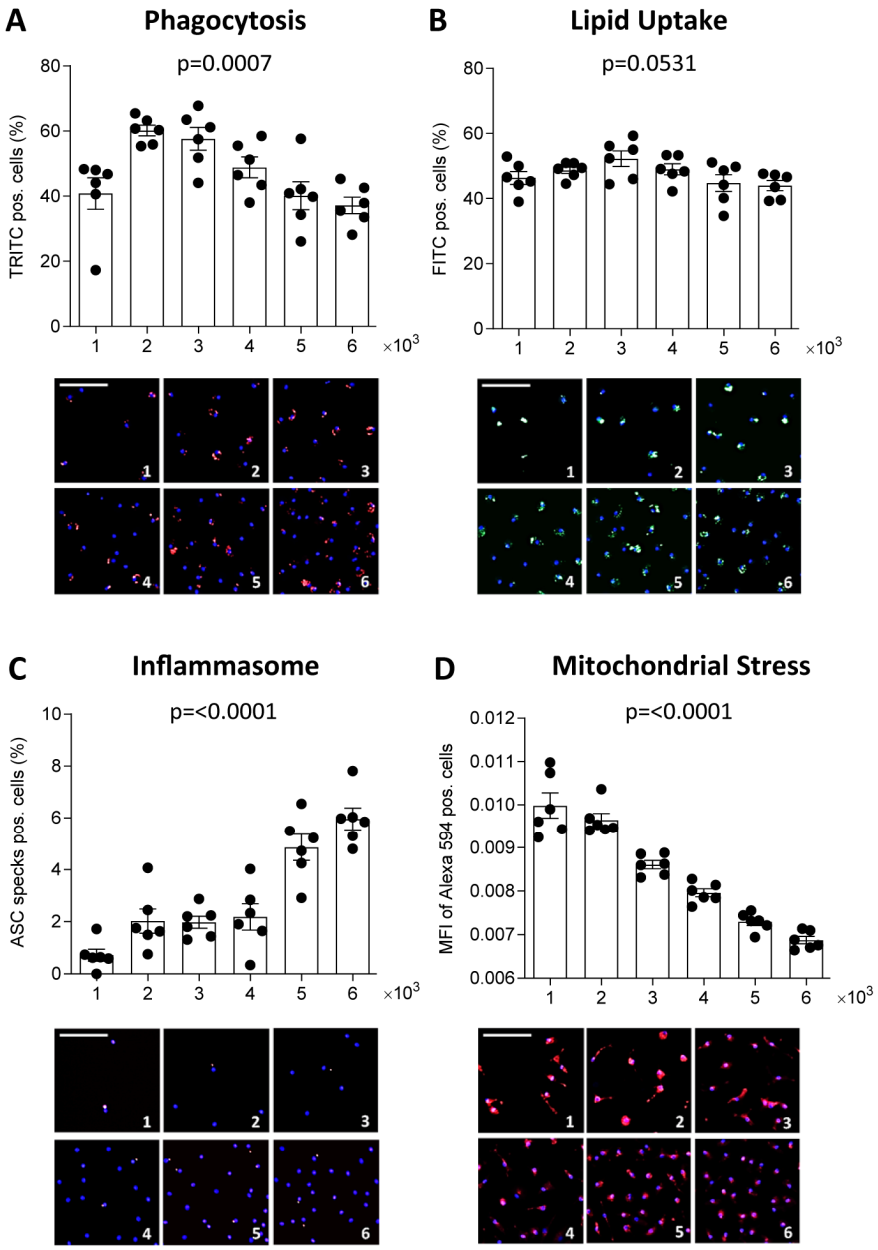

Figure 2: Density affects human primary MΦ function

CD14-positive monocytes were isolated from PBMCs of 6 healthy donors, pooled and seeded at the respective densities (1-6 x 10^3 cells/mm²) and differentiated to MΦ using 100 ng/ml macrophage colony-stimulating factor (M-CSF) for 7 days. Phagocytic activity (A, red), oxLDL uptake (B, green), inflammasome activation (C, red), and mitochondrial stress (D, red) were assessed using the MacroScreen platform. Hoechst was used for nuclear labelling (blue). The scale bar in the representative fluorescent images refers to 50 µM. The indicated p-values refer to overall significance, multiple comparison significance can be found in **Supplementary Table 2**. MFI: Mean fluorescence intensity.

Colony formation may contribute to density-dependent functional effects

We observed that THP-1 MΦ formed colonies in culture, especially if cultured at higher densities. Thus, we set out to study if at least part of the density-dependent functional changes may be attributed to changes in the colony-forming growth pattern of THP-1 cells. We assessed the association between the functional outcome of an index cell with its distance to the closest neighbouring cell. Index cells that were close to neighbouring cells had higher proliferation rates compared to MΦ in more scarcely populated niches (**Figure 3A**). However, at very low seeding density (0.2 x 10^3 cells/mm^2), MΦ proliferation was low regardless of the index cell's distance to neighbouring cells, suggesting proliferation to be linked to colony formation. Similarly, we found that at a seeding density of 0.2 x 10^3 cells/mm^2, MΦ with neighbouring cells in close proximity had taken up fewer fluorescent beads compared to equally dense MΦ seeded at higher densities (**Figure 3B**), a finding that was less pronounced for the uptake of oxLDL (**Figure 3C**). Interestingly, a similar proximity effect on phagocytosis and lipid uptake in MDM (**Figure 3D** and **3E**), in which we did not observe colony formation in culture, was not apparent. These findings suggest that MΦ only exert certain functions beyond a local cell density threshold.

Functional differences between MDM of different donors may arise from density differences

Inter-donor variability has previously been proposed to compromise reproducibility of *in vitro* experiments with MDM (21, 22). Therefore, we looked at functions of MDM from 6 healthy donors (A-F) plated at the same density (13,000 cells/well). A significance matrix with the p-values of all group comparisons can be found in **Supplementary Table 3**. Differences in the number of nuclei (**Figure 4A**), phagocytosis (**Figure 4B**), oxLDL uptake (**Figure 4C**), inflammasome activation (**Figure 4D**) and mitochondrial stress (**Figure 4E**) between donors were apparent. Interestingly, MDM from donors A and B, which showed higher phagocytic activity and oxLDL uptake, also had a higher number of nuclei compared to the other donors. This suggests that functional differences between MDM obtained from different donors may well be related to inter-donor differences in density, possibly resulting from differences in adherence and survival capacity.

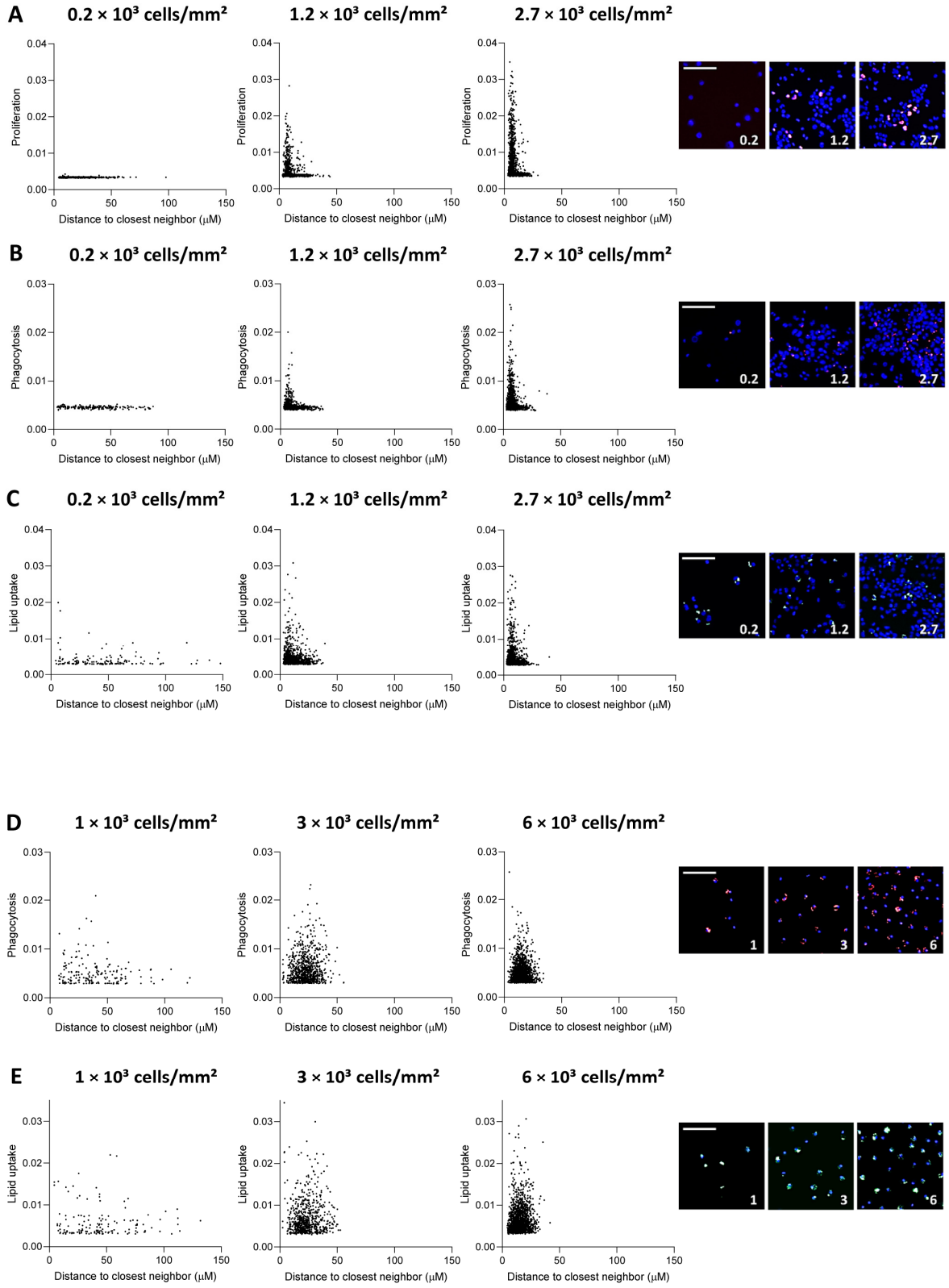

Figure 3: Distance to neighbouring cells influences THP-1 MΦ function

Distance to closest neighbour was plotted against mean fluorescence intensity (MFI) per cell for proliferation (A), phagocytosis (B) and lipid uptake (C) assays in THP-1 MΦ, and (D) phagocytosis and (E) lipid uptake assay in primary MDM, for 3 plating densities each. The scale bar corresponds to 50 µm.

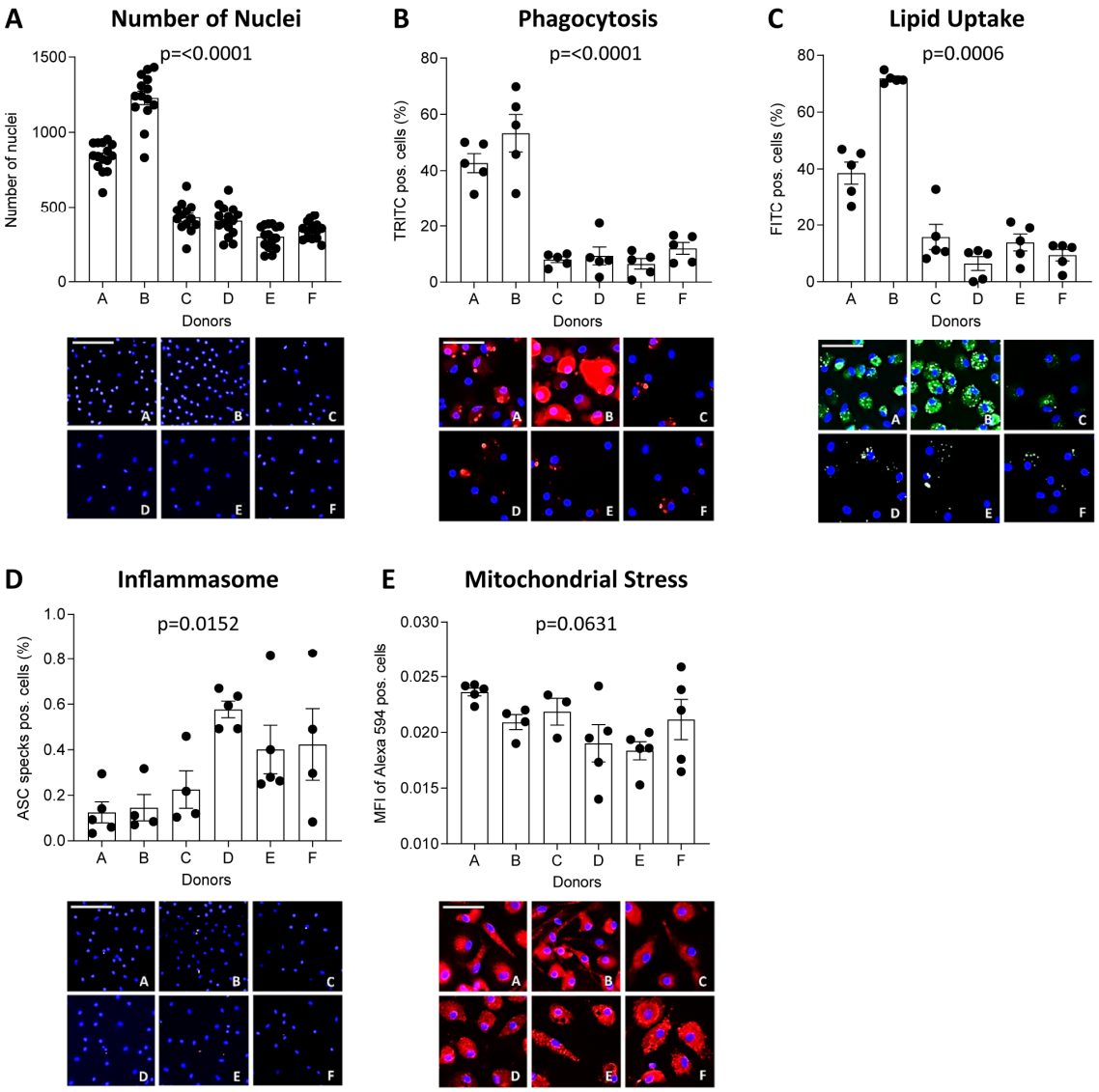

Figure 4: MΦ function differs between donors

CD14-positive monocytes of 6 healthy donors were seeded at 13,000 cells/well and differentiated into MΦ for 7 days using 100 ng/ml macrophage colony-stimulating factor (M-CSF). The number of nuclei per donor at experimentation (A) is given. Their functional phenotype was assessed using the MacroScreen platform: phagocytosis (B, red), lipid uptake (C, green), inflammasome activation (D, red), and mitochondrial stress (E, red). The scale bar corresponds to 25 µM. The indicated p-values refer to overall significance, multiple comparison significance can be found in Supplementary Table 3. MFI: Mean fluorescence intensity.

Discussion

In vitro studies are an indispensable step in the screening of genes or drugs and the safety testing of compounds, before costly and time-consuming pre-clinical *in vivo* studies may commence (23). Parameters that should be considered for robust *in vitro* testing include the culture medium and supplements such as growth factors or antibiotics, the culture dish and its coating, and culture maintenance (24). In this study, we have shown that culture density, a frequently overlooked factor, is an at least equally important parameter with major impact on MΦ assay outcome. As we show, density affects the functional phenotype of both THP-1 MΦ and primary MDM, with individual functions showing distinct density responses. Moreover, our data suggest the distance of index cells to their neighbour cells to influence functionality of THP-1 MΦ but less so of MDM, and the functional profiles and density response to vary considerably between donors.

The effect of low and high culture density on individual MΦ functions has been studied previously. In BMDM, secretion of TNF-α and other cytokines (MCP-1, RANTES, MIP-1α and MIP-1β) was found to increase with cell density (9). However, another study found BMDM at higher density to secrete less pro-inflammatory cytokines, including IL-6 and TNF-α (13). These contradicting results may be explained by differences in applied seeding densities in the two studies, as these were approximately 10 times higher in the latter study. Although our study did not look at BMDM, our THP-1 MΦ results do support a decrease of cytokine secretion with increasing density. However, at the lowest density, cytokine secretion by THP-1 MΦ was at most marginal, suggesting a defective response of sparsely seeded MΦ to toll-like receptor (TLR) activation, potentially due to quiescence or compromised viability.

Although phagocytosis and lipid uptake are both clearance mechanisms, they showed a divergent density response pattern in both THP-1 MΦ and MDM. Previously, THP-1 MΦ seeded at a lower density were found to show a 5-fold higher accumulation of esterified cholesterol after exposure to acetylated LDL (acLDL), which the authors attributed to increased scavenger receptor activity and acLDL degradation (15). Moreover, murine peritoneal IC-21 MΦ showed decreased phagocytosis of latex beads when seeded at a higher density (14), which partly concurs with our findings in human primary MDM and can be attributed to the limited availability of beads per cell. Bead concentration should be increased if cells are cultured at higher density to ensure sufficient bead availability for all actively phagocytosing cells.

Primary cells or cell lines are frequently and often interchangeably used in MΦ *in vitro* studies; the latter offering the advantages of easier availability and culture maintenance, and a uniform genetic background which may increase reproducibility (21). A serious disadvantage of cell lines is that compared to primary cells, they are to a certain degree de-differentiated and show clear transcriptional and functional differences. For example, the murine J774A.1 MΦ cell line and BMDM were found to respond differently to mycobacterial infection (25). Often myeloma-

derived or immortalised cell lines have aberrant contact inhibition and growth patterns (26); indeed, we found the proximity of neighbouring cells to have a greater impact on THP-1 MΦ than MDM function. In THP-1 MΦ, this may be attributed to increased proliferation at closer proximity which is absent at lower density, and suggests quorum sensing to induce functional changes locally at sites of colony formation. Comparing primary human monocytes with the monocytic cell lines U-937, HL-60, and THP-1, the latter were found to most closely resemble primary monocytes (27). Nevertheless, in contrast to primary MDM, cell line-derived MΦ do not capture inter-donor variability. This might be evaded by iPSC-derived MΦ, although Vaughan-Jackson et al. recently demonstrated density-related effects also in iPSC, including a more rounded and less elongated morphology, decreased cytokine secretion, and altered surface marker expression at higher density (28). However, it could be argued that also primary MΦ in monocultures *in vitro* do not mirror the *in vivo* conditions, where MΦ are embedded in a local heterogenous tissue microenvironment with implications for cell function (21). The complex cellular and molecular microenvironment tissue MΦ are exposed to *in vivo* cannot be mimicked by exposure to a single or a few selected stimuli such as LPS and interferon (IFN) -γ, or IL-4 and IL-10, as commonly done (29, 30).

Of note, we did not observe any indications for increased acidification of the culture medium which could explain the observed density effects and even at the highest density, the total cell number was most likely too low to deplete key nutrients. However, the comparability of our results on THP-1 MΦ and MDM may be impeded because different seeding densities had to be used due to the proliferating nature of the THP-1 cell line. In addition, the culturing process of MDM (7 days) and THP-1 MΦ (2 days PMA stimulation and 1 day resting) differs considerably. An extended resting period (5 days after 3 days PMA stimulation) has been shown to yield THP-1 MΦ with a phenotype closer to MDM (31). Moreover, the functional profile we provide here is not comprehensive as it only includes measurements of 5 cellular readouts and 5 cytokines. Future studies could reveal if the observed culture density effects also apply to other functions such as efferocytosis, susceptibility to apoptosis, production of reactive oxygen species (ROS), and metabolic differences.

In conclusion, our study highlights the importance of culture density for *in vitro* MΦ assay outcome and pleads for more awareness and closer monitoring of differences in cell density between conditions. This is particularly important for the THP-1 cell line which demonstrated more pronounced density effects compared to primary MDM, and when treatments are suspected to act pro-apoptotic or favour cell detachment or proliferation, which in turn impacts cell density. Moreover, a sufficiently large donor pool should be used in experiments with primary MDM to account for inter-donor variability, as the number of cells after differentiation and culture differed between donors despite seeding at the same density. Disregarding density differences may lead to secondary effects on MΦ functions, and thus misinterpretation of findings.

Author contributions

A.V.R., J.N., L.T., P.G. and E.A.L.B. contributed to the conception and design of the study; A.V.R., J.M.A.D. and J.N. carried out the experiments; C.L. performed the bioinformatic analyses; P.G., L.T., J.C.S. and E.A.L.B. contributed to the interpretation of results; A.V.R. wrote the manuscript with input from all authors.

Funding

This work was supported by the European Research Area Network Joint Transnational Call for Cardiovascular Disease (ERA-CVD; JTC-2017t100 AtheroMacHete to P.G. and E.A.L.B.), the Netherlands Organisation for Scientific Research (NWO)/São Paulo Research Foundation (FAPESP; DNAMoving to L.T. and E.A.L.B.), NWO-STW (#13568 Barcoding the Obese to E.A.L.B., L.T, and A.V.R.), NWO-VIDI (#91718364 to J.C.S.) and ASPASIA grant (#015.013.064 to J.S.C.), the Dutch Heart Foundation (Dekker 2020T042 to P.G.) and the Chinese Scholarship Council (CSC, #201706990018 to C.L.).

Conflict of interest

The authors declare that the research was conducted in the absence of any commercial or financial relationships that could be construed as a potential conflict of interest.

References

1. Rodell CB, Koch PD, Weissleder R. Screening for New Macrophage Therapeutics. Theranostics. 2019;9(25):7714-29.
2. Wynn TA, Chawla A, Pollard JW. Macrophage Biology in Development, Homeostasis and Disease. Nature. 2013;496(7446):445-55.
3. Zhang C, Yang M, Ericsson AC. Function of Macrophages in Disease: Current Understanding on Molecular Mechanisms. Front Immunol. 2021;12.
4. Baker M. Reproducibility: Respect Your Cells! Nature. 2016;537(7620):433-5.
5. Hirsch C, Schildknecht S. In Vitro Research Reproducibility: Keeping up High Standards. Front Pharmacol. 2019;10.
6. Guilliams M, Scott CL. Does Niche Competition Determine the Origin of Tissue-Resident Macrophages? Nat Rev Immunol. 2017;17(7):451-60.
7. Postat J, Olekhnovitch R, Lemaître F, Bousso P. A Metabolism-Based Quorum Sensing Mechanism Contributes to Termination of Inflammatory Responses. Immunity. 2018;49(4):654-665.e5.
8. Miller MB, Bassler BL. Quorum Sensing in Bacteria. Ann Rev of Microbiol. 2001;55(1):165-99.
9. Muldoon JJ, Chuang Y, Bagheri N, Leonard JN. Macrophages Employ Quorum Licensing to Regulate Collective Activation. Nat Commun. 2020;11(1):878.
10. Chen C-C, Wang L, Plikus MV, Jiang TX, Murray PJ, Ramos R, et al. Organ-Level Quorum Sensing Directs Regeneration in Hair Stem Cell Populations. Cell. 2015;161(2):277-90.
11. Sharma RK, Goswami B, Das Mandal S, Guha A, Willard B, Ray PS. Quorum Sensing by Gelsolin Regulates Programmed Cell Death 4 Expression and a Density-Dependent Phenotype in Macrophages. J Immunol. 2021;207(5):1250-64.
12. Zhuang JC, Wogan GN. Growth and Viability of Macrophages Continuously Stimulated to Produce Nitric Oxide. Proc Natl Acad Sci U S A. 1997;94(22):11875-80.
13. Lee CM, Hu J. Cell Density During Differentiation Can Alter the Phenotype of Bone Marrow-Derived Macrophages. Cell Biosci. 2013;3(1):30.
14. Vishniakova KS, Kireev II, Dunina-Barkovskaya AY. Effects of Cell Culture Density on Phagocytosis Parameters in IC-21 Macrophages. Biochemistry (Mosc) Suppl Ser A: Membr Cell Biol. 2011;5(4):355-63.
15. Rodriguez A, Kafonek SD, Georgopoulos A, Bachorik PS. Cell Density Can Affect Cholesteryl Ester Accumulation in the Human THP-1 Macrophage. J Lipid Res. 1994;35(11):1909-17.
16. Trout KL, Holian A. Factors Influencing Multinucleated Giant Cell Formation in Vitro. Immunobiology. 2019;224(6):834-42.
17. Boechat N, Bouchonnet F, Bonay M, Grodet A, Pelicic V, Gicquel B, et al. Culture at High Density Improves the Ability of Human Macrophages to Control Mycobacterial Growth. Journal Immunol. 2001;166(10):6203-11.
18. Fontaine MAC, Jin H, Gagliardi M, Rousch M, Wijnands E, Stoll M, et al. Blood Milieu in Acute Myocardial Infarction Reprograms Human Macrophages for Trauma Repair. Adv Sci (Weinh). 2023;10(5):2203053.
19. Lamprecht MR, Sabatini DM, Carpenter AE. Cellprofiler: Free, Versatile Software for Automated Biological Image Analysis. Biotechniques. 2007;42(1):71-5.
20. Redgrave TG, Roberts DC, West CE. Separation of Plasma Lipoproteins by Density-Gradient Ultracentrifugation. Anal Biochem. 1975;65(1-2):42-9.
21. Chanput W, Mes JJ, Wichers HJ. THP-1 Cell Line: An in Vitro Cell Model for Immune Modulation Approach. Int Immunopharmacol. 2014;23(1):37-45.
22. Rey-Giraud F, Hafner M, Ries CH. In Vitro Generation of Monocyte-Derived Macrophages under Serum-Free Conditions Improves Their Tumor Promoting Functions. PLoS One. 2012;7(8):e42656.
23. Sivinski SE, Mamedova LK, Rusk RA, Elrod CC, Swartz TH, McGill JM, et al. Development of an in Vitro Macrophage Screening System on the Immunomodulating Effects of Feed Components. J Anim Sci Biotechnol. 2020;11(1):89.
24. Riss TL, Moravec RA, Duellman SJ, Niles AL. Treating Cells as Reagents to Design Reproducible Assays. SLAS Discov. 2021;26(10):1256-67.
25. Andreu N, Phelan J, de Sessions PF, Cliff JM, Clark TG, Hibberd ML. Primary Macrophages and J774 Cells Respond Differently to Infection with Mycobacterium Tuberculosis. Sci Rep. 2017;7(1):42225.

26. Rennert K, Nitschke M, Wallert M, Keune N, Raasch M, Lorkowski S, et al. Thermo-Responsive Cell Culture Carrier: Effects on Macrophage Functionality and Detachment Efficiency. J Tissue Eng. 2017;8:2041731417726428.
27. Riddy DM, Goy E, Delerive P, Summers RJ, Sexton PM, Langmead CJ. Comparative Genotypic and Phenotypic Analysis of Human Peripheral Blood Monocytes and Surrogate Monocyte-Like Cell Lines Commonly Used in Metabolic Disease Research. PLoS One. 2018;13(5):e0197177.
28. Vaughan-Jackson A, Stodolak S, Ebrahimi KH, Johnson E, Reardon PK, Dupont M, et al. Density dependent regulation of inflammatory responses in macrophages. Front Immunol. 2022;13.
29. Chen H-J, Li Yim AYF, Griffith GR, de Jonge WJ, Mannens MMAM, Ferrero E, et al. Meta-Analysis of in Vitro-Differentiated Macrophages Identifies Transcriptomic Signatures That Classify Disease Macrophages in Vivo. Front Immunol. 2019;10.
30. Luque-Martin R, Mander PK, Leenen PJM, Winther MPJ. Classic and New Mediators for in Vitro Modelling of Human Macrophages. J Leukoc Biol. 2021;109(3):549-60.
31. Daigneault M, Preston JA, Marriott HM, Whyte MKB, Dockrell DH. The Identification of Markers of Macrophage Differentiation in PMA-Stimulated THP-1 Cells and Monocyte-Derived Macrophages. PLoS One (2010) 5(1):e8668.

Supplementary material

Supplementary Table 1

Significance matrix with p-values of group comparisons in functional assays on THP-1 macrophages. Density conditions are indicated as × 10^3 cells/mm^2.

Phagocytosis (corresponding to Fig. 1A)						
× 10^3	**0.4**	**0.7**	**1.2**	**1.7**	**2.2**	**2.7**
0.2	0.1523	<0.0001	<0.0001	<0.0001	<0.0001	<0.0001
0.4		0.0341	<0.0001	<0.0001	<0.0001	<0.0001
0.7			<0.0001	<0.0001	<0.0001	<0.0001
1.2				0.3623	0.0018	<0.0001
1.7					0.2933	0.0145
2.2						0.8149
Lipid Uptake (corresponding to Fig. 1B)						
× 10^3	**0.4**	**0.7**	**1.2**	**1.7**	**2.2**	**2.7**
0.2	>0.9999	<0.0001	<0.0001	<0.0001	<0.0001	<0.0001
0.4		<0.0001	<0.0001	<0.0001	<0.0001	<0.0001
0.7			<0.0001	<0.0001	<0.0001	<0.0001
1.2				0.0504	0.0006	<0.0001
1.7					0.6558	0.0183
2.2						0.5003
Inflammasome (corresponding to Fig. 1C)						
× 10^3	**0.4**	**0.7**	**1.2**	**1.7**	**2.2**	**2.7**
0.2	0.5259	0.5661	0.3857	0.2411	0.2054	0.163
0.4		>0.9999	0.885	0.0899	0.04	0.0124
0.7			0.2864	0.0061	0.0017	0.0007
1.2				0.0424	0.0014	<0.0001
1.7					0.9603	0.1122
2.2						0.3429
Mitochondrial Stress (corresponding to Fig. 1D)						
× 10^3	**0.4**	**0.7**	**1.2**	**1.7**	**2.2**	**2.7**
0.2	0.6803	0.4296	<0.0001	<0.0001	<0.0001	<0.0001
0.4		0.9996	<0.0001	<0.0001	<0.0001	<0.0001
0.7			<0.0001	<0.0001	<0.0001	<0.0001
1.2				0.9255	0.0055	0.0016
1.7					0.0864	0.0271
2.2						0.9953
Proliferation (corresponding to Fig. 1E)						
× 10^3	**0.4**	**0.7**	**1.2**	**1.7**	**2.2**	**2.7**
0.2	N/A	N/A	N/A	N/A	N/A	N/A
0.4		0.1936	<0.0001	<0.0001	0.0005	<0.0001
0.7			0.0018	0.0002	0.0001	<0.0001
1.2				0.0123	0.0353	0.0002
1.7					0.1985	0.0006
2.2						>0.9999

IL-10 (corresponding to Fig. 1F)							
× 10^3	0.2	0.4	0.7	1.2	1.7	2.2	2.7
CTRL	>0.9999	0.062	0.2215	>0.9999	>0.9999	>0.9999	>0.9999
0.2		0.0096	0.0419	0.2625	>0.9999	>0.9999	>0.9999
0.4			>0.9999	>0.9999	>0.9999	>0.9999	0.3101
0.7				>0.9999	>0.9999	>0.9999	0.9146
1.2					>0.9999	>0.9999	>0.9999
1.7						>0.9999	>0.9999
2.2							>0.9999
IL-6 (corresponding to Fig. 1G)							
× 10^3	0.2	0.4	0.7	1.2	1.7	2.2	2.7
CTRL	>0.9999	0.0509	0.2621	>0.9999	>0.9999	>0.9999	>0.9999
0.2		0.0077	0.0509	0.2621	>0.9999	>0.9999	>0.9999
0.4			>0.9999	>0.9999	>0.9999	>0.9999	0.2621
0.7				>0.9999	>0.9999	>0.9999	>0.9999
1.2					>0.9999	>0.9999	>0.9999
1.7						>0.9999	>0.9999
2.2							>0.9999
IL-1β (corresponding to Fig. 1H)							
× 10^3	0.2	0.4	0.7	1.2	1.7	2.2	2.7
CTRL	0.0117	<0.0001	<0.0001	<0.0001	<0.0001	<0.0001	0.0002
0.2		<0.0001	<0.0001	<0.0001	<0.0001	<0.0001	<0.0001
0.4			0.1783	0.0003	<0.0001	<0.0001	<0.0001
0.7				0.0485	0.0001	<0.0001	<0.0001
1.2					0.071	0.0033	<0.0001
1.7						0.7457	0.0013
2.2							0.0279
IL-8 (corresponding to Fig. 1I)							
× 10^3	0.2	0.4	0.7	1.2	1.7	2.2	2.7
CTRL	>0.9999	<0.0001	<0.0001	<0.0001	0.0001	0.0306	0.7575
0.2		<0.0001	<0.0001	<0.0001	<0.0001	0.0239	0.6845
0.4			0.1068	<0.0001	<0.0001	<0.0001	<0.0001
0.7				0.0003	<0.0001	<0.0001	<0.0001
1.2					0.0132	<0.0001	<0.0001
1.7						0.1334	0.0023
2.2							0.429
TNF-α (corresponding to Fig. 1J)							
× 10^3	0.2	0.4	0.7	1.2	1.7	2.2	2.7
CTRL	0.9934	<0.0001	<0.0001	<0.0001	<0.0001	0.0036	0.6971
0.2		<0.0001	<0.0001	<0.0001	<0.0001	0.0008	0.2876
0.4			0.0035	<0.0001	<0.0001	<0.0001	<0.0001
0.7				0.0119	<0.0001	<0.0001	<0.0001
1.2					0.0043	0.0001	<0.0001
1.7						0.5181	0.002
2.2							0.0903

Supplementary Table 2

Significance matrix with p-values of group comparisons in functional assays on primary monocyte-derived macrophages. Density conditions are indicated as × 10^3 cells/mm^2.

Phagocytosis (corresponding to Fig. 2A)					
× 10^3	**2**	**3**	**4**	**5**	**6**
1	0.1624	0.3698	>0.9999	>0.9999	>0.9999
2		>0.9999	>0.9999	0.0322	0.0061
3			>0.9999	0.0848	0.0184
4				>0.9999	>0.9999
5					>0.9999
Lipid Uptake (corresponding to Fig. 2B)					
× 10^3	**2**	**3**	**4**	**5**	**6**
1	0.9515	0.2974	0.9248	0.991	0.9543
2		0.7995	>0.9999	0.7022	0.5291
3			0.8482	0.1028	0.0563
4				0.6413	0.4681
5					0.9997
Inflammasome (corresponding to Fig. 2C)					
× 10^3	**2**	**3**	**4**	**5**	**6**
1	0.2428	0.2771	0.1483	<0.0001	<0.0001
2		>0.9999	0.9998	0.0004	<0.0001
3			0.9993	0.0003	<0.0001
4				0.0009	<0.0001
5					0.419
Mitochondrial Stress (corresponding to Fig. 2D)					
× 10^3	**2**	**3**	**4**	**5**	**6**
1	>0.9999	>0.9999	0.1386	0.004	<0.0001
2		>0.9999	0.2979	0.0113	0.0003
3			>0.9999	0.639	0.0552
4				>0.9999	0.8267
5					>0.9999

Supplementary Table 3

Significance matrix with p-values of group comparisons in the functional assays on primary monocyte-derived macrophages of 6 different donors.

Number of Nuclei (corresponding to Fig. 4A)					
Donor	**B**	**C**	**D**	**E**	**F**
A	<0.0001	<0.0001	<0.0001	<0.0001	<0.0001
B		<0.0001	<0.0001	<0.0001	<0.0001
C			0.9900	0.0159	0.2431
D				0.0637	0.5600
E					0.8538
Phagocytosis (corresponding to Fig. 4B)					
Donor	**B**	**C**	**D**	**E**	**F**
A	0.3138	<0.0001	<0.0001	<0.0001	<0.0001
B		<0.0001	<0.0001	<0.0001	<0.0001
C			0.9998	0.9996	0.9647
D				0.9921	0.9943
E					0.8760
Lipid Uptake (corresponding to Fig. 4C)					
Donor	**B**	**C**	**D**	**E**	**F**
A	>0.9999	>0.9999	0.0430	>0.9999	0.3545
B		0.1310	0.0012	0.1059	0.0184
C			>0.9999	>0.9999	>0.9999
D				>0.9999	>0.9999
E					>0.9999
Inflammasome (corresponding to Fig. 4D)					
Donor	**B**	**C**	**D**	**E**	**F**
A	>0.9999	>0.9999	0.0184	0.7632	0.9243
B		>0.9999	0.0839	>0.9999	>0.9999
C			0.4614	>0.9999	>0.9999
D				>0.9999	>0.9999
E					>0.9999
Mitochondrial Stress (corresponding to Fig. 4E)					
Donor	**B**	**C**	**D**	**E**	**F**
A	0.6611	0.9417	0.1130	0.0515	0.6918
B		0.9969	0.8945	0.7127	>0.9999
C			0.6961	0.4899	0.9991
D				0.9986	0.8029
E					0.5745

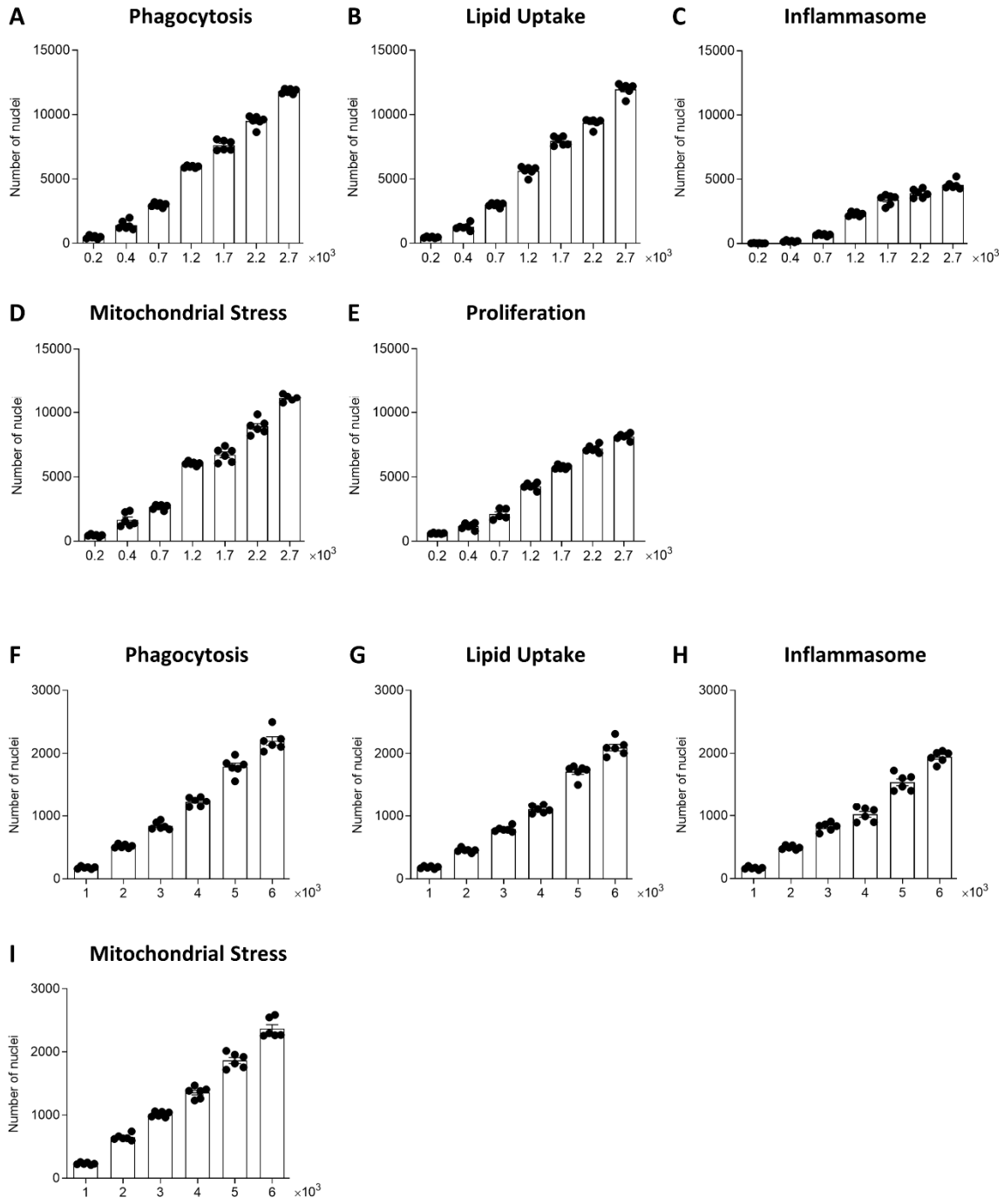

Supplementary Figure 1

(A-E) Number of nuclei in functional assays on THP-1 macrophages. (F-I) Number of nuclei in functional assays on primary monocyte-derived macrophages. Density conditions are indicated as x 10^3 cells/mm^2.

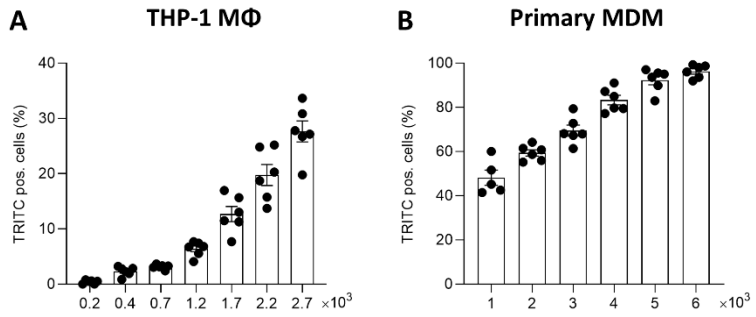

Supplementary Figure 2

(A) THP-1 cells were seeded at the respective densities (0.2-2.7 x 10^3 cells/mm²) and differentiated with 2000 nM PMA for 48 hours followed by a resting period of 24 hours. Phagocytic activity was assessed with the MacroScreen platform using an increasing concentration of substrate (zymosan-coated beads) relative to seeding density. (B) CD14-positive monocytes were isolated from PBMCs of 6 healthy donors, pooled and seeded at the respective densities (1-6 x 10^3 cells/mm²), and differentiated into MΦ using 100 ng/ml macrophage colony-stimulating factor (M-CSF) for 7 days. Phagocytic activity was assessed using a constant ratio of zymosan-coated beads relative to seeding density. Density conditions are indicated as x 10^3 cells/mm^2


5

Chapter 5

M-CSF and GM-CSF induce distinct changes in functional phenotype during monocyte-to-macrophage differentiation

AV Ruder, [illegible], J Kanenborg, L Temmerman, L Bonaguro, E De-Domenico, T Ulas, CG Schalkwijk, MMCP Donners, JC Sluimer, P Goossens, EAL Biessen

Submitted


6

Chapter 6

Magnetic resonance imaging contrast-enhancement with superparamagnetic iron oxide nanoparticles amplifies macrophage foam cell apoptosis in human and murine atherosclerosis

FME Segers, AV Ruder, MM Westra, T Lammers, SM Dadfar, K Roemhild, TS Lam, ME Kooi, KBJM Cleutjens, FK Verheyen, GWH Schurink, GR Haenen, TJC van Berkel, I Bot, B Halvorsen, JC Sluimer* and EAL Biessen*

* Authors contributed equally

Adapted from *Cardiovascular Research. 2022;118(17):3346-59*

Abstract

(Ultra) Small superparamagnetic iron oxide nanoparticles, (U)SPIO, are widely used as magnetic resonance imaging contrast media and assumed to be safe for clinical applications in cardiovascular disease. As safety tests largely relied on normolipidemic models, not fully representative of the clinical setting, we investigated the impact of (U)SPIOs on disease-relevant endpoints in hyperlipidemic models of atherosclerosis. RAW264.7 foam cells, exposed *in vitro* to ferumoxide (dextran-coated SPIO), ferumoxtran (dextran-coated USPIO), or ferumoxytol [carboxymethyl (CM) dextran-coated USPIO] (all 1 mg Fe/ml) showed increased apoptosis and reactive oxygen species accumulation for ferumoxide and ferumoxtran, whereas ferumoxytol was tolerated well. Pro-apoptotic ($TUNEL^+$) and pro-oxidant activity of ferumoxide (0.3 mg Fe/kg) and ferumoxtran (1 mg Fe/kg) were confirmed in plaque, spleen, and liver of hyperlipidemic apolipoprotein E-knockout ($ApoE^{-/-}$) (n=9/group) and low-density lipoprotein receptor-knockout ($LDLR^{-/-}$) (n=9-16/group) mice that had received single IV injections compared to saline-treated controls. Again, ferumoxytol treatment (1 mg Fe/kg) failed to induce apoptosis or oxidative stress in these tissues. Concomitant antioxidant treatment (EUK-8/EUK-134) largely prevented these effects *in vitro* (-68%, $p < 0.05$) and in plaques from $LDLR^{-/-}$ mice (-60%, $p < 0.001$, n=8/group). Repeated ferumoxtran injections of $LDLR^{-/-}$ mice with pre-existing atherosclerosis enhanced plaque inflammation and apoptosis but did not alter plaque size. Strikingly, carotid artery plaques of endarterectomy patients who received ferumoxtran (2.6 mg Fe/kg) before surgery (n=9) also showed 5-fold increased apoptosis (18.2 versus 3.7% respectively; $p=0.004$) compared to controls who did not receive ferumoxtran. Mechanistically, neither coating nor particle size seemed accountable for the observed cytotoxicity of ferumoxide and ferumoxtran. In conclusion, ferumoxide and ferumoxtran, but not ferumoxytol, induced apoptosis of lipid-laden macrophages in human and murine atherosclerosis, potentially impacting disease progression in patients with advanced atherosclerosis. Past and ongoing clinical trials with iron-based contrast agents in elderly, hyperlipidemic and/or cardiovascular patients should evaluate tissue apoptosis and monitor future cardiovascular complications well beyond the imaging timeframe. Safety studies of newly developed iron-based contrast agents should also be performed in hyperlipidemic settings.

Introduction

Functional imaging is widely employed to detect rupture-prone atherosclerotic plaques in coronary artery disease and carotid artery disease patients at risk of clinical symptoms (1). Rupture-prone plaques are typified by extensive lipid deposition, inflammation, matrix degradation, and cell death. These factors eventually lead to fibrous cap rupture and subsequent formation of an atherothrombus (2, 3).

Several passive and active molecular imaging modalities have been considered to identify high-risk plaques, including ^{18}F-fluoro-deoxyglucose-guided positron emission tomography-computed tomography (PET-CT), marking plaque inflammation and contrast-enhanced magnetic resonance imaging (MRI), respectively. MRI offers the advantage of superior spatial resolution, especially when using small (50-150 nm; SPIO) and ultrasmall (15-30 nm; USPIO) superparamagnetic iron oxide nanoparticles to enhance signal contrast (4-10). Upon systemic administration, both formulations are rapidly cleared by the reticuloendothelial system of lung and liver and by renal excretion, while accumulation in heart and brain is less pronounced, maximising signal to noise (11). USPIO extravasation and uptake by macrophages are considerably increased in inflammation (12-14), and vascular macrophages in the atherosclerotic plaque, in abdominal aneurysm, and in the infarcted or inflamed heart show avid accumulation of these particles (6, 9, 15-19), rendering them useful for cardiovascular disease imaging.

Extensive toxicology studies led to the assumption that (U)SPIO are safe for clinical application (20-22). However, this notion is merely based on studies in normolipidemic animal and cell culture models. In the hyperlipidemic setting of atherosclerosis, vascular macrophages will acquire a foam cell phenotype, with intracellular free cholesterol deposits, and increased production of reactive oxygen species (ROS) and susceptibility to apoptosis (23, 24). Moreover, upon uptake USPIO will accumulate in endo-lysosomes, where their coating will be degraded and the entrapped iron oxide cargo released (25, 26). Besides prolonging the imaging signal, (25, 26) this will also foster an oxidative stress response, which may well be detrimental to macrophage survival. Moreover, monocyte-derived macrophages were reported to enhance inflammatory cytokine secretion upon exposure to iron oxide particles (27). This suggests that (U)SPIO toxicity data obtained in normolipidemic, inflammatory macrophages *in vitro* may not be representative of the clinical situation. This prompted us to study (U)SPIO in macrophage foam cells, and in murine and human atherosclerosis to elucidate potentially unfavourable effects under clinically relevant conditions.

Methods

Cell culture

The RAW264.7 murine macrophage cell line was grown in DMEM, containing 10% foetal bovine serum (heat-inactivated for 30 minutes at 56 °C), 2 mmol/L L-glutamine, 100 U/ml penicillin and 100 µg/ml streptomycin (all from PAA), at 37 °C in a humidified atmosphere (5% CO_2).
Human very-low-density lipoprotein (hVLDL) was isolated from human serum of healthy volunteers by discontinuous density gradient centrifugation (using KBr; 40,000 rpm for 22 hours) (28). The VLDL fraction was collected and dialysed against phosphate-buffered saline (PBS) containing 1 mM EDTA. RAW264.7 cells were incubated with hVLDL (50 µg/ml) for 20 hours and replaced by medium with or without ferumoxide (100 µg Fe/ml, Guerbet) or two types of ultrasmall iron oxide nanoparticles (100 µg Fe/ml): ferumoxtran (Guerbet), and ferumoxytol (RIENSO, Takeda; EU tradename for Feraheme, AMAG Pharmaceuticals). Cells were pre-treated with EUK-8 antioxidant 2 hours prior to ferumoxtran treatment (25 µM; Merck Chemicals Ltd.). Viability of RAW cells was assessed using MTT assay (3-(4,5-dimethylthiazol-2-yl)-2,5-diphenyl-tetrazoliumbromide; Sigma). Apoptosis was quantified in ≥3 fields per well, 20x magnification after terminal deoxynucleotidyl transferase dUTP nick-end labelling (TUNEL) (Roche Diagnostics), or by flow cytometry of Annexin V-Oregon green (120 ng/ml).

Iron content

Ferumoxtran (100 µg Fe/ml) uptake by RAW264.7 macrophages and foam cells was determined after incubation for 1 hour at 37 °C. Quantitative determination of iron uptake by inductively coupled plasma atomic emission spectroscopy (ICP-AES; Optima 3300 RL, Perkin Elmer) was carried out after mineralisation of the pellet with HNO_3 (3 hours at 80 °C).

Animals and tissue harvesting

All animal work was performed in compliance with the Dutch government and directive 2010/63/EU guidelines and approved by national and local review boards (AVD1070020185705). Male low-density lipoprotein receptor-knockout ($LDLR^{-/-}$) or apolipoprotein E-knockout ($ApoE^{-/-}$) mice (aged 12 weeks) were obtained from the local animal facility. Animals were housed in the laboratory animal facility of Leiden University under standard conditions. Food and water were provided *ad libitum* during the entire experiment. All animals were housed in individually ventilated cages (GM500, Techniplast) in groups of up to 5 animals per cage, with bedding (corn cob, Technilab-BMI) and cage enrichment. Cages were changed weekly, reducing handling of the mice to one handling per week during non-intervention periods.
A pilot study was done with $ApoE^{-/-}$ mice (n=3/group) that received a single dose of saline, ferumoxide (0.3 mg Fe/kg), or ferumoxtran (1 mg Fe/kg) after 9 weeks on a Western-type diet (WTD, 0.25% cholesterol, 15% cocoa butter; SDS). Based on this, a sample size of 8 single mice

per group was calculated by power analysis. No inclusion or exclusion criteria were set. Cages were randomly located on the racks. LDLR$^{-/-}$ (n=9/group) were fed a WTD for 3 weeks, after which they received weekly intravenous injections of saline or ferumoxtran and fed a WTD for 5 consecutive weeks. LDLR$^{-/-}$ (n=8/group) fed a WTD for 14 weeks received either saline, ferumoxtran, antioxidant EUK-134 (10 mg/kg, Cayman Chemicals), or ferumoxtran with EUK-134, whereby EUK-134 was administered intraperitoneally 1 hour prior to the intravenous injection of ferumoxtran. In a third experiment, male LDLR$^{-/-}$ (n=9/group) fed a WTD for 9 weeks received a single saline, or ferumoxytol (1 mg Fe/kg) injection. In all experiments, 24 hours after the final injection, mice were anaesthetised using a single dose of pentobarbital (100 mg/kg i.p.), subjected to blood sampling and *in situ* perfusion-fixation through the left cardiac ventricle. Aortic root, liver and spleen were collected for cryosectioning using a Leica CM 3050S Cryostat (Leica Instruments).

Human tissue collection

Atherosclerotic carotid arteries (n=18) were obtained at surgery from patients treated with ferumoxtran (2.6 mg Fe/kg, single dose, n=9) and historic control patients (n=9) matched for age, sex and plaque type (Table 1) to analyse apoptosis in plaque sections (6). Inclusion and exclusion criteria were described before (6). Sample size was calculated based on interpatient MRI enhancement. Collection, storage, and use of tissue and patient data were performed in agreement with institutional ethical guidelines and the principles outlined in the Declaration of Helsinki and approved by the Maastricht University Medical Center Medical Ethical Committee (MEC00-078b) (6). Subjects gave informed consent prior to the inclusion and were enrolled consecutively between 2000 and 2002. Samples were processed and classified based on plaque morphology as described previously (29).

Histology and morphometry

Aortic root cryosections (10 µm) were stained with Oil Red O (Sigma) and MoMa-2 (1:50; Serotec) to detect lipid deposits and macrophage content, respectively. Secondary antibody goat anti-rat IgG-AP (1:100; Sigma) and enzyme substrate nitro-blue tetrazolium chloride with 5-bromo-4-chloro-3'-indolyphosphate p-toluidine salt (NBT-BCIP, DAKO) were used for MoMa-2 visualisation. The primary outcome of apoptotic cells in liver, spleen and atherosclerotic plaque was detected using TUNEL (Roche Diagnostics) and visualised using Nova-Red (DAKO) for mouse and AEC (Sigma) for human sections. Human atherosclerotic plaques were stained with 8OH-dG (Japan Institute for the Control of Aging, clone N45.1), TUNEL and cleaved caspase for apoptosis, CD68 to detect ROS, apoptosis, and macrophages, respectively. Quantitative morphometric analysis of Oil Red O, MoMa-2 and TUNEL was performed using Leica Qwin image analysis software and a Leica-DM-RE microscope (Leica Imaging Systems). Cells were marked as apoptotic when double positive for TUNEL and DAPI. High-sensitive Perl's iron staining was performed to visualise iron nanoparticles. Following quenching of endogenous peroxidases by hydrogen peroxide (0.3% in methanol), slides were incubated for 90 minutes in

1:1 solution of 2% HCl + 2% potassium hexacyanoferrate Fe^{2+}. After washing, slides were incubated for 20 minutes in 3,3′-diaminobenzidine (DAB, DAKO). Slides were counterstained with Nuclear Fast Red. Negative control sections incubated with DAB only were negative. Outcome and data analysis were done blindly.

Electron microscopy

Tissue fragments of carotid endarterectomy specimens of ~1 mm^3 were fixed overnight in 2.5% glutaraldehyde (Ted Pella), post-fixed in 1% osmium tetroxide solution, dehydrated, and embedded in epoxy resin. Semi-thin (1 µm) serial sections were stained with toluidine blue to localise microvessels. Ultra-thin sections (70-90 nm) were mounted on Formvar (1595 E, Merck)-coated 75 mesh copper grids, and counterstained with uranyl acetate and lead citrate before analysis on a Philips CM100 transmission electron microscope.

Trolox equivalent antioxidant capacity

The Trolox equivalent antioxidant capacity (TEAC) gives the concentration of 2,2'-azino-bis (3-ethylbenzthiazoline-6-sulfonic acid) diammonium salt (ABTS) radicals that can be scavenged by serum. It is a measure of antioxidant capacity. The TEAC was determined in serum that was deproteinated with a final concentration of 5% trichloroacetic acid (TCA), as described previously (30). The samples were incubated with an ABTS radical solution for 5 minutes and subsequently, the reduction in absorbance at 734 nm, reflecting the extent of radical scavenging, was quantified. This is related to that of the reference antioxidant Trolox and is expressed as µM Trolox equivalents. The TEAC value gives the concentration of Trolox that has the same capacity.

Uric Acid

Uric acid was determined in serum that was deproteinated with a final concentration of 5% TCA, using HPLC. A Hypersil BDS C-18 end-capped column, 125 x 4 mm, particle size 5 µm (Agilent, Palo Alto), was used, with a mobile phase of 0.1% trifluoroacetic acid (v/v) in water. UV detection was performed at 292 nm.

IL1-β ELISA

IL1-β, secreted in supernatant medium of RAW264.7 cells, was measured as suggested by the manufacturer (Invitrogen).

Quantitative RT-PCR

Quantitative RT-PCR analysis was performed to determine mRNA expression of apoptosis and oxidative stress related genes in RAW264.7 cells, foam cells and ferumoxtran-treated foam cells. Total RNA extracts isolated using the guanidium isothiocyanate (GTC) method (31) were transformed into cDNA using RevertAid M-MuLV reverse transcriptase (Fermentas, Burlington,

Canada) according to manufacturer's protocol. Quantitative gene expression analysis was performed with the SYBR-Green technology on a 7500 fast Real-Time PCR apparatus (Applied Biosystems). All Ct values were normalised to the stable-expressed reference gene hypoxanthine phospho-ribosyltransferase (HPRT). Supplementary Table 1 shows a detailed overview of the different primer pairs (Eurogentec), which were designed using NCBI primer blast.

Serum cholesterol analysis

Total cholesterol concentration in serum was determined using an enzymatic colorimetric assay (Roche Diagnostics). Precipath I (Roche Diagnostics) was used as an internal standard. Absorbance was measured at 490 nm. Cholesterol distribution over the different lipoprotein fractions was determined by fractionation of 30 µl serum using a Superose 6 column (3.2 x 300 mm; SMART system, Pharmacia). Cholesterol content of the effluent was determined as described above.

Dextran uptake assay

RAW264.7 cells were seeded at 75,000 cells per well in a 96-well black clear-bottom imaging microplate (Corning) in DMEM medium with 4.5 g/L D-glucose and pyruvate (Gibco) supplemented with 10% heat-inactivated (30 minutes at 56 °C) foetal bovine serum (SERANA) and 1% penicillin-streptomycin, and left to attach for 2 hours (37 °C, 5% CO_2). Supernatant of cells was either replaced with 1, 2.4, or 4 µM TRITC-labelled dextran (ThermoFisher Scientific). After 1 hour (37 °C, 5% CO_2), cells were washed with DMEM and nuclei were stained with Hoechst 33342 (Sigma) in DMEM for 10 minutes (37 °C, 5% CO_2). Cells were imaged using the BD Pathway 855 (BD Biosciences) and analysed with CellProfiler software 4.0.4 (32).

Chemicals for synthesis of iron particles

Ferric chloride anhydrous, ferrous chloride tetrahydrate, 1,10-phenanthroline, hydroxylamine hydrochloride, dextran and carboxymethyl (CM) dextran were purchased from Sigma. Trisodium citrate dihydrate, citric acid, hydrogen chloride, ammonium hydroxide (NH_4OH) and sodium hydroxide were obtained from Carl Roth.

Synthesis of citrate-coated iron particles

Citrate-coated iron particles were prepared via the standard co-precipitation technique. Briefly, 8 mmol of ferric chloride was dissolved in 10 ml of deionised water (from here on water) and mixed for 5 minutes under mechanical stirring and nitrogen atmosphere. Subsequently, 4 mmol of ferrous chloride tetrahydrate was added to the solution and mixed for a further 5 minutes at room temperature. The pH of the solution was adjusted to 11.0 by adding 80 ml of 1 M aqueous ammonia solution drop-wisely, and vigorously stirred at room temperature for 30 minutes. The formed black-coloured iron oxide nanoparticles were decanted using a

permanent magnet and washed at least three times with 500 ml of water. Afterwards, 20 ml of 0.1 M hydrochloric acid was added to the particles and sonicated for 10 minutes. Following, 2.5 g trisodium citrate dihydrate in 10 ml of water were added to the mixture and was stirred at 80 °C for 2 hours. The citrate-coated polydisperse particles were separated using a permanent magnet and then resuspended in 35 ml of water. Finally, the suspension was passed through a 0.2 µm filter to remove larger particles.
This highly polydisperse crude batch was subjected to five sequential rounds of centrifugation to obtain monodispersed iron particle subfractions. As depicted in Supplementary Figure 1, the supernatant obtained after 20 minutes of centrifugation at 14,000 rpm is referred to as Citrate S (USPIO size). The precipitate was resuspended in water and centrifuged again at progressively lower speed. The monodisperse batch obtained after 5 centrifugation cycles is referred to as Citrate L (SPIO size).

Synthesis of dextran-coated iron particles

Dextran-coated iron particles were prepared via the standard co-precipitation technique, under a nitrogen atmosphere. Briefly, 1 mmol of ferric chloride was dissolved in 2 ml of water and mixed for 5 min under mechanical stirring and nitrogen atmosphere. Subsequently, 0.5 mmol of ferrous chloride tetrahydrate in 1 ml of water was added to the solution and mixed for 5 minutes at room temperature after which pH was adjusted to 11.0 (1 M aqueous ammonia). The suspension was stirred at 0 °C for 1 or 30 minutes to obtain differently sized particles and an aqueous solution of dextran (1 kDa or 10 kDa; 1 gr) or CM dextran (10-20 kDa, 1 gr), filtered over a 200 nm syringe filter, was added. The temperature was slowly increased to 80 °C and was kept at that temperature for 60 minutes. Afterwards, the solution was cooled down to room temperature. The formed black-coloured iron oxide particles were sonicated for 20 minutes. Following, the solution was dialyzed for 24 hours against 5 L of water (25 kDa cut-off, SnakeSkin™ dialysis membrane, ThermoFisher Scientific). Finally, the suspension was passed through a 0.2 µm filter to remove the aggregates. Also here, the highly polydisperse starting batch was fractionated by size via two sequential rounds of centrifugation as described above (14,000 rpm, 20 minutes (S batch) and 7,000 rpm, 10 minutes (L batch)).

Characterisation of synthesized iron particles

Particle size and size distribution, Zeta potential, average hydrodynamic diameter (Dh) and polydispersity index (PDI) of the particles were measured by dynamic light scattering using a Zetasizer Nano-ZS instrument (Malvern Instruments) at 25 °C. The machine was equipped with a 633 nm He–Ne laser and a detector at angle of 173°. The samples were diluted and sonicated in a water bath prior to size analysis. Iron concentration was measured using 1,10-phenanthroline assay as described previously (33). Finally, the absorbance was detected at 510 nm using an Infinite M200 Pro TECAN reader (TECAN).

Apoptosis assay

RAW264.7 cells were seeded at 6000 cells per well in a 96-well black clear-bottom imaging microplate (Corning) in DMEM medium with 4.5 g/L D-glucose and pyruvate (Gibco) supplemented with 10% heat-inactivated (30 minutes at 56 °C) foetal bovine serum (SERANA) and 1% penicillin-streptomycin, and left to attach for 24 hours (37 °C, 5% CO_2). Supernatant of cells was either replaced with 50 µg/ml hVLDL in DMEM or fresh DMEM. After 20 hours (37 °C, 5% CO_2), cells were incubated with iron particles (100 µg Fe/ml) small (S) or large (L) in size with different coatings (citrate, dextran, or CM dextran) in DMEM or fresh DMEM for 1 hour (37 °C, 5% CO_2). Nuclei were stained with Hoechst 33342 (Sigma) in DMEM for 10 minutes (37 °C, 5% CO_2). After washing with Annexin binding buffer (10 mM HEPES, 140 mM NaCl, 5 mM $CaCl_2$; pH 7.37), cells were incubated with 2.5 ng/µl Annexin V for 15 minutes (37 °C, 5% CO_2). Cells were imaged using the BD Pathway 855 (BD Biosciences) and analysed with CellProfiler software 4.0.4 (17).

Statistical analysis

Data are expressed as mean ± SEM. Normal distribution was assessed by Shapiro-Wilkes normality test, followed by Student's t-test or ANOVA for normal distributed data or a non-parametric Mann-Whitney U test or Kruskal-Wallis to compare two or more groups. Sidak or Dunn's multiple comparison test followed significant changes demonstrated by ANOVA or Kruskal-Wallis respectively. Results were considered statistically different when $p < 0.05$.

Results

Iron oxide nanoparticles induce macrophage foam cell apoptosis in vitro*, plaque, liver and spleen* in vivo

RAW264.7 foam cells were formed by preloading with 50 µg/ml hVLDL for 20 hours. 90-minute treatment with the dextran-coated USPIO ferumoxtran (100 µg Fe/ml) increased apoptosis of foam cells compared to normolipidemic RAW macrophages (**Figure 1A**) in a time- and hVLDL concentration-dependent manner (**Figure 1E**). Specifically, foam cells showed apoptotic morphology (blebbing and shrinkage) and 4-fold enhanced TUNEL positivity (**Figure 1A-C**), despite similar iron uptake as normolipidemic macrophages (**Figure 1D**). Together, these data indicate that ferumoxtran preferentially induced apoptosis in lipid-laden foam cells.

These findings were confirmed *in vivo* in ApoE$^{-/-}$ mice fed a WTD for 9 weeks before receiving a single dose of the SPIO platform ferumoxide (0.3 mg Fe/kg), of ferumoxtran (1 mg Fe/kg), or saline. Even these subclinical doses of ferumoxide or ferumoxtran markedly enhanced TUNEL-positive apoptosis in atherosclerotic plaque compared to saline controls (**Figure 2A-D**). As expected from the short follow-up time, plaque size was not affected 24 hours after treatment (**Figure 2E**), also excluding that observed effects were biased by differences in plaque stage.

Superparamagnetic iron oxide nanoparticles induce apoptosis in murine liver and spleen in vivo

Notably, apoptosis was not only limited to atherosclerotic plaques, as macrophage-rich liver and spleen of ApoE$^{-/-}$ mice also showed significant 2.5- to 4-fold increases in TUNEL-positive cells after only a single dose of ferumoxide or ferumoxtran treatment (**Figure 2F** and **2G**). TUNEL-positive cells in the spleen were exclusively localised in the red pulp area (**Supplementary Figure 2**), which harbours mainly marginal metallophilic macrophages. These data clearly show that ferumoxide and ferumoxtran treatment both enhance apoptosis in atherosclerotic lesions and other macrophage-rich tissue in hyperlipidemic mice.

Repeated iron oxide injection shows smaller, but less stable plaques

The effect of ferumoxtran on atherosclerotic lesion progression was studied in LDLR$^{-/-}$ mice fed a WTD for 3 weeks to develop initial lesions and then subjected to weekly ferumoxtran injections (1 mg Fe/kg) for another 5 weeks. Ferumoxtran-treated mice again showed a 5.4-fold increase in TUNEL-positive plaque cells compared to controls (**Figure 2H-J**). Most apoptotic cells were foam cells, and few endothelial and smooth muscle cells, as inferred from cell morphology and location. Repeated ferumoxtran treatment prevented weight gain, but increased serum levels of total, VLDL, and LDL cholesterol (**Supplementary Figure 3**). These findings are in agreement with a study showing that selective depletion of monocytes/macrophages in circulation and peripheral tissue results in increased (V)LDL-derived cholesterol levels with reduced atherogenesis (34). Indeed, atherosclerotic plaque size was reduced in ferumoxtran-treated mice (**Figure 2K**), despite the moderate serum cholesterol

increase. This observation concurs with known effects of enhanced apoptosis on early atherosclerosis (2). Notwithstanding increased apoptosis, plaque macrophage content was increased in ferumoxtran-treated mice (**Figure 2L**), possibly reflective of influx of new phagocytes upon apoptotic eat-me signals.

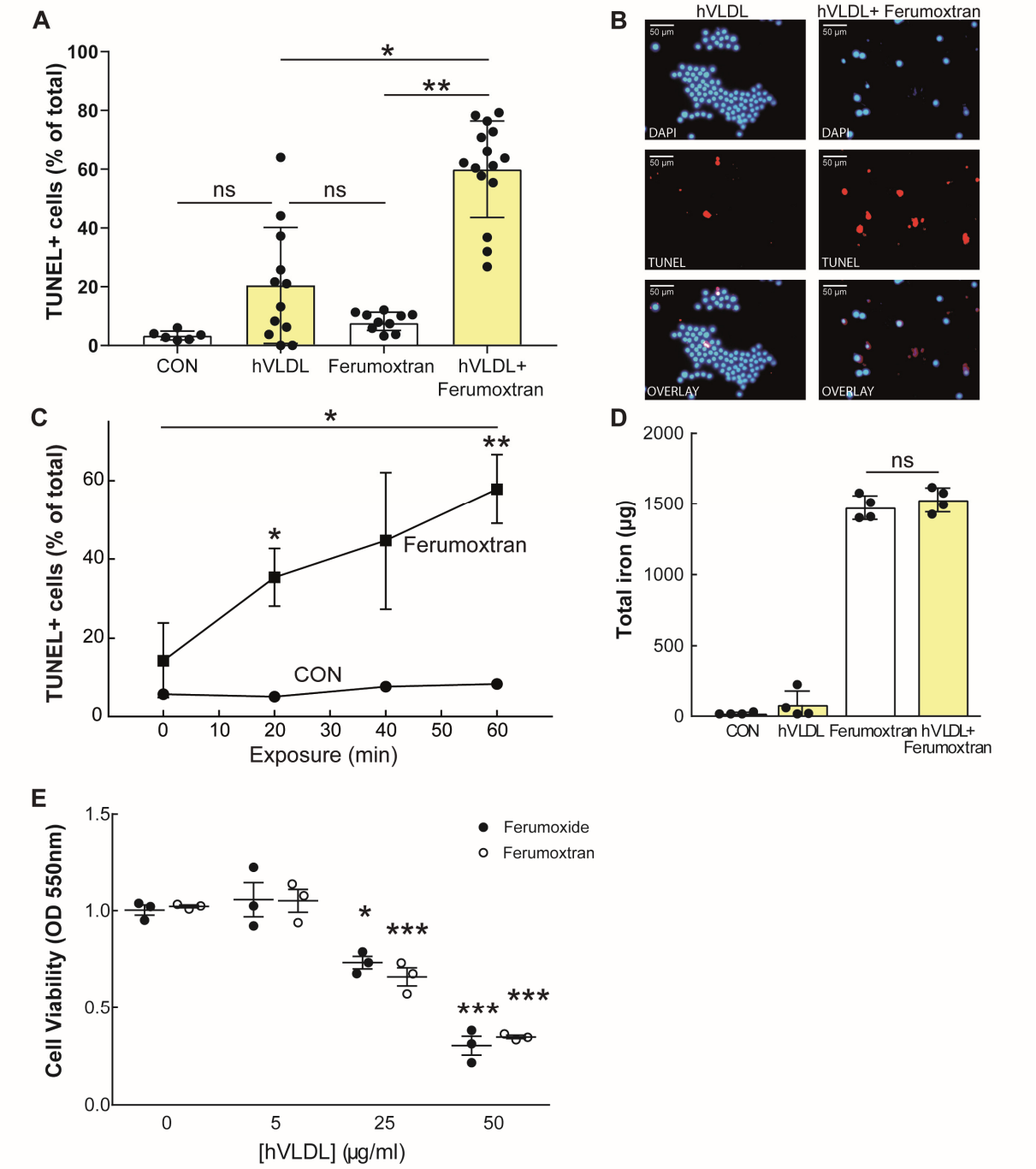

Figure 1: Ferumoxtran exposure increases apoptosis of RAW264.7 foam cells compared to normolipidemic macrophages

(A) RAW264.7 cells were transformed into foam cells (20 hours incubation with hVLDL 50 µg/ml) and incubated with ferumoxtran (USPIO, 100 µg Fe/ml). (B) Fluorescent microscopic pictures of DAPI and TUNEL-stained foam cells incubated with or without ferumoxtran for 1.5 hours. (C) RAW264.7 control macrophages (circles) and foam cells (squares) were harvested at different time points and cytospins were analysed for TUNEL in 3 random fields

of view (magnification 20x; 412 ± 104 cells/cytospin were analysed). (D) The ability of macrophages and foam cells to take up iron-based contrast media was quantitatively analysed using an ICP-AES assay. (E) Cell viability after ferumoxide (100 µg Fe/ml, black circles) or ferumoxtran treatment (white circles) of RAW264.7 cells with different lipid loading were determined using a cytotoxic MTT assay. Data are mean ± SEM (n=3), 4-12 technical replicates, and representative of 3 independent experiments. Statistics: unpaired student's t-test, * p <0.05, ** p <0.01 and *** p <0.001 compared to control conditions. CON: control.

Antioxidant treatment prevents iron oxide nanoparticle-induced apoptosis in vitro *and* in vivo

As iron oxide metabolism has been suggested to lead to oxidative stress (25, 26), we investigated whether this could explain ferumoxtran-induced apoptosis. 24 hours after ferumoxtran injection, serum antioxidant levels were increased as shown by increased uric acid concentration with a consequential increase in TEAC (**Figure 3A** and **3B**), a common response to oxidative stress exposure (35). Uric acid is an established oxidative stress marker. Although uric acid was previously shown to display moderate antioxidant activity, this seems outweighed by its pro-oxidant and pro-inflammatory effects (36). In addition, plaque oxidant damage (8OH-dG) showed a trend to increase (data not shown), and quantitative RT-PCR of ferumoxtran-treated and control foam cells revealed a strong upregulation of oxidative stress-related p22phox (also known as neutrophil cytochrome b light chain), and the pro-apoptotic BCL-2-associated X protein (Bax) and X-linked inhibitor of apoptosis (XIAP) genes (**Figure 3C**). Although nanoparticle-induced ROS have been shown to activate the NLR family pyrin domain containing protein 3 (NLRP3) inflammasome (37), ferumoxtran did neither enhance serum interleukin-1β (IL-1β), nor mRNA expression of IL-1β and NLRP3 in liver and spleens *in vivo* (data not shown). Importantly, ferumoxtran-augmented apoptosis could be prevented by EUK-8 and its more lipophilic O-methyl derivative EUK-134, both antioxidants with superoxide dismutase, catalase, and oxyradical scavenging properties (38). Antioxidant treatment resulted in normalisation of ferumoxtran-induced apoptosis *in vitro* (**Figure 3D**), as well as in $LDLR^{-/-}$ mice with advanced atherosclerosis (**Figure 3E-J**).

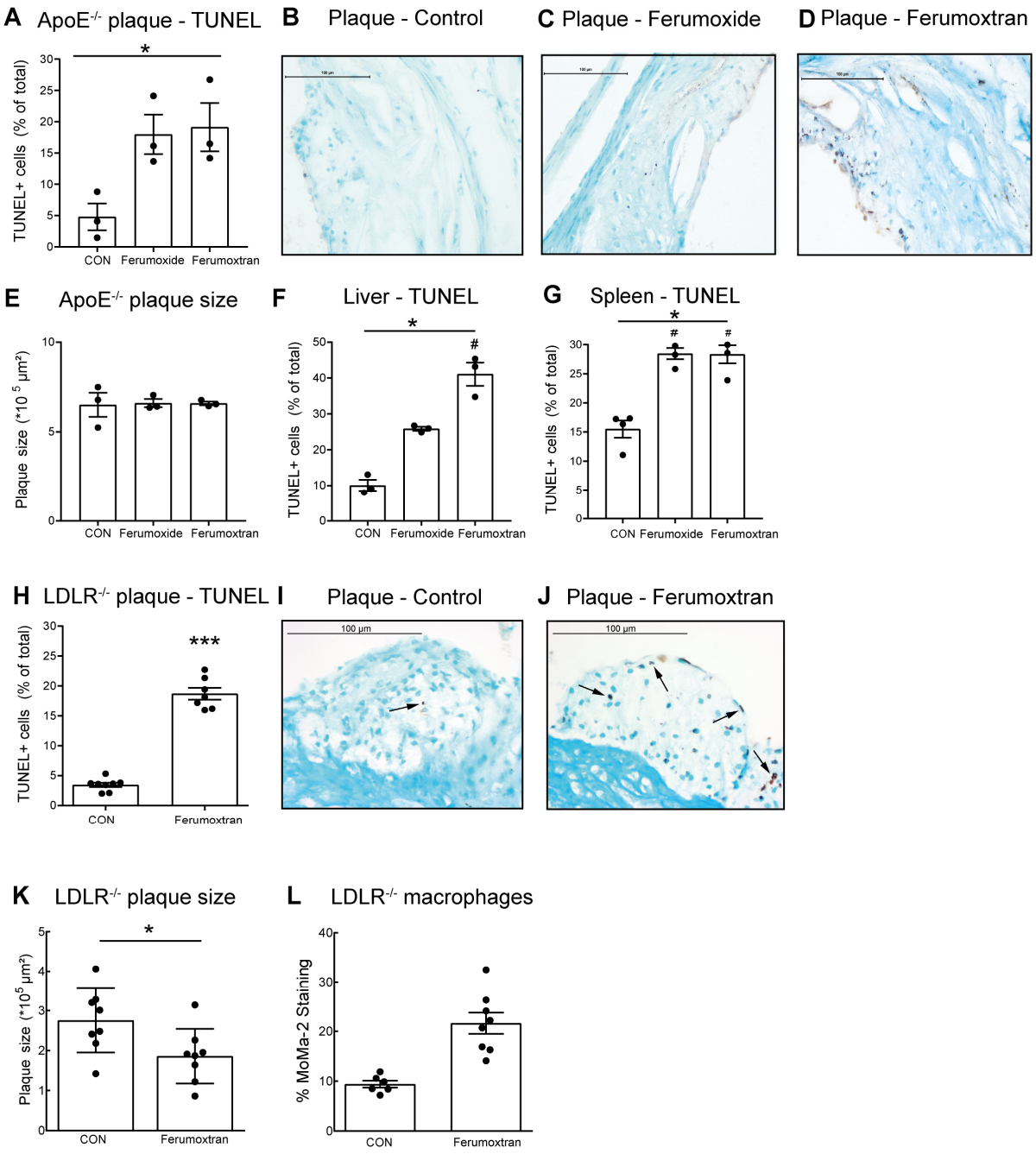

Figure 2: Ferumoxide and ferumoxtran increase apoptosis in atherosclerotic lesions in hyperlipidemic ApoE$^{-/-}$ and LDLR$^{-/-}$ mice

(A) ApoE$^{-/-}$ mice with advanced atherosclerosis were injected once with NaCl 0.9% (n=3), ferumoxide (0.3 mg Fe/kg; n=3) or ferumoxtran (1 mg Fe/kg; n=3). TUNEL-positive cells in the atherosclerotic plaques of the aortic root were quantified and normalised to total cell count. * indicates p-value <0.05 for Kruskal-Wallis across 3 groups, not significant changes in Dunn's post-hoc testing between individual groups. (B) Representative image of TUNEL staining of plaques in control, (C) ferumoxide or (D) ferumoxtran-treated mice. Scale bar in (B) to (D) corresponds to 100 µm. (e) Plaque area of ApoE$^{-/-}$ was determined by computer-assisted morphometric analysis of Oil Red O-stained section. (F) The percentage of TUNEL-positive cells was quantified in liver and (G) spleen of ApoE$^{-/-}$ mice controls and mice receiving a single ferumoxide or ferumoxtran dose. * indicates p-value <0.05 for Kruskal-Wallis across 3 groups, # p-value <0.05 in Dunn's post-hoc testing versus control. (H) LDLR$^{-/-}$ mice with initial plaques were fed a high cholesterol diet and received weekly intravenous injections with NaCl 0.9% (control group, n=8) or ferumoxtran (n=8). The percentage of TUNEL-positive cells was quantified in the atherosclerotic plaques of the aortic root. Unpaired student's t-test, * p <0.05 and *** p <0.001 compared to control conditions.

(I) Representative image of TUNEL staining of plaques in control, and (J) ferumoxtran-treated LDLR$^{-/-}$ mice. (K) Plaque area (Oil Red O) and (L) the percentage of macrophages (MoMa-2-positive) cells were quantified in plaques of control LDLR$^{-/-}$ and mice repeatedly treated with ferumoxtran. Statistics: unpaired student's t-test, * p <0.05 and *** p <0.001 compared to control conditions. Data are mean ± SEM. CON: control.

Superparamagnetic iron oxide nanoparticles associated with enhanced human plaque apoptosis

As ferumoxtran has been widely used as contrast agent for MRI detection of inflammatory human atherosclerosis (6, 9), the potential impact of ferumoxtran treatment on human disease was studied in carotid endarterectomy samples. Samples were collected from symptomatic patients that had received ferumoxtran (2.6 mg Fe/kg I.V., n=9) 2-11 days prior to surgery, and from control patients (n=9), matched for sex, age and plaque phenotype (**Table 1**) (6). All patients were eligible, gave informed consent, and completed all steps of the protocol, and were thus included in the analysis. Notably, the dose used in our mouse model experiments was almost 3 times lower than that used for the clinical study. Electron microscopy detected ferumoxtran mainly in macrophages and smooth muscle cells (**Figure 4A-C**). The percentage of TUNEL-positive apoptotic cells (**Figure 3D-J**; 3.7 ± 1.4 (95% CI of mean: 0.5-6.9) versus 18.2 ± 5.3 (95% CI: 5.9-30.5) for the control and ferumoxtran group, respectively), as well as the number of apoptotic cells per plaque area (33.4 ± 11.1 (95% CI: 7.9-59.0) versus 191.2 ± 48.0 (95% CI: 80.5-301.9) for the control and ferumoxtran group, respectively) was increased 4-fold in atherosclerotic plaque from ferumoxtran-treated compared to untreated patients. Most apoptotic cells were macrophage foam cells (**Figure 4K** and **4L**). TUNEL-positive cells co-localised with CD68-positive macrophages (**Figure 4E** and **4H**) and activated caspase-3 (**Figure 4F** and **4I**). Thus, the use of ferumoxtran in patients with cardiovascular disease aggravated plaque apoptosis, and possibly subsequent plaque instability.

Table 1: Patient characteristics

Patients characteristics		Control (n=9)	Ferumoxtran (n=9)
Gender	Male %; male/female	89%; 8/1	89%; 8/1
Age	Years ± SD	64.6 ± 2.9	63.9 ± 3.2
Plaque type	Thin/thick cap fibroatheroma	67% (n=6)	67% (n=6)
	Intraplaque/luminal thrombus	33% (n=3)	33% (n=3)
Clinical stage	Symptomatic %	100%	100%
Stenosis	Patients % with >70%	100%	100%

No significant p-values.

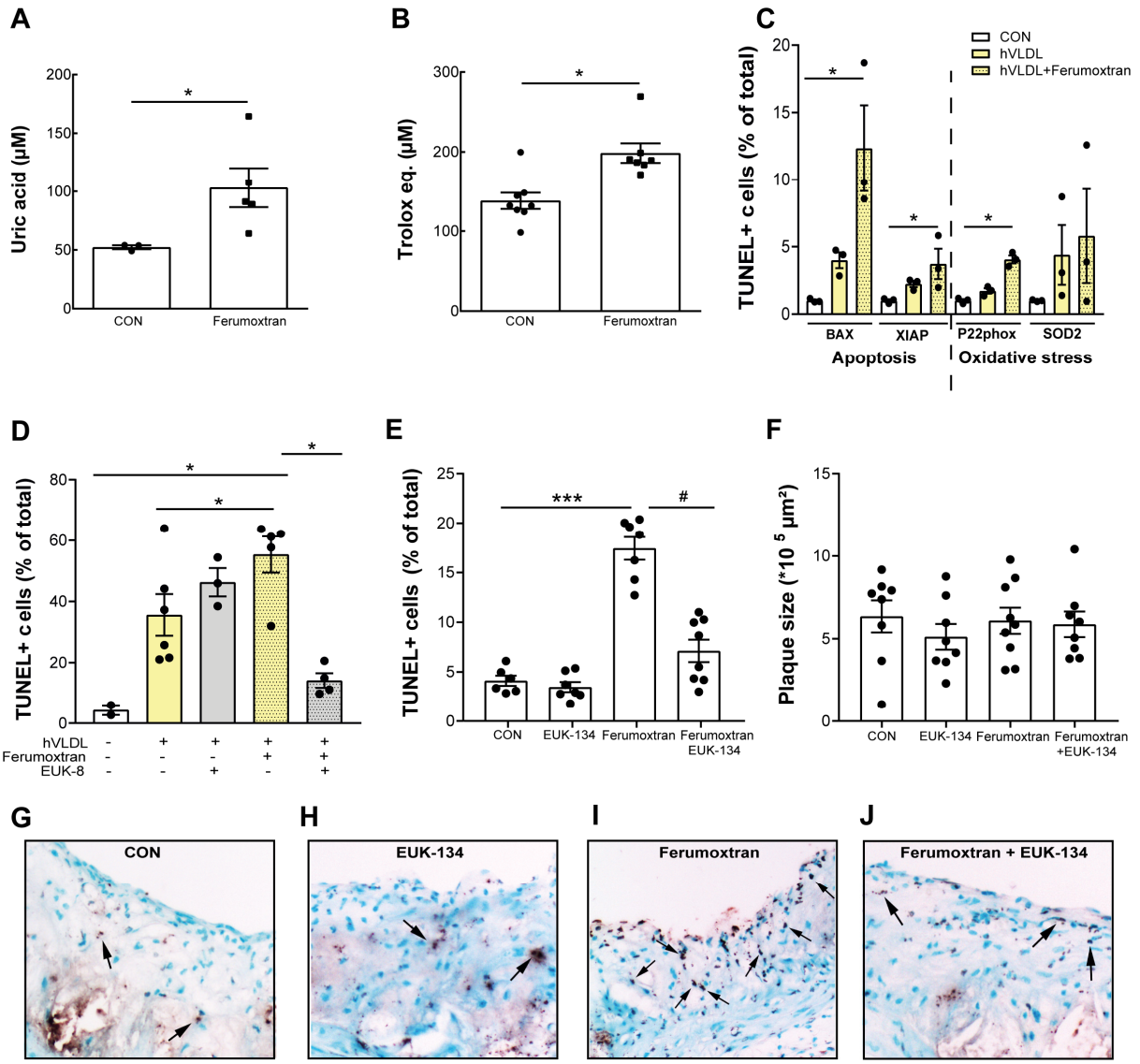

Figure 3. Ferumoxtran triggers ROS-induced apoptosis *in vitro* and *in vivo*

(A) Serum uric acid and (B) Trolox equivalent antioxidant capacity were increased in serum samples of LDLR$^{-/-}$ mice 24 hours after ferumoxtran injection compared to control, a common response to oxidant stress exposure. Statistics: unpaired Student's t-test. Data are mean ± SEM. (C) Gene expression levels of apoptosis- and oxidative stress-related genes of RAW untreated macrophages (white bars), hVLDL–treated foam cells (yellow bars), and hVLDL–treated foam cells exposed to 100 µg/ml ferumoxtran (yellow dotted bars). (D) RAW264.7 cells transformed into foam cells with hVLDL (yellow bars) were incubated with ferumoxtran (dotted filling) to induce apoptosis. Pre-treatment of hVLDL foam cells with antioxidant (grey bars) prior to ferumoxtran reduced apoptosis. Untreated RAW264.7 cells were used as a control (white bars). Cells were harvested, cytospins were made and apoptotic cells quantified by TUNEL analysis in 4 randomly chosen field of views (20x magnification; average 93 ± 27 cells/FOV analysed). Data are mean ± SEM, include 3-6 technical replicates, and are representative of three independent experiments. Statistics: * p <0.05, and p <0.001 versus control (Kruskal-Wallis; Dunn's multiple comparison). (E) LDLR$^{-/-}$ mice on a high cholesterol diet for 6 weeks received a single treatment with either saline (n=8), saline with antioxidant EUK-134 (10 mg/kg, n=8), ferumoxtran alone (1000 µg Fe/kg, n=9), or ferumoxtran with EUK-134 (n=9). The percentage of TUNEL-positive cells was quantified in the atherosclerotic plaques of the aortic root. Statistics: * p <0.05, and p <0.001 versus control (ANOVA; Sidak's multiple comparison). (F) Plaque area (Oil Red O) was quantified in plaques of LDLR$^{-/-}$ treated once with saline, EUK-134, ferumoxtran, or ferumoxtran with EUK-134. (G) Representative image of TUNEL staining of plaques in saline, (H) EUK-134, (I) ferumoxtran, or (J) ferumoxtran with EUK-134 treated LDLR$^{-/-}$ mice. Data are mean ± SEM. CON: control.

New USPIO formulation does not enhance macrophage apoptosis in vitro *or* in vivo

The newly developed CM dextran-coated USPIO ferumoxytol has recently been approved by the U.S. Food and Drug Administration to treat anaemia in chronic kidney patients (39). In light of the initial controversy regarding acute side-effects at time of injection (40) and its use in clinical trials of several cardiovascular diseases (8, 15-19, 41), this new generation USPIO was also tested *in vivo* and *in vitro*. In contrast to prior USPIO formulations, ferumoxytol did not enhance apoptosis in plaques or liver of hypercholesterolemic LDLR$^{-/-}$ mice (**Figure 5A-G**). In line, ferumoxytol did not enhance foam cell apoptosis *in vitro*, despite positive Perl's iron staining (**Figure 5H-J**). This supports a favourable safety profile of ferumoxytol for cardiovascular imaging, in line with recent safety reports (42), and in contrast to ferumoxtran and ferumoxide, the use of which may have side effects on atherosclerotic plaque stability.

Table 2: Nanoparticle characteristics

Feature	Ferumoxide	Ferumoxtran	Ferumoxytol
SPIO/USPIO	SPIO	USPIO	USPIO
Particle size (nm)	120-180	31 ± 5	28 ± 4
Crystal core size (nm)	5	6	6.7
Polydispersity index	n.a.	0.374 ± 0.019	0.252 ± 0.018
Half-life (hours)	2-3	30	15
Coating	Dextran	Dextran	Carboxymethyl dextran
Zeta potential ζ (mV)	n.a.	-27 ± 7.1	-43.9 ± 8.4
Macrophage uptake (pg Fe/cell)*	5.0-7.0	0.5 ± 1.8	1.0-1.5
Mechanism uptake	SRA1	SRA1	SRA1
Clinical dose mg/kg	0.6	4	2.7

Integrated data from (59-61, 64) and own measurements; * THP-1 with 200 µg Fe/ml for 24 hours; SRA1: scavenger receptor A-mediated; n.a.: information not available.

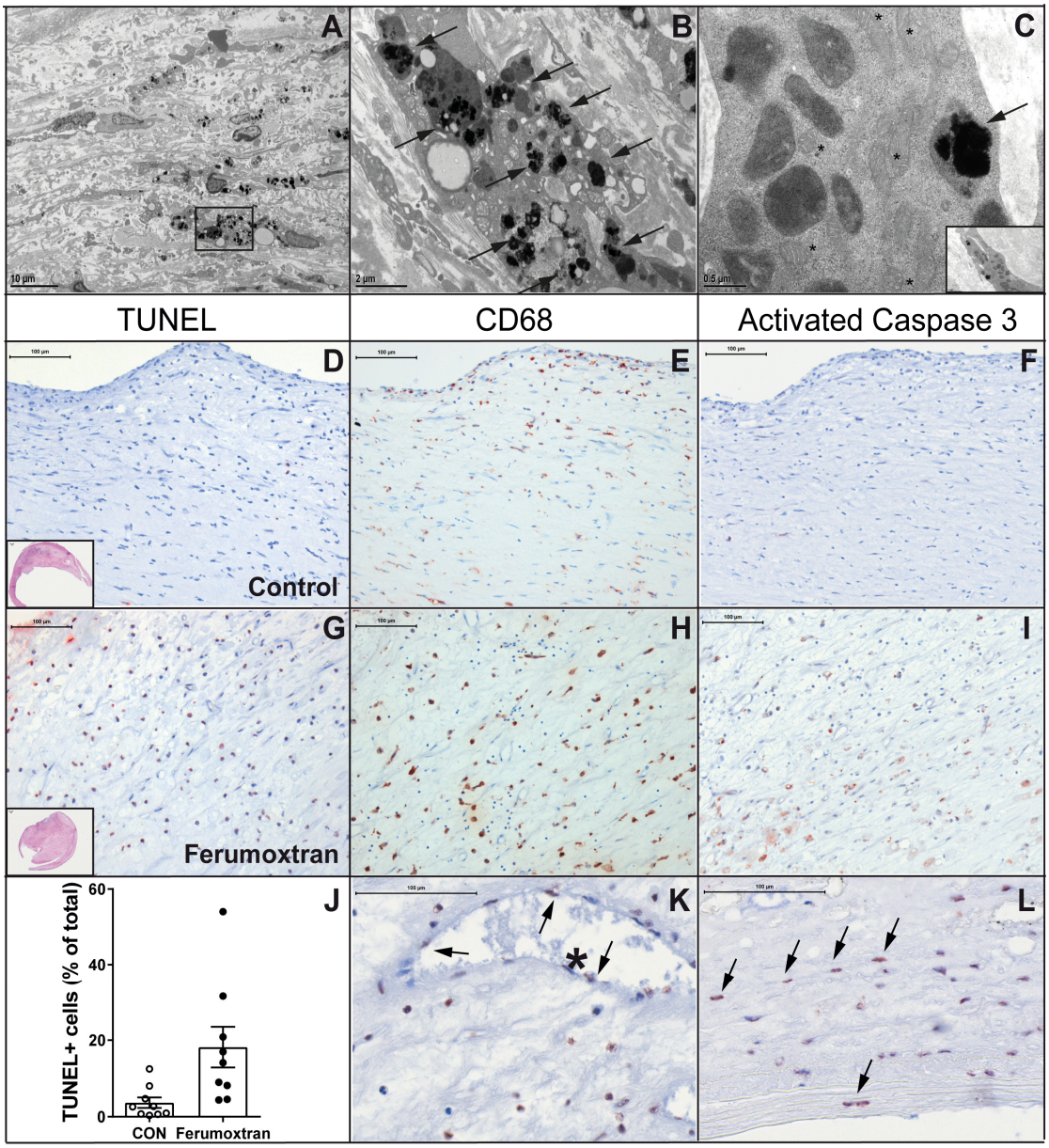

Figure 4: Ferumoxtran increases apoptosis in human carotid atherosclerotic lesions

(A) Electron microscopy shows human carotid atherosclerotic plaque with accumulation of superparamagnetic iron oxide nanoparticles, scale bar corresponds to 10 µm. Boxed region shows particle-laden macrophages, represented in (B) high-power view of macrophage with intracellular ferumoxtran (arrows). Scale bar corresponds to 2 µm. (C) Smooth muscle cell with numerous mitochondria (*) also showing intracellular accumulation of ferumoxtran nanoparticles (arrow). Insert shows origin of smooth muscle cell. Scale bar corresponds to 0.5 µm. (D) Atherosclerotic lesions obtained from symptomatic patients undergoing carotid endarterectomy and receiving no injection (n=9; D-F) or a single dose of ferumoxtran (2.7 mg/kg IV, n=9; G-I) prior to surgery. Sections were stained with TUNEL (AEC red precipitate; D,G). Apoptotic TUNEL-positive cells co-localise with macrophages and activated caspase-3 on serial sections stained respectively with CD68 (red precipitate; E, H), (F) activated caspase 3 (red precipitate; F, I). Scale bars in (D) to (I) corresponds to 100 µm. (H) Apoptosis was quantified as TUNEL-positive cells per total cell count. (K) Arrows indicate TUNEL-positive nuclei in endothelial cells lining an intraplaque microvessel and (L) smooth muscle cells. Scale bars in (K) and (L) correspond to 100 µm. Data are mean ± SEM. Statistics: ** p=0.004 (Mann-Whitney compared to control). CON: control.

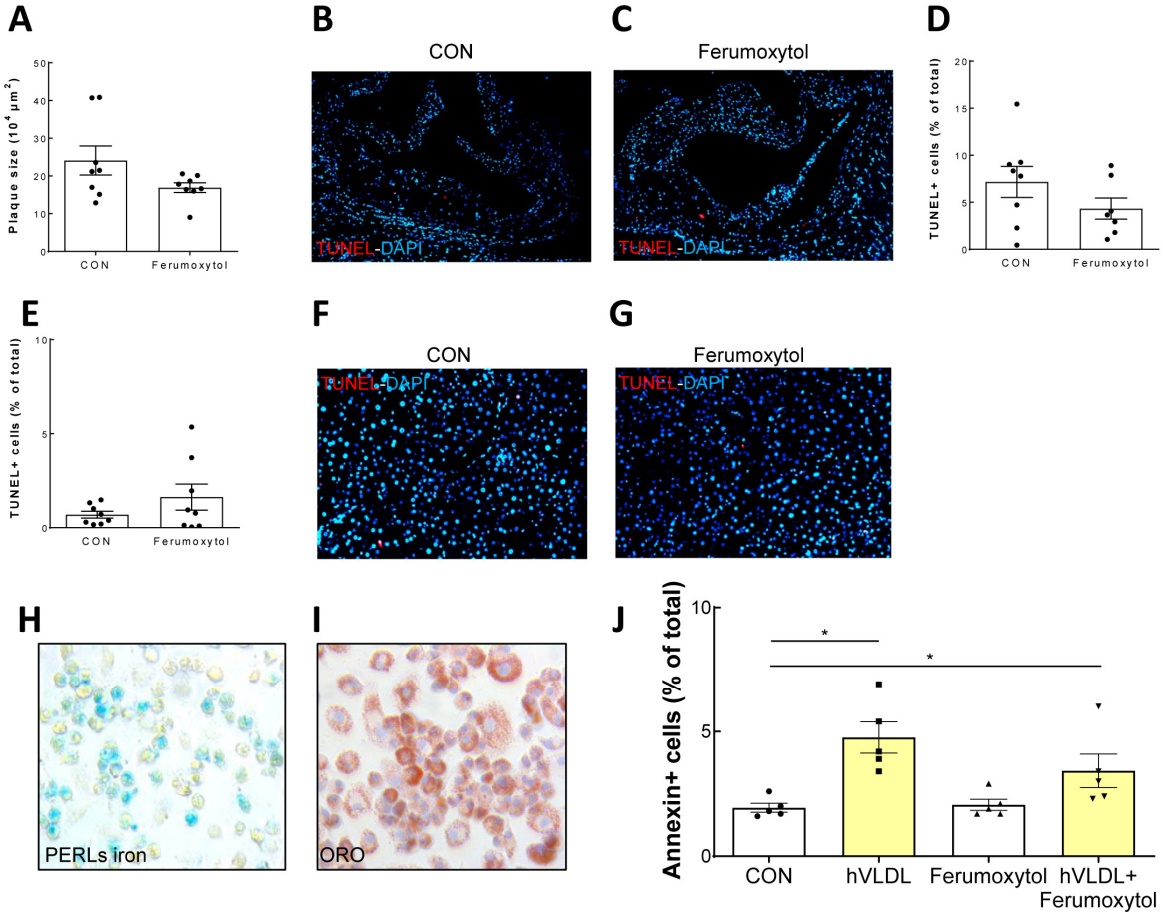

Figure 5: Ferumoxytol does not enhance apoptosis *in vivo* or *in vitro*

(A) Plaque area at sacrifice of LDLR$^{-/-}$ mice with early atherosclerosis which were fed a high cholesterol diet for 9 weeks after single weekly intravenous injections with NaCl 0.9% (control group, n=8) or ferumoxytol (n=8). Representative images of apoptotic cells detected by TUNEL in atherosclerotic plaques of the aortic root of LDLR$^{-/-}$ mice injected with saline (control; B) or ferumoxytol (C), with corresponding quantification (D). Quantification (E) and representative images of apoptotic cells detected by TUNEL in liver of LDLR$^{-/-}$ mice injected with saline (control; F) or ferumoxytol (G). (H) Perl's iron staining of RAW264.7 cells, incubated with hVLDL and ferumoxytol, detects iron accumulation. (I) Oil Red O staining of RAW264.7 cells, incubated with hVLDL and ferumoxytol, confirmed massive lipid accumulation. (J) The percentage of apoptotic, Annexin V-positive cells was quantified by flow cytometry of RAW264.7 cells incubated with or without hVLDL, in the absence or presence of ferumoxytol (n=5-8 technical replicates per group). Data are mean ± SEM. * p <0.05, (unpaired Mann-Whitney test or Kruskal-Wallis with Dunn's multiple comparison test, compared to control). CON: control.

Dextran coating and particle size are not associated with enhanced macrophage apoptosis

Since ferumoxide and ferumoxtran particles are coated with dextran, while ferumoxytol particles are coated with negatively charged CM dextran, the effect of iron particle coating on macrophage apoptosis was investigated. Dextran was avidly taken up by RAW264.7 macrophages (Figure 6A and 6B) but, compared to the untreated control, no significant induction of apoptosis in both foam cells and normolipidemic macrophages was observed (Figure 6C and 6D). Moreover, no significant difference in apoptosis was observed in both normolipidemic and hVLDL-laden RAW264.7 cells incubated with iron nanoparticles coated with citrate, dextran, or CM dextran (Supplementary Figure 4). Particle size itself also did not appear to be a major determinant of USPIO-induced apoptosis (Supplementary Figure 4). Taken together, these findings suggest that neither particle size nor coating accounts for the difference in apoptosis induction found between ferumoxtran and ferumoxytol.

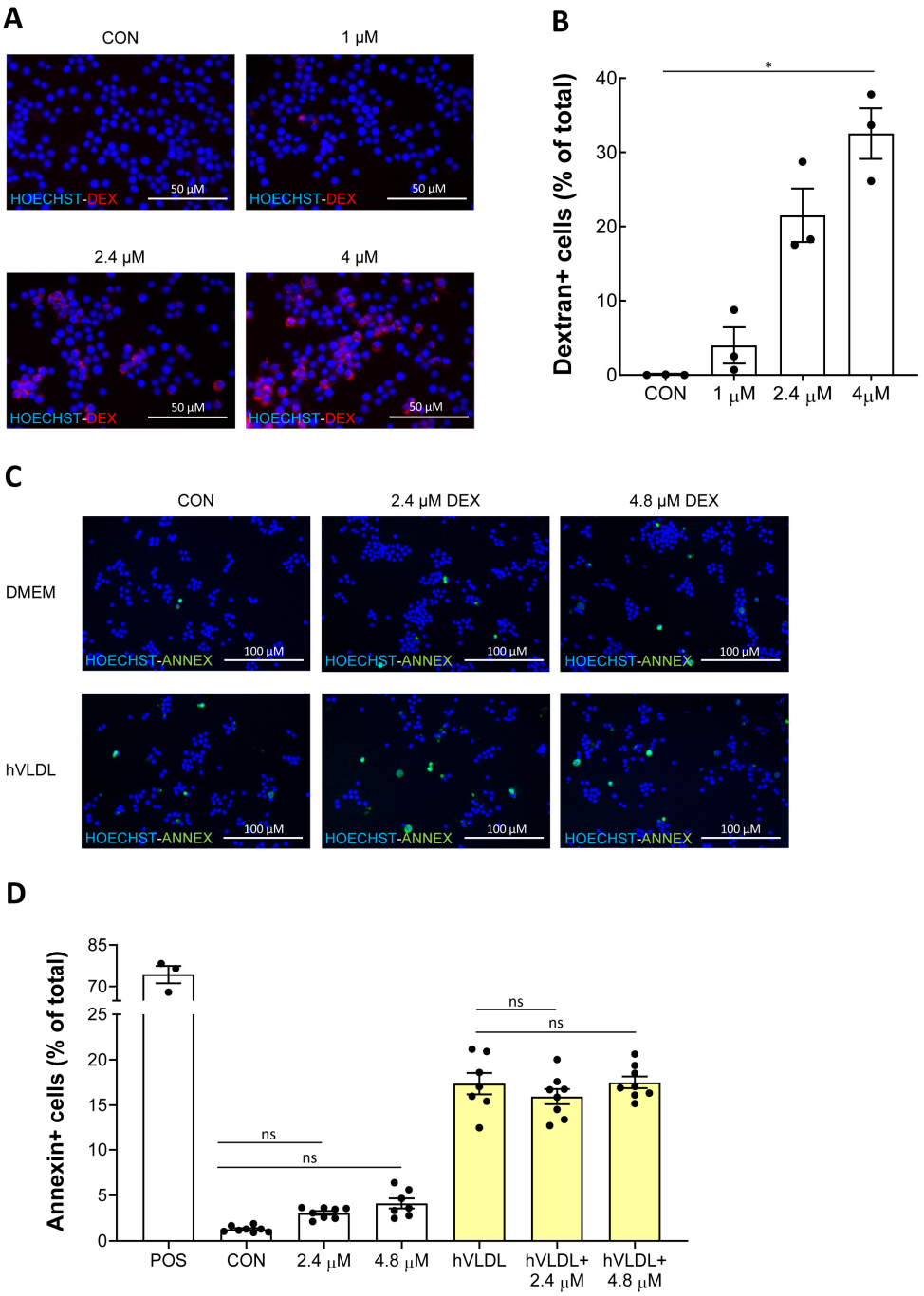

Figure 6: Dextran does not increase apoptosis in RAW foam cells compared to normolipidemic macrophages
(A) Fluorescent microscopic pictures of RAW264.7 incubated with 1 µM, 2.4 µM or 4 µM TRITC-dextran for 1 hour or untreated RAW264.7 (CON) and stained with Hoechst 33342. Per well, 9 fluorescent images were taken and merged, corresponding to around 2700 cells imaged per well, with 3 technical replicates per condition. Scale bars correspond to 50 µm. (B) Quantification of (A), percentage of cells positive for TRITC-dextran. (C) Fluorescent microscopic pictures of RAW264.7 transformed into foam cells with hVLDL (yellow bars) or normolipidemic cells (white bars) exposed to 2.4 µM or 4.8 µM dextran or fresh DMEM for 1 hour. Untreated cells served as control (CON), RAW264.7 cells treated with 1 µM staurosporine for 20 hours served as positive control (POS). Cells were stained with Annexin V and Hoechst 33342. 9 fluorescent images were taken and merged per well, corresponding to around 4400 cells imaged per well, with 3 (POS) or 7-8 technical replicates per conditions. Scale bars correspond to 100 µm. (D) Quantification of (C), percentage of cells positive for Annexin V. Data are presented as mean ± SEM and representative of three independent experiments (C, D). Statistics: * p <0.05 (Kruskal-Wallis with Dunn's multiple comparison test).

Discussion

Collectively, our findings indicate that administration of previous formulations of superparamagnetic iron oxide nanoparticles enhances apoptosis in murine and human atherosclerosis. Despite the large body of evidence supporting the safety of superparamagnetic iron oxide nanoparticles (20, 21), concern is growing that (U)SPIO uptake may lead to intracellular release of iron ions, generation of oxidative stress, and DNA damage, and that it will promote thrombogenicity in the heart (25, 43, 44). Our study shows that ferumoxide and ferumoxtran induce apoptosis and ROS in lipid-laden macrophages and that its effects can be prevented by antioxidant treatment *in vivo* and *in vitro*, pointing to iron oxide-induced oxidative stress as causative factor for USPIO-induced apoptosis. In support of this finding, bare USPIO was seen to induce endothelial cell apoptosis *in vitro,* which was also mediated by USPIO-related ROS, and reversed by antioxidant treatment (45, 46). In fact, we observed occasional endothelial apoptosis in atherosclerotic plaque after treatment with dextran-coated ferumoxide (SPIO), and to a lesser extent ferumoxtran (USPIO). The apparent preference for foam cell apoptosis may be explained by the increased susceptibility to apoptosis of lipid-laden foam cells subjected to a second stressor (23).

Moreover, repeated ferumoxtran treatment of mice with early atherosclerosis not only led to enhanced plaque apoptosis but also increased plaque macrophage accumulation. Interestingly, this did not translate in progressive plaque growth. Although the jury is still out on this notion, increased macrophage apoptosis has indeed been suggested to impede plaque progression in early-stage atherosclerosis as phagocytic clearance of apoptotic cells is fully operative at this stage (34, 47, 48). In contrast, in advanced plaques with compromised efferocytosis (49), accumulating apoptotic cell debris and secondary necrosis will directly promote plaque progression by expansion of the necrotic core and inflammation (2, 50). As ferumoxtran exacerbated plaque apoptosis in mice and patients with advanced atherosclerosis, this raises concerns regarding potentially deleterious effects on plaque progression and destabilisation. This is especially true considering the prolonged residence time of USPIO platforms in tissue. In fact, in porcine heart, USPIO persisted for several months after intracardiac injection of USPIO-labelled stem cells (51). However, our cardiovascular disease (CVD) cohort, with its limited group size, is not fit to draw any conclusions on USPIO treatment-associated clinical adverse events.

Considering the widespread cardiovascular and non-cardiovascular clinical use of USPIO, our findings may have broader impact. USPIO-based imaging has been used for the diagnosis of tumour metastases, autoimmune diseases, rheumatoid arthritis, for targeted stem cell transfer to the infarcted heart, and for treatment of anaemia in patients with chronic kidney disease (21, 51-53). Although ferumoxtran has been discontinued in 2010 (51-54), several trials have been started to test the potential of similar USPIO platforms for diagnosis of prostate cancer (55, 56), head and neck squamous cell carcinoma (57), and aortic dissection (58). Most

applications involve elderly patient populations, expected to suffer from moderate to advanced atherosclerosis. Nevertheless, ferumoxytol, a new generation USPIO equipped with a CM dextran coating, appears to display a safer profile for cardiovascular disease. Biodistribution, macrophage uptake route and speed, and intracellular release of USPIO entrapped iron are dependent on particle and iron core size and composition, coating chemistry and charge and will define the particle's pro-oxidant and pro-apoptotic activity. Dextran-coated SPIOs ferumoxide and ferumoxtran, while differently sized, both acted pro-apoptotic, suggesting that coating (chemistry) may be critical (Table 2) (59-61). However, it has previously been shown that blocking CD206 or CD11b does not reduce SPIO uptake by macrophages, indicating that interaction of the dextran coating with carbohydrate receptors does not notably contribute to SPIO uptake (62). Our data show that dextran polymers of similar size and molecular concentration as the derived SPIO were completely inert, suggesting that particle charge or subtle factors in the SPIO production process may be critical. Net macrophage uptake (and thus gross iron oxide availability) of ferumoxide was highest, followed by ferumoxytol and ferumoxtran (59, 63), which underpins that particle intrinsic factors are decisive. Ferumoxytol uptake, while higher than that of ferumoxtran, did not enhance apoptosis. As ferumoxytol and ferumoxtran differ in coating chemistry and charge (negatively charged CM dextran versus non-ionic dextran) (61), but not in particle size and core composition, this suggests that the former factors are indeed instrumental in its toxicity. The lack of toxicity of citrate- versus dextran-versus CM dextran-coated USPIO particles (33) of similar size, suggest however that the driving determinant may be even more subtle, and relate to differences in coating density or heterogeneity. Nevertheless, our study may reassure recent investigators and their patients on safe use of ferumoxytol (8, 16, 17, 21, 41, 42, 63).

In conclusion, iron-based contrast agents, such as ferumoxide and ferumoxtran increase apoptosis in human and murine atherosclerotic plaque, an effect that can be prevented by antioxidants. Their administration to patients with advanced lesions may result in plaque destabilisation. Although ferumoxytol appears to have a safe cardiovascular profile, our findings indicate that caution should be exercised when applying other iron-based contrast agents in patients with clinical atherosclerosis or other inflammatory disorders that involve lipid-laden macrophages.

Author contributions

F.M.E.S., T.J.C.B. and E.A.L.B. were responsible for conception and design. All authors were involved in analysis and interpretation of data. F.M.E.S., A.V.R., I.B., T.J.C.B., B.H., J.C.S., and E.A.L.B. drafted the manuscript, or revised it critically for important intellectual content. All authors gave final approval of the submitted manuscript and agree to be accountable for all aspects of the work in ensuring that questions related to the accuracy or integrity of any part of the work are appropriately investigated and resolved.

Funding

This work was supported by the Dutch Heart Foundation (Established Investigator NHS 2003T201 to E.A.L.B.; Senior Postdoc 2016T060 to J.C.S.), Guerbet, two VENI fellowships (916.86.04 to I.B.; 016.116.017 to J.C.S.), a VIDI fellowship of the Netherlands Organisation of Scientific Research (NWO; 0.16.186.364 to J.C.S.), an ERC consolidator grant (864121 to T.L.); the German Research Foundation (GRK/RTG2375: 331065168 to T.L.), and the Leducq Foundation Transatlantic Network of Excellence “Modulating autophagy to treat CVD“ (15CVD04 to J.C.S).

Conflicts of interest

The principal investigator (E.A.L.B.) has received financial support for this work from Guerbet.

References

1. Fayad ZA, Fuster V, Fallon JT, Jayasundera T, Worthley SG, Helft G, et al. Noninvasive in vivo human coronary artery lumen and wall imaging using black-blood magnetic resonance imaging. Circulation. 2000;102(5):506-10.
2. Moore KJ, Tabas I. Macrophages in the pathogenesis of atherosclerosis. Cell. 2011;145(3):341-55.
3. Virmani R, Kolodgie FD, Burke AP, Finn AV, Gold HK, Tulenko TN, et al. Atherosclerotic Plaque Progression and Vulnerability to Rupture Angiogenesis as a Source of Intraplaque Hemorrhage. Arterioscler Thromb Vasc Biol. 2005;25(10):2054-61.
4. Briley-Saebo KC, Mani V, Hyafil F, Cornily JC, Fayad ZA. Fractionated Feridex and positive contrast: in vivo MR imaging of atherosclerosis. Magn Reson Med. 2008;59(4):721-30.
5. Dadfar SM, Roemhild K, Drude NI, von Stillfried S, Knüchel R, Kiessling F, et al. Iron oxide nanoparticles: Diagnostic, therapeutic and theranostic applications. Adv Drug Deliv Rev. 2019;138:302-25.
6. Kooi ME, Cappendijk VC, Cleutjens KB, Kessels AG, Kitslaar PJ, Borgers M, et al. Accumulation of ultrasmall superparamagnetic particles of iron oxide in human atherosclerotic plaques can be detected by in vivo magnetic resonance imaging. Circulation. 2003;107(19):2453-8.
7. Ruehm SG, Corot C, Vogt P, Kolb S, Debatin JF. Magnetic resonance imaging of atherosclerotic plaque with ultrasmall superparamagnetic particles of iron oxide in hyperlipidemic rabbits. Circulation. 2001;103(3):415-22.
8. Smits LP, Tiessens F, Zheng KH, Stroes ES, Nederveen AJ, Coolen BF. Evaluation of ultrasmall superparamagnetic iron-oxide (USPIO) enhanced MRI with ferumoxytol to quantify arterial wall inflammation. Atherosclerosis. 2017;263:211-8.
9. Trivedi RA, JM UK-I, Graves MJ, Cross JJ, Horsley J, Goddard MJ, et al. In vivo detection of macrophages in human carotid atheroma: temporal dependence of ultrasmall superparamagnetic particles of iron oxide-enhanced MRI. Stroke. 2004;35(7):1631-5.
10. Zheng KH, Schoormans J, Stiekema LCA, Calcagno C, Cicha I, Alexiou C, et al. Plaque Permeability Assessed With DCE-MRI Associates With USPIO Uptake in Patients With Peripheral Artery Disease. JACC Cardiovasc Imaging. 2019;12(10):2081-3.
11. Hanini A, Schmitt A, Kacem K, Chau F, Ammar S, Gavard J. Evaluation of iron oxide nanoparticle biocompatibility. Int J Nanomedicine. 2011;6:787-94.
12. Olzinski AR, Turner GH, Bernard RE, Karr H, Cornejo CA, Aravindhan K, et al. Pharmacological inhibition of C-C chemokine receptor 2 decreases macrophage infiltration in the aortic root of the human C-C chemokine receptor 2/apolipoprotein E-/- mouse: magnetic resonance imaging assessment. Arterioscler Thromb Vasc Biol. 2010;30(2):253-9.
13. Rogers WJ, Basu P. Factors regulating macrophage endocytosis of nanoparticles: implications for targeted magnetic resonance plaque imaging. Atherosclerosis. 2005;178(1):67-73.
14. von Zur Muhlen C, von Elverfeldt D, Bassler N, Neudorfer I, Steitz B, Petri-Fink A, et al. Superparamagnetic iron oxide binding and uptake as imaged by magnetic resonance is mediated by the integrin receptor Mac-1 (CD11b/CD18): implications on imaging of atherosclerotic plaques. Atherosclerosis. 2007;193(1):102-11.
15. Richards JM, Semple SI, MacGillivray TJ, Gray C, Langrish JP, Williams M, et al. Abdominal aortic aneurysm growth predicted by uptake of ultrasmall superparamagnetic particles of iron oxide: a pilot study. Circ Cardiovasc Imaging. 2011;4(3):274-81.
16. Stirrat CG, Alam SR, MacGillivray TJ, Gray CD, Dweck MR, Dibb K, et al. Ferumoxytol-enhanced magnetic resonance imaging in acute myocarditis. Heart. 2018;104(4):300-5.
17. Stirrat CG, Alam SR, MacGillivray TJ, Gray CD, Dweck MR, Raftis J, et al. Ferumoxytol-enhanced magnetic resonance imaging assessing inflammation after myocardial infarction. Heart. 2017;103(19):1528-35.
18. Investigators MRS. Aortic Wall Inflammation Predicts Abdominal Aortic Aneurysm Expansion, Rupture, and Need for Surgical Repair. Circulation. 2017;136(9):787-97.
19. Lagan J, Naish JH, Simpson K, Zi M, Cartwright EJ, Foden P, et al. Substrate for the Myocardial Inflammation-Heart Failure Hypothesis Identified Using Novel USPIO Methodology. JACC Cardiovasc Imaging. 2021;14(2):365-76.
20. Bourrinet P, Bengele HH, Bonnemain B, Dencausse A, Idee JM, Jacobs PM, et al. Preclinical safety and pharmacokinetic profile of ferumoxtran-10, an ultrasmall superparamagnetic iron oxide magnetic resonance contrast agent. Invest Radiol. 2006;41(3):313-24.

21. Macdougall IC, Strauss WE, McLaughlin J, Li Z, Dellanna F, Hertel J. A randomized comparison of ferumoxytol and iron sucrose for treating iron deficiency anemia in patients with CKD. Clin J Am Soc Nephrol. 2014;9(4):705-12.
22. Muller K, Skepper JN, Posfai M, Trivedi R, Howarth S, Corot C, et al. Effect of ultrasmall superparamagnetic iron oxide nanoparticles (Ferumoxtran-10) on human monocyte-macrophages in vitro. Biomaterials. 2007;28(9):1629-42.
23. Devries-Seimon T, Li Y, Yao PM, Stone E, Wang Y, Davis RJ, et al. Cholesterol-induced macrophage apoptosis requires ER stress pathways and engagement of the type A scavenger receptor. J Cell Biol. 2005;171(1):61-73.
24. Hung YC, Hong MY, Huang GS. Cholesterol loading augments oxidative stress in macrophages. FEBS Lett. 2006;580(3):849-61.
25. Briley-Saebo K, Bjornerud A, Grant D, Ahlstrom H, Berg T, Kindberg GM. Hepatic cellular distribution and degradation of iron oxide nanoparticles following single intravenous injection in rats: implications for magnetic resonance imaging. Cell Tissue Res. 2004;316(3):315-23.
26. Fayad ZA, Razzouk L, Briley-Saebo KC, Mani V. Iron oxide magnetic resonance imaging for atherosclerosis therapeutic evaluation: still "rusty?". J Am Coll Cardiol. 2009;53(22):2051-2.
27. Guildford AL, Poletti T, Osbourne LH, Di Cerbo A, Gatti AM, Santin M. Nanoparticles of a different source induce different patterns of activation in key biochemical and cellular components of the host response. J R Soc Interface. 2009;6(41):1213-21.
28. Redgrave TG, Roberts DC, West CE. Separation of plasma lipoproteins by density-gradient ultracentrifugation. Anal Biochem. 1975;65(1-2):42-9.
29. Virmani R, Kolodgie FD, Burke AP, Farb A, Schwartz SM. Lessons from sudden coronary death: a comprehensive morphological classification scheme for atherosclerotic lesions. Arterioscler Thromb Vasc Biol. 2000;20(5):1262-75.
30. Fischer MA, Gransier TJ, Beckers LM, Bekers O, Bast A, Haenen GR. Determination of the antioxidant capacity in blood. Clin Chem Lab Med. 2005;43(7):735-40.
31. Chomczynski P, Sacchi N. Single-step method of RNA isolation by acid guanidinium thiocyanate-phenol-chloroform extraction. Anal Biochem. 1987;162(1):156-9.
32. Lamprecht MR, Sabatini DM, Carpenter AE. CellProfiler: free, versatile software for automated biological image analysis. Biotechniques. 2007;42(1):71-5.
33. Dadfar SM, Camozzi D, Darguzyte M, Roemhild K, Varvarà P, Metselaar J, et al. Size-isolation of superparamagnetic iron oxide nanoparticles improves MRI, MPI and hyperthermia performance. J Nanobiotechnology. 2020;18(1):22.
34. Stoneman V, Braganza D, Figg N, Mercer J, Lang R, Goddard M, et al. Monocyte/macrophage suppression in CD11b diphtheria toxin receptor transgenic mice differentially affects atherogenesis and established plaques. Circ Res. 2007;100(6):884-93.
35. Ames BN, Cathcart R, Schwiers E, Hochstein P. Uric acid provides an antioxidant defense in humans against oxidant- and radical-caused aging and cancer: a hypothesis. Proc Natl Acad Sci U S A. 1981;78(11):6858-62.
36. Esen AM, Akcakoyun M, Esen O, Acar G, Emiroglu Y, Pala S, et al. Uric acid as a marker of oxidative stress in dilatation of the ascending aorta. Am J Hypertens. 2011;24(2):149-54.
37. Zhou R, Yazdi AS, Menu P, Tschopp J. A role for mitochondria in NLRP3 inflammasome activation. Nature. 2011;469(7329):221-5.
38. Rong Y, Doctrow SR, Tocco G, Baudry M. EUK-134, a synthetic superoxide dismutase and catalase mimetic, prevents oxidative stress and attenuates kainate-induced neuropathology. Proc Natl Acad Sci U S A. 1999;96(17):9897-902.
39. Lu M, Cohen MH, Rieves D, Pazdur R. FDA report: Ferumoxytol for intravenous iron therapy in adult patients with chronic kidney disease. Am J Hematol. 2010;85(5):315-9.
40. FDA. FDA Drug Safety Communication: FDA strengthens warnings and changes prescribing instructions to decrease the risk of serious allergic reactions with anemia drug Feraheme (ferumoxytol). 2016. Available from: https://www.fda.gov/drugs/drug-safety-and-availability/fda-drug-safety-communication-fda-strengthens-warnings-and-changes-prescribing-instructions-decrease.
41. Usman A, Patterson AJ, Yuan J, Cluroe A, Patterson I, Graves MJ, et al. Ferumoxytol-enhanced three-dimensional magnetic resonance imaging of carotid atheroma- a feasibility and temporal dependence study. Sci Rep. 2020;10(1):1808.

42. Wetmore JB, Weinhandl ED, Zhou J, Gilbertson DT. Relative Incidence of Acute Adverse Events with Ferumoxytol Compared to Other Intravenous Iron Compounds: A Matched Cohort Study. PLoS One. 2017;12(1):e0171098.
43. Shen Y, Huang Z, Liu X, Qian J, Xu J, Yang X, et al. Iron-induced myocardial injury: an alarming side effect of superparamagnetic iron oxide nanoparticles. J Cell Mol Med. 2015;19(8):2032-5.
44. Nemmar A, Beegam S, Yuvaraju P, Yasin J, Tariq S, Attoub S, et al. Ultrasmall superparamagnetic iron oxide nanoparticles acutely promote thrombosis and cardiac oxidative stress and DNA damage in mice. Part Fibre Toxicol. 2016;13(1):22.
45. Buyukhatipoglu K, Clyne AM. Superparamagnetic iron oxide nanoparticles change endothelial cell morphology and mechanics via reactive oxygen species formation. J Biomed Mater Res A. 2011;96(1):186-95.
46. Zhu M-T, Wang B, Wang Y, Yuan L, Wang H-J, Wang M, et al. Endothelial dysfunction and inflammation induced by iron oxide nanoparticle exposure: Risk factors for early atherosclerosis. Toxicol Lett. 2011;203(2):162-71.
47. Babaev VR, Chew JD, Ding L, Davis S, Breyer MD, Breyer RM, et al. Macrophage EP4 deficiency increases apoptosis and suppresses early atherosclerosis. Cell Metab. 2008;8(6):492-501.
48. Boesten LS, Zadelaar AS, van Nieuwkoop A, Hu L, Teunisse AF, Jochemsen AG, et al. Macrophage p53 controls macrophage death in atherosclerotic lesions of Apolipoprotein E deficient mice. Atherosclerosis. 2009;207(2):399-404.
49. Schrijvers DM, De Meyer GR, Kockx MM, Herman AG, Martinet W. Phagocytosis of apoptotic cells by macrophages is impaired in atherosclerosis. Arterioscler Thromb Vasc Biol. 2005;25(6):1256-61.
50. Thorp E, Li G, Seimon TA, Kuriakose G, Ron D, Tabas I. Reduced apoptosis and plaque necrosis in advanced atherosclerotic lesions of Apoe-/- and Ldlr-/- mice lacking CHOP. Cell Metab. 2009;9(5):474-81.
51. Kawamura M, Miyagawa S, Fukushima S, Saito A, Miki K, Ito E, et al. Enhanced survival of transplanted human induced pluripotent stem cell-derived cardiomyocytes by the combination of cell sheets with the pedicled omental flap technique in a porcine heart. Circulation. 2013;128(11 Suppl 1):S87-94.
52. Harisinghani MG, Barentsz J, Hahn PF, Deserno WM, Tabatabaei S, van de Kaa CH, et al. Noninvasive detection of clinically occult lymph-node metastases in prostate cancer. N Engl J Med. 2003;348(25):2491-9.
53. Beckmann N, Falk R, Zurbrugg S, Dawson J, Engelhardt P. Macrophage infiltration into the rat knee detected by MRI in a model of antigen-induced arthritis. Magn Reson Med. 2003;49(6):1047-55.
54. Bietenbeck M, Florian A, Sechtem U, Yilmaz A. The diagnostic value of iron oxide nanoparticles for imaging of myocardial inflammation – quo vadis? JCMR. 2015;17(1):54.
55. NIH. Ferumoxtran-10-enhanced MRI in Prostate Cancer Patients. Available from: https://ClinicalTrials.gov/show/NCT04261777.
56. NIH. Radio Guided Lymph Node Dissection in Oligometastatic Prostate Cancer Patients. Available from: https://ClinicalTrials.gov/show/NCT04300673.
57. NIH: Validation of USPIO-enhanced MRI for Detection of Lymph Node Metastases in Head and Neck Carcinoma. Available from: https://ClinicalTrials.gov/show/NCT03817307.
58. NIH: Magnetic Resonance Imaging (MRI) for Aortic Dissection to Visualise Inflammation. Available from: https://ClinicalTrials.gov/show/NCT03948555.
59. Modo MMJJ, Bulte JWM. Molecular and cellular MR imaging. Boca Raton: CRC Press; 2007.
60. Alam SR, Stirrat C, Richards J, Mirsadraee S, Semple SI, Tse G, et al. Vascular and plaque imaging with ultrasmall superparamagnetic particles of iron oxide. J Cardiovasc Magn Reson. 2015;17(1):83.
61. Wang G, Serkova NJ, Groman EV, Scheinman RI, Simberg D. Feraheme (Ferumoxytol) Is Recognized by Proinflammatory and Anti-inflammatory Macrophages via Scavenger Receptor Type AI/II. Mol Pharm. 2019;16(10):4274-81.
62. Chao Y, Karmali PP, Simberg D. Role of carbohydrate receptors in the macrophage uptake of dextran-coated iron oxide nanoparticles. Adv Exp Med Biol. 2012;733:115-23.
63. Yancy AD, Olzinski AR, Hu TC, Lenhard SC, Aravindhan K, Gruver SM, et al. Differential uptake of ferumoxtran-10 and ferumoxytol, ultrasmall superparamagnetic iron oxide contrast agents in rabbit: critical determinants of atherosclerotic plaque labeling. J Magn Reson Imaging. 2005;21(4):432-42.
64. Said B, McCart JA, Libutti SK, Choyke PL. Ferumoxide-enhanced MRI in patients with colorectal cancer and rising CEA: surgical correlation in early recurrence. Magn Reson Imaging. 2000;18(3):305-9.

Supplementary material

Supplementary Table 1
Primer sequences.

Gene	Forward primer	Reverse primer
p22phox	5’-GCCATTGCCAGTGTGATCTA -3’	5’-AATGGGAGTCCACTGCTCAC-3’
XIAP	5'-GAGTTCTGATAGGAATTTCCCAAATT-3'	5'-AACGACCCGTGCTTCATATTCT-3'
Bax	5'-CGTGGTTGCCCTCTTCTACTTT-3	5’-TGATCAGCTCGGGCACTTTA-3
SOD2	5'-ACGTTGGATGGCTTTCTCGTCTTCAGCACC-3'	5'-ACGTTGGATGTTCTGCCTGGAGCCCAGATAC-3'
IL-1β	5'-TACCTGTGGCCTTGGGCCTCAA-3'	5'-GCTTGGGATCCACACTCTCCAGCT-3'
NLRP3	5'-GCACCAACCGGAGCCTCACT-3'	5'-AGCGCCCCAACCACAGTCTC -3'
HPRT	5'-TTGCTCGAGATGTCATGAAGGA-3'	5'-AGCAGGTCAGCAAAGAACTTATAG-3'

Supplementary Table 2
Characteristics of synthesized nanoparticles. Values are given ± SD. PDI: Polydispersity Index.

Name	Citrate		1 kD-Dextran		10 kD-Dextran		CM-Dextran	
Coating	Citrate		Dextran (1 kD)		Dextran (10 kD)		Carboxymethylated dextran (10-20 kD)	
	S	L	S	L	S	L	S	L
Particle size (nm)	26 ± 1	115 ± 1	25 ± 2	107 ± 2	30 ± 2	105 ± 1	39 ± 3	110 ± 3
PDI	0.099 ± 0.005	0.113 ± 0.008	0.189 ± 0.015	0.138 ± 0.007	0.191 ± 0.011	0.154 ± 0.009	0.191 ± 0.011	0.144 ± 0.007
Zeta potential (mV)	-45 ± 7.1	-53.9 ± 9.3	-26.1 ± 6.2	-21.4 ± 7.1	-19.5 ± 5.1	-16.3 ± 4.1	-37.2 ± 3.4	-39.9 ± 5.2

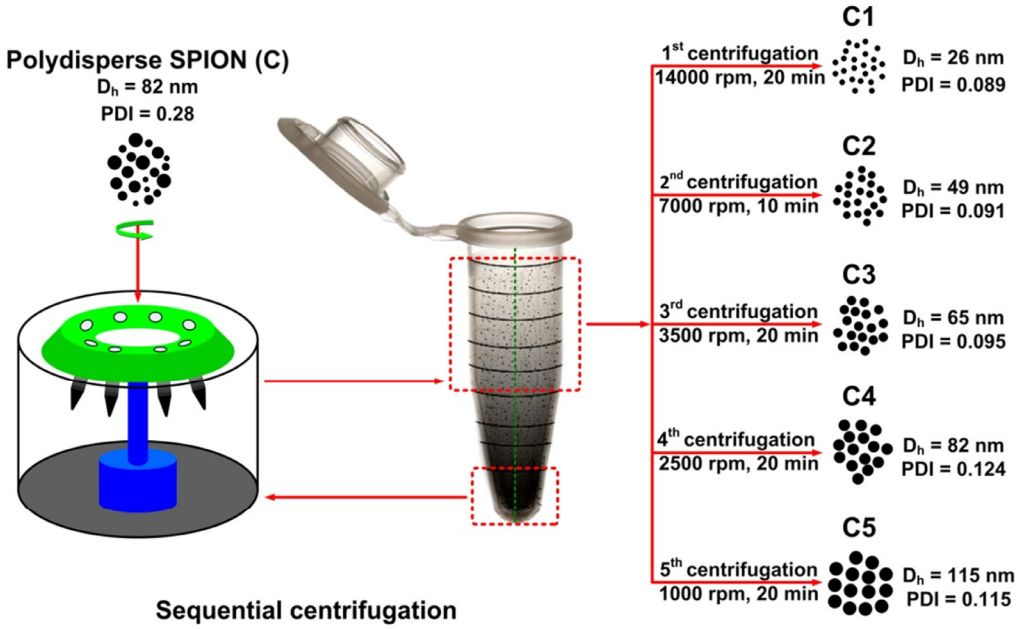

Supplementary Figure 1: Iron oxide particle synthesis

Iron oxide particle fractionation strategy via sequential centrifugation. Schematic overview of the centrifugation protocol to obtain monodispersed iron oxide particle with different hydrodynamic diameters from a crude mixture of polydisperse particles. The polydisperse sample (C) was transferred into 1.5 ml Eppendorf tubes and centrifuged at 14,000 rpm for 20 minutes. The resulting 1 ml of supernatant was collected (1st centrifugation sample, referred to as Citrate S). 0.1 ml of the bottom compartment in the Eppendorf tube was resuspended in water and again centrifuged, and the top 1 ml was collected. These steps were repeated multiple times to yield Citrate L particles (5th centrifugation). The image is reproduced from Dadfar et al., J. Nanobiotechnology 2020 (33).

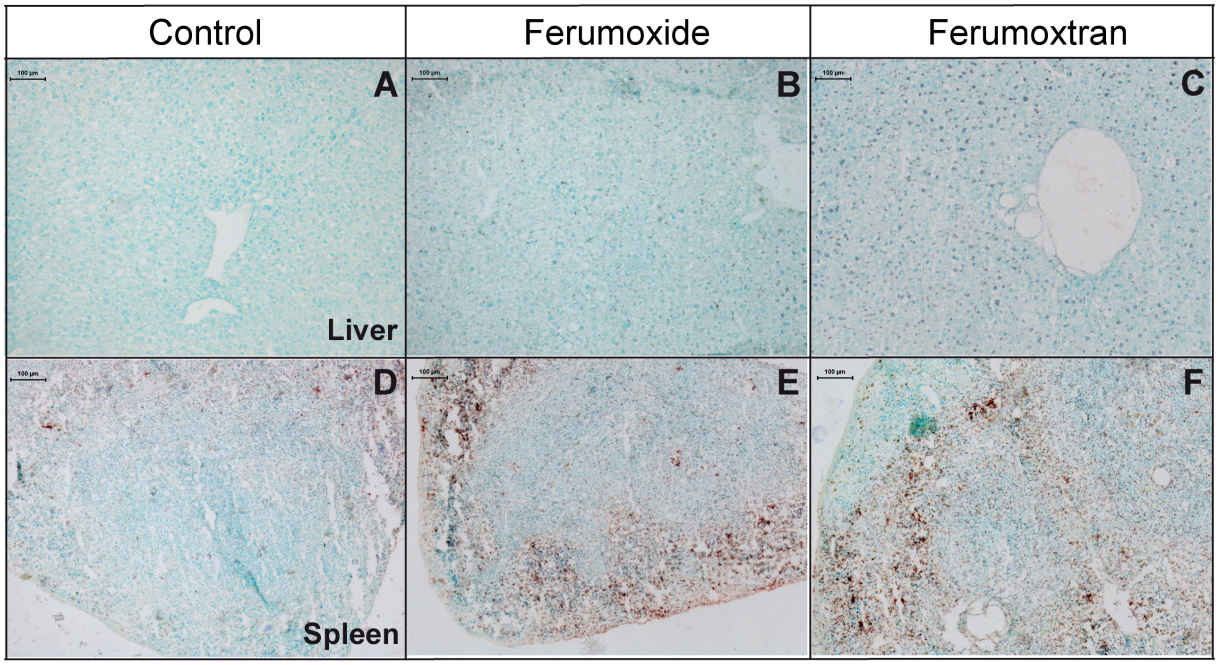

Supplementary Figure 2: Apoptosis in liver and spleen of ferumoxide/ferumoxtran-treated mice
(A) Representative image of TUNEL staining of liver and (B) spleen of single-treated control, ferumoxide or ferumoxtran-treated ApoE$^{-/-}$ mice.

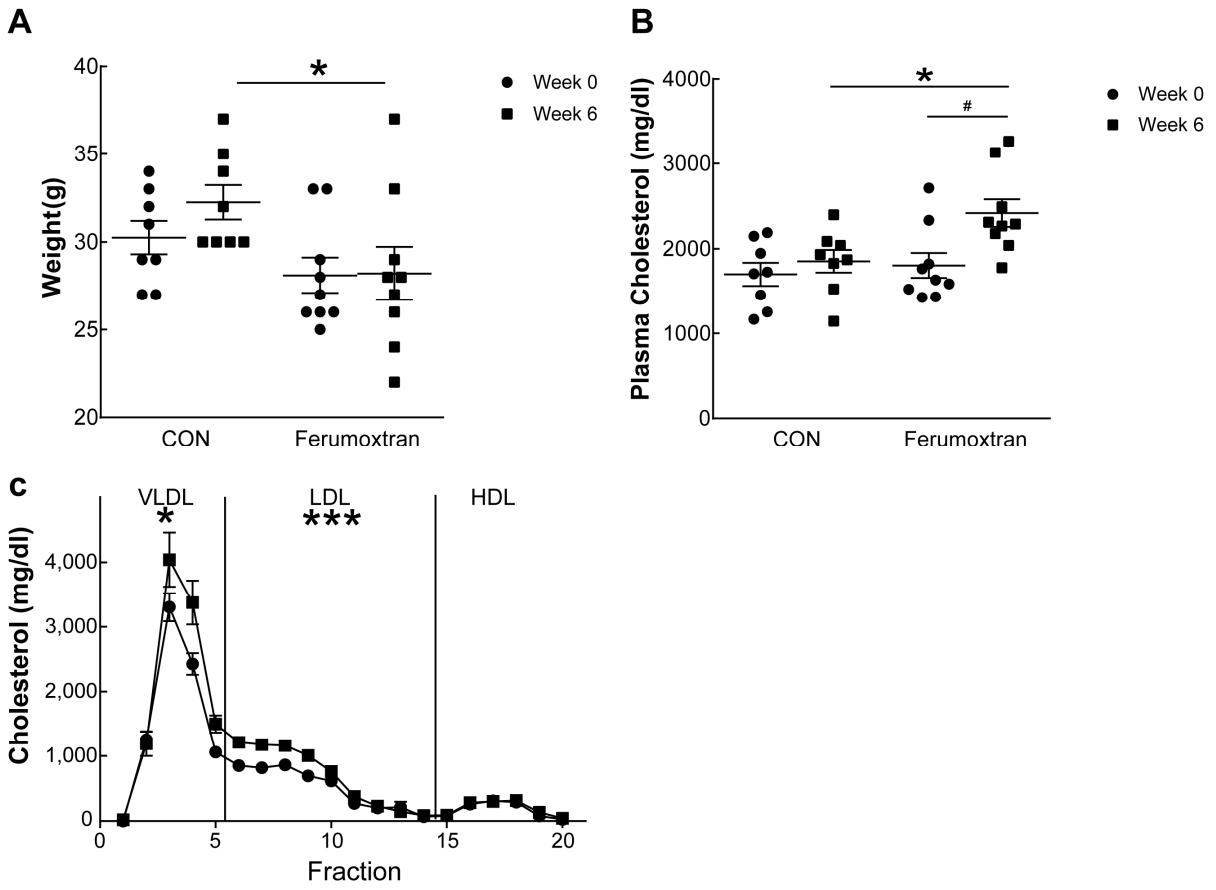

Supplementary Figure 3: Repeated *in vivo* ferumoxtran injections affect weight and cholesterol levels in hyperlipidemic LDLR$^{-/-}$ mice

(A) Weight and (B) serum cholesterol of LDLR$^{-/-}$ mice before and after 5-week treatment with NaCl 0.9% (control group, n=8) or ferumoxtran (n=8). (C) Lipoprotein fraction analysis of control (circles) and ferumoxtran-treated mice (squares) was performed using SMART analysis to identify differences in lipoprotein profiles. Data are mean ± SEM. Statistics: * p <0.05 (unpaired Mann-Whitney U compared to control week 0); # p <0.05 (unpaired Mann-Whitney U compared to ferumoxtran week 0). VLDL: very-low-density lipoprotein; LDL: low-density lipoprotein; HDL: high-density lipoprotein.

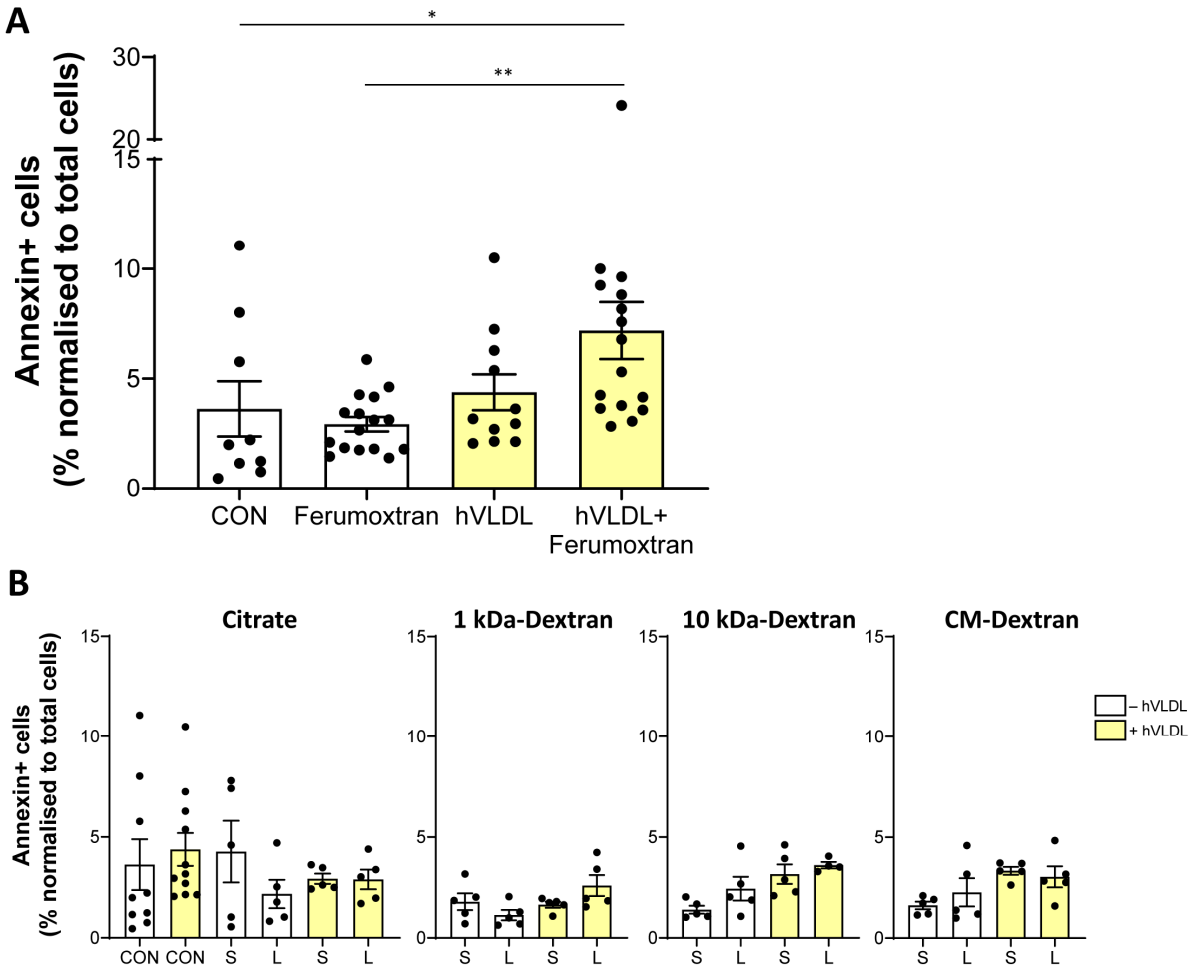

Supplementary Figure 4: Apoptotic effect of ferumoxtran in RAW264.7 foam cells may not be attributed to iron particle coating or particle size

(A) RAW264.7 cell transformed into foam cells with hVLDL (yellow bars) or normolipidemic cells (white bars) were incubated with ferumoxtran (100 µg Fe/ml) for 1 hour or (B) small (S) or large (L) iron particles coated with citrate, dextran, or carboxymethylated dextran (see **Supplementary Table 2** for particle characteristics) or left untreated (CON). Cells were stained with Annexin V and Hoechst 33342 for fluorescence microscopic imaging. Per well, 9 fluorescent images were taken and merged, including around 5000 cells images per well, with 5-16 technical controls per condition. The percentage of Annexin V-positive cells was normalised to the total number of cells per well. Data are presented as mean ± SEM. Statistics: * $p < 0.05$ and ** $p < 0.01$ (Kruskal-Wallis with Dunn's multiple comparison test).


7

Chapter 7

Reprogramming of human macrophages by the blood milieu of SARS-CoV-2-infected patients is predictive of respiratory function decline

AV Ruder, T Ueland, L Temmerman, AM Dyrhol-Riise, A Barratt-Due, TV Lerum, P Aukrust, TB Dahl, EAL Biessen* and B Halvorsen*

* Authors contributed equally

In preparation


8

Chapter 8

General discussion

Main findings of this thesis

Macrophages (MΦ) are implicated in all stages of atherosclerosis (1). They are well-known for their phenotypic plasticity and for sensing their microenvironment (2). However, how the functional phenotype of fully differentiated MΦ is influenced at monocyte stage, during monocyte-to-MΦ differentiation, and by the microenvironment is still largely unknown.

The studies presented in this thesis aimed to address this gap and have led to the following main findings:

1) MΦ phenotype is imprinted at monocytic precursor stage, as MΦ derived from different monocyte subsets have distinct functional phenotypes (Chapter 3).
2) MΦ phenotype is dependent on cues from neighbouring cells, as culture density strongly affects MΦ function *in vitro* (Chapter 4).
3) MΦ phenotype is primed by growth factors during monocyte-to-MΦ differentiation, as macrophage colony-stimulating factor (M-CSF) and granulocyte-macrophage colony-stimulating factor (GM-CSF) induce specific differentiation trajectories that yield functionally and transcriptionally distinct MΦ (Chapter 5).
4) MΦ phenotype is shaped by environmental cues, as nanoparticle treatment (Chapter 6) or the systemic environment reflecting coronavirus disease 2019 (COVID-19) (Chapter 7) induce functional changes.

Altogether, these findings indicate that MΦ phenotype is at least partly determined before differentiation to MΦ is completed. This, in turn, will influence their environment-specific response. In this general discussion, I will consider the implications of functional changes at monocyte stage or during differentiation for the MΦ response to environmental cues. Moreover, I will address the origin and role of embryonic and monocyte-derived MΦ *in vivo* and discuss to what extent their phenotype can be mimicked using MΦ models *in vitro*. The employed functional profiling methodology relied heavily on the MacroScreen functionomics platform. Therefore, I will also elaborate on its merits and potential future applications, as well as its limitations. Finally, I will discuss outstanding questions and perspectives for further research.

Sensitive sensors: MΦ responses to disease environments captured by the MacroScreen

In all experimental chapters of this thesis (Chapters 3-7), the MacroScreen platform was used to measure several key functions of MΦ, including phagocytosis, inflammasome activation, and oxidised low-density lipoprotein (oxLDL) uptake. The MacroScreen platform is built on automated microscopy and fluorescence-based functional assays at microscale, allowing rapid high-content analysis (HCA) of MΦ function. In principle, the MacroScreen can be used with

any adherent cell type, although optimisation of the functional assays and attention to culture density, as shown in Chapter 4, are required for each cell type. The extension of the MacroScreen to other cell types was demonstrated in Chapter 3, where we performed functional measurements on monocytes, and in Chapter 7, where we measured collagen production and morphological features of alveolar fibroblasts. In addition, the MacroScreen is compatible with various pre-treatment protocols, such as incubation with drug compounds (Chapter 6), and stimulation with patient serum or conditioned medium (Chapter 7), among others. This offers the possibility of pre-clinical evaluation of candidate drugs using human primary cells to either complement or even circumvent animal testing. Moreover, it allows the study of MΦ phenotype in disease contexts *in vitro* by using patient material to reflect the (micro)environment MΦ encounter *in vivo* more accurately.

In Chapter 7, we used patient serum to mimic the systemic environment in COVID-19 and to elucidate the role of MΦ. In (severe) COVID-19, the monocyte-derived MΦ pool in the lung will expand as a consequence of progressive monocyte influx (3, 4). Due to massive pulmonary oedema (5), alveolar MΦ will be exposed to the systemic disease environment not only at monocyte stage in the blood but also after infiltrating the lung. We found increased apoptosis and phagocytic activity of MΦ stimulated with serum of COVID-19 patients compared to healthy subjects, a functional adaptation that was sustained even at 3 months after hospitalisation. This could be an indication of a failing regression of COVID-19 but could also reflect an intrinsic pre-disposition of the hospitalised patients. Interestingly, phagocytic capacity was also found to be the main predictor of impaired lung function and clinical outcome. The observed increased phagocytosis of MΦ exposed to serum of patients with a poor prognosis might be attributed to the activation of certain pattern-recognition receptors (PRRs) by pathogen-associated (PAMPs) or danger-associated molecular patterns (DAMPs) (6, 7) to promote debris clearance, and prevent secondary necrosis and inflammation to reduce injury. However, MΦ activation via PRRs may also culminate in macrophage activation syndrome (MAS), the excessive activation of MΦ that underlies a cytokine storm (8). COVID-19 has been associated with an increased risk for cardiovascular disease (CVD) after infection, including dysrhythmia, myocarditis, and ischemic heart disease (9). Previously, MΦ phenotype in response to the systemic environment of acute myocardial infarction (AMI) was investigated with the MacroScreen (10), using a similar setup as in Chapter 7. Interestingly, increased phagocytosis was also observed in this study, hinting at a similar functional response of MΦ. However, a more sophisticated comparison of MΦ functional profiles between COVID-19 and AMI is required to draw substantive conclusions regarding the relevance of this connection, which may well reflect the ongoing inflammation in both pathologies.

In this thesis, we have demonstrated that MΦ phenotype may be influenced by the respective growth factors driving monocyte-to-MΦ differentiation. For alveolar MΦ, development and maintenance are largely dependent on GM-CSF (11). Moreover, GM-CSF levels in circulation

were found to be increased in hospitalised COVID-19 patients compared to healthy subjects (12). Thus, in Chapter 7, we have used GM-CSF for the differentiation of MΦ before their exposure to COVID-19 patient serum. In Chapter 5, we have found distinct functional and transcriptional profiles induced by GM-CSF and M-CSF, with overall lower phagocytic activity, uptake of oxLDL, and interleukin (IL) -6 secretion in GM-CSF-differentiated MΦ. Strikingly, several ongoing clinical trials are investigating GM-CSF inhibition but, paradoxically, also GM-CSF administration for COVID-19 therapy (13). Underlying these contrary approaches is the idea of regulating the hyperactive immune response in COVID-19 on the one hand, and on the other, facilitating alveolar MΦ function to promote tissue repair and to protect against secondary infections (13). However, MΦ will likely be exposed to both M-CSF and GM-CSF simultaneously *in vivo*, and both CSFs have been shown to influence alveolar and interstitial MΦ (11). Thus, an indication of local CSF levels in the lung in COVID-19 would be necessary to understand their contribution to MΦ phenotype and mimic it *in vitro*. Moreover, increased proportions of intermediate and non-classical monocytes were found in patients with post-acute sequelae of COVID-19 (PASC; also referred to as Long COVID) (14). Considering the pronounced functional differences between MΦ derived of different monocyte subsets as we have shown in Chapter 3, further studies using MΦ differentiated from different monocyte subsets could help unravel MΦ phenotype in PASC.

Like two peas in a pod? Resemblance of *in vitro* MΦ models to MΦ *in vivo*

Human MΦ are commonly cultured *in vitro* for their use in biological assays or screening tools, whether they are maintained as cell lines or as primary MΦ derived from blood monocytes. Several *in vitro* models of MΦ have been used in this thesis, including human monocyte-derived MΦ (Chapters 3-5 and 7), human MΦ derived from the THP-1 acute monocytic leukaemia cell line (Chapter 4), or the murine RAW264.7 virus-immortalised MΦ cell line (Chapter 6). However, next to advantages and disadvantages regarding availability and reproducibility, MΦ cell lines and primary MΦ differ functionally, as we have demonstrated in Chapter 4. In particular, we showed that THP-1-derived MΦ and primary monocyte-derived MΦ are affected by culture density, with a more profound impact on the former. Thus, it is crucial to not only ensure equal seeding density, but also to take density differences at the timepoint of experimental readout into account when interpretating *in vitro* experiments. However, considering density differences may be challenging in assays such as the apoptosis assay, where (initial) cell density may be obscured by pro-apoptotic effects of the compound or treatment being tested, like the pre-treatment with very-low-density lipoprotein (VLDL) or iron oxide nanoparticles used in Chapter 6. In addition, human primary MΦ are often obtained by isolating CD14-positive monocytes from peripheral blood mononuclear cells (PBMCs) and differentiating them into MΦ, disregarding the functional phenotype of MΦ derived of intermediate and non-classical monocytes that may be distinct, as we have shown in Chapter 3. Moreover, it could be argued that monocyte-derived MΦ may only resemble MΦ originating from infiltrating monocytes, thus reflecting inflammatory MΦ rather than tissue-resident MΦ.

Tissue-resident MΦ may self-maintain without or with limited contribution of monocyte-derived MΦ at steady-state or, depending on the organ, require constant replenishment by MΦ derived from recruited monocytes (15). They are seeded in sequential haematopoietic waves during embryonic development, in which they are first generated in the yolk sac, and later in the foetal liver (16). Circulating monocytes in adulthood arise from haematopoietic stem cells (HSCs) in the bone marrow or, in inflammation and injury, from extramedullary monocyte reservoirs like the spleen (17). Considering this difference in origin, the question arises whether part of MΦ heterogeneity can be attributed to their ontogeny. Bonnardel and Guilliams proposed that monocyte-derived MΦ at steady-state are similar but not identical to embryonic MΦ in tissue, resulting in different functional responses to inflammation. Alternatively, they suggest that the response to microenvironmental cues superimposes any retained functions from their precursors (18). Xue et al. found local context-induced epigenetic rewiring to partly overrule the epigenetic imprint of the progenitors. Nevertheless, strong inflammatory stimuli acting at transcriptional level could often overrule this environmental epigenetic imprint (19). The findings of this thesis indicate that MΦ phenotype may not exclusively be attributed to the plastic response to their microenvironment but is at least partly retained from their monocyte precursors (Chapter 3). However, how ontogeny influences the function of MΦ in tissue remains to be investigated by fate-mapping approaches *in vivo* (18). These utilise the differential expression of markers between haematopoietic and embryonic MΦ and are thus highly dependent on the specificity of their expression. However, common models like the $Cx3cr1^{CreER}$ or $Flt3^{Cre}$ mouse strains have been reported to label both HSC-derived MΦ and the tissue-resident MΦ population (20). A more specific option could be Ms4a3-based lineage tracing, as it was proposed to allow discrimination between monocyte-derived MΦ and embryonic tissue-resident MΦ (21). Besides, observations in mice are only partly transferable to humans, as the overlap of markers and cell subtypes between the two species is not exact (22).

In vitro, tissue-resident MΦ may be modelled by using MΦ derived from induced pluripotent stem cells (iPSCs). MΦ from iPSCs (iMΦ) are generated by replicating the embryonic seeding of MΦ, starting with the formation of mesoderm, followed by the induction of haematopoietic differentiation and commitment to the myeloid lineage, and finally the differentiation to MΦ (23). This stepwise protocol is intricately orchestrated by different combinations of differentiation factors, albeit with large differences in the protocols used (24). However, how closely iMΦ will resemble tissue-resident MΦ depends on how closely their niche and contained cues can be emulated *in vitro*. In this thesis, we have focused on MΦ function in atherosclerosis (Chapters 5 and 6) and COVID-19 (Chapter 7), where MΦ derived from recruited monocytes are involved in the pathogenic process (25, 26). Nevertheless, to identify MΦ functions that contribute to the development and progression of disease, it is crucial to understand MΦ phenotype at steady-state. It is expected that the MacroScreen will be suitable for high-throughput functional analysis of iMΦ which could contribute to a deeper

understanding of the tissue-resident MΦ phenotype. Ultimately, more complex experimental models starting with the co-culture of multiple cell types, to organoids, to *ex vivo* experiments using human tissue, are required to verify these findings.

MΦ as multi-tools: MΦ functions unaccounted for by the MacroScreen

The MacroScreen allows measurement of many MΦ functions important in atherosclerosis and other inflammatory diseases. These include phagocytosis, lipid uptake, inflammasome activation, mitochondrial function, and cytokine secretion. However, some relevant functions are still not covered by the MacroScreen and should be added for a more comprehensive characterisation of MΦ phenotype.

Oxidative stress by the dysregulated production of reactive oxygen species (ROS) contributes to atherogenesis (27) and is implicated in the oxidation of low-density lipoprotein (LDL) and cellular damage (28). Unfortunately, our efforts to set up a robust assay to measure oxidative stress in MΦ using the MacroScreen were unsuccessful, despite various fluorescent probes (H_2DCFDA or CellROX) and stimulation protocols (using H_2O_2, PMA, t-BOOH, or menadione) tested. Interestingly, this seems to concern mainly primary MΦ, as ROS measurement by H_2DCFDA in other cell types (fibroblasts) and cell lines (THP-1) was more robust and reproducible in our hands. Due to their inherent oxidative burst to defend against bacteria (29), MΦ may be habituated to and protected from high levels of ROS, impeding the stimulation of ROS production *in vitro*. Moreover, high background fluorescence intensity with high variation between wells was observed. This might indicate that the probe is not retained intracellularly but pumped out by MΦ, suggesting that the use of fluorescent probes might not be suitable to measure ROS in primary MΦ. Oxidative burst may be measured as conversion of nitric oxide to nitrite by the widely-used Griess assay after stimulation with LPS (30).

Impaired efferocytosis contributes to the growth and vulnerability of atherosclerotic plaques (31). While phagocytosis of zymosan-coated particles is one of the functional measurements included in the MacroScreen (Chapter 3-5 and 7), an assay to measure uptake of apoptotic cells, which utilises a mechanism different from phagocytosis (32), is still being optimised. For this, apoptotic Jurkat T cells were labelled with fluorescent Annexin V which is also used in the apoptosis assay. However, it was difficult to distinguish Jurkat cells within MΦ from Jurkat cells on top of MΦ in the fluorescent images acquired with the MacroScreen. To circumvent this, Jurkat cells were labelled with pHrodo-Annexin V that is fluorescent only in acidic environments like the MΦ lysosome. Unfortunately, a drop in intracellular pH is a hallmark of apoptotis (33), and Annexin V bound to phosphatidylserine (PS) may be exposed to the intracellular acidic environment as PS is translocated to the inner membrane leaflet (34). This could explain why a fluorescent signal was also observed in Jurkat cells clearly outside of MΦ. A possible solution to this would be to use a different or additional marker next to Annexin V to label apoptotic Jurkat cells, such as a pHrodo-coupled antibody against T cell marker CD3.

MΦ are professional antigen-presenting cells that express major histocompatibility complex (MHC) class II molecules on which they present peptides derived of exogenous proteins to T cells (35). Thus, MΦ may tune the adaptive immune response to be more atherogenic by activating T_H1 cells, or more atheroprotective by activating regulatory T cells (36). An assay using fluorescent labelling of surface MHC II could be used as a measure of antigen presentation, although this would not allow any conclusions about the expression of co-stimulatory molecules, antigen-MHC II stability and binding affinity, and the T cell subsets activated. Alternatively, a co-culture system using a known antigen such as ovalbumin and labelled OT-II CD4+ T cells could be used to assess T cell activation and proliferation, a more relevant read-out for the efficiency of antigen presentation.

Foam cell formation is one of the hallmarks of atherosclerosis (37). An assay measuring oxLDL uptake is already included in the MacroScreen and was employed in Chapters 3-5 and 7. In Chapter 6, we generated foam cells using VLDL before assessing apoptosis using the MacroScreen. However, as the formation of foam cells is attributable to disbalanced influx/efflux, it can also result from impaired cholesterol efflux (38). To measure cholesterol efflux, MΦ could be loaded with fluorescently-labelled cholesterol, similar to the oxLDL uptake assay. Cholesterol efflux could be quantified by comparing the fluorescence intensity and percentage of cholesterol-positive MΦ directly after cholesterol loading to MΦ after releasing the labelled cholesterol into fresh culture medium. In addition, the amount of cholesterol released to the culture medium could be assessed as fluorescence intensity with a plate reader (39).

Another important function of MΦ not covered by our panel yet is extracellular matrix degradation capacity, needed for the migration through tissue, among other purposes. MΦ secrete cathepsins which are cysteine/serine proteases, and matrix metalloproteinases (MMPs) which are zinc-dependent proteases (40, 41). In atherosclerosis, MMPs contribute to plaque rupture by degrading the collagen-rich fibrous cap (42). Moreover, in severe COVID-19, MMPs may promote lung tissue remodelling, fibrosis, and tissue damage (43). MMP activity could be measured using a fluorogenic MMP substrate (44) on both cell lysate and conditioned medium to include both membrane-bound and secreted MMPs, respectively. Additionally, as MMP activity may be pericellular or focused to podosomes, MΦ could be cultured in wells pre-coated with fluorescently-labelled gelatine and degradation could be quantified as the area devoid of fluorescent signal (45).

Ultimately, for the MacroScreen platform to be utilised for screening purposes, it will be necessary to link the *in vitro* setting to the *in vivo* setting. This could be realised by using one set of phenotype markers in both settings, which in turn requires thorough understanding of MΦ phenotypic heterogeneity *in vivo*. In the atherosclerotic plaque, at least three major MΦ populations with distinct phenotypes may be distinguished, including foam cell MΦ (expressing

CD9, LGALS3, PLIN2), inflammatory MΦ (expressing IL1B, CASP1, CASP4 or TLR4, TNF), and resident-like MΦ (LYVE-1, CD206), although recent single-cell studies have described numerous subpopulations (46, 47). In summary, the assay-based setup of the MacroScreen platform allows the addition of assays to measure other functions, and could be linked to the *in vivo* setting through the use of a pre-defined set of phenotypic markers in the future.

Outstanding questions and perspectives

As our current understanding of the functional phenotype of MΦ is still only scratching the surface, many questions remain unresolved, but many opportunities for further research arise. A first opportunity concerns the study of MΦ phenotype constituted in monocyte-to-MΦ differentiation with a combination of M-CSF and GM-CSF, which would be closer to the *in vivo* setting. This would require quantitative measurements of M-CSF and GM-CSF levels in homeostasis and disease contexts *in vivo* to determine a representative ratio that could be used *in vitro*. In a pilot experiment related to Chapter 5, we used different ratios of M-CSF and GM-CSF and assessed the functional phenotype during differentiation, obtaining preliminary evidence that GM-CSF overrides the M-CSF differentiation trajectory. A second opportunity relates to the role of monocyte-derived MΦ in COVID-19. In Chapter 7, we have studied the functional response of fully differentiated MΦ to COVID-19 patient serum but did not account for any phenotypic imprinting that may have occurred in the monocytic precursors that were exposed to the systemic COVID-19 disease environment in circulation. This could be investigated by already stimulating monocytes with COVID-19 patient serum, differentiating them to MΦ, and assessing their phenotype using the MacroScreen. Moreover, monocytes of COVID-19 patients themselves could be used to investigate whether monocytes harbour a pre-disposition to the severity or duration of the disease. A third challenge concerns the functions of the three human monocytes subsets, which we studied in Chapter 3. The role of each monocyte subset, especially the proportionally smaller intermediate and non-classical subsets, remains to be elucidated. As discussed in Chapter 2, non-classical monocytes have been proposed to patrol the vasculature, raising the possibility that their function is limited to the vasculature and that they generally do not extravasate. Thus, it would be interesting to investigate whether they respond to or rely on blood-related factors, possibly derived from thrombocytes or erythrocytes, to exert their patrolling function. Moreover, their patrolling behaviour would make non-classical monocytes interesting cells to study in atherogenesis, as they might enter atherosclerotic lesions upon endothelial dysfunction where they could be involved in debris clearance and lipid uptake.

Concluding remarks

This thesis investigated MΦ phenotype using the MacroScreen platform. We found the functional phenotype of MΦ to be determined by monocytic origin, growth factors during monocyte-to-MΦ differentiation, and their environment. A more holistic picture of MΦ

phenotype may be obtained by considering all these levels at which phenotypic modulation may occur. In the current age of single-cell RNA-sequencing and high-parameter flow cytometry broadening our view of monocyte and MΦ heterogeneity, it will become inevitable to functionally characterise the identified (sub)populations. This may be facilitated by the MacroScreen which allows cost-effective high-throughput measurement of several functional parameters. Moreover, the addition of other functional assays and cell types such as human or murine iMΦ to the MacroScreen may further refine the profiling of MΦ phenotype in the future. Ultimately, a thorough understanding of MΦ phenotype will be instrumental to the development of MΦ-targeted screening models and therapies for atherosclerosis and other inflammatory diseases.

References

1. Barrett TJ. Macrophages in Atherosclerosis Regression. Arterioscler Thromb Vasc Biol. 2020;40(1):20-33.
2. Biswas SK, Mantovani A. Macrophage plasticity and interaction with lymphocyte subsets: cancer as a paradigm. Nat Immunol. 2010;11(10):889-96.
3. Velu PP, Lucas CD, Conway Morris A. Post-mortem dissection of COVID-19: a pathogenic role for macrophages? Intensive Care Med. 2021;47(11):1322-5.
4. Wendisch D, Dietrich O, Mari T, von Stillfried S, Ibarra IL, Mittermaier M, et al. SARS-CoV-2 infection triggers profibrotic macrophage responses and lung fibrosis. Cell. 2021;184(26):6243-61.e27.
5. Cui X, Chen W, Zhou H, Gong Y, Zhu B, Lv X, et al. Pulmonary Edema in COVID-19 Patients: Mechanisms and Treatment Potential. Front Pharmacol. 2021;12:664349.
6. Uribe-Querol E, Rosales C. Phagocytosis: Our Current Understanding of a Universal Biological Process. Front Immunol. 2020;11:1066.
7. Roh JS, Sohn DH. Damage-Associated Molecular Patterns in Inflammatory Diseases. Immune Netw. 2018;18(4):e27.
8. Kosyreva A, Dzhalilova D, Lokhonina A, Vishnyakova P, Fatkhudinov T. The Role of Macrophages in the Pathogenesis of SARS-CoV-2-Associated Acute Respiratory Distress Syndrome. Front Immunol. 2021;12:682871.
9. Xie Y, Xu E, Bowe B, Al-Aly Z. Long-term cardiovascular outcomes of COVID-19. Nat Med. 2022;28(3):583-90.
10. Fontaine MAC, Jin H, Gagliardi M, Rousch M, Wijnands E, Stoll M, et al. Blood Milieu in Acute Myocardial Infarction Reprograms Human Macrophages for Trauma Repair. Adv Sci (Weinh). 2023;10(5):2203053.
11. Draijer C, Penke LRK, Peters-Golden M. Distinctive Effects of GM-CSF and M-CSF on Proliferation and Polarization of Two Major Pulmonary Macrophage Populations. J Immunol. 2019;202(9):2700-9.
12. Huang C, Wang Y, Li X, Ren L, Zhao J, Hu Y, et al. Clinical features of patients infected with 2019 novel coronavirus in Wuhan, China. Lancet. 2020;395(10223):497-506.
13. Lang FM, Lee KM, Teijaro JR, Becher B, Hamilton JA. GM-CSF-based treatments in COVID-19: reconciling opposing therapeutic approaches. Nat Rev Immunol. 2020;20(8):507-14.
14. Patterson BK, Francisco EB, Yogendra R, Long E, Pise A, Rodrigues H, et al. Persistence of SARS CoV-2 S1 Protein in CD16+ Monocytes in Post-Acute Sequelae of COVID-19 (PASC) up to 15 Months Post-Infection. Front Immunology. 2022;12:746021.
15. Ginhoux F, Guilliams M. Tissue-Resident Macrophage Ontogeny and Homeostasis. Immunity. 2016;44(3):439-49.
16. Hoeffel G, Ginhoux F. Ontogeny of Tissue-Resident Macrophages. Front Immunol. 2015;6:486.
17. Wolf AA, Yáñez A, Barman PK, Goodridge HS. The Ontogeny of Monocyte Subsets. Front Immunol. 2019;10:1642.
18. Bonnardel J, Guilliams M. Developmental control of macrophage function. Curr Opin Immunol. 2018;50:64-74.
19. Xue J, Schmidt Susanne V, Sander J, Draffehn A, Krebs W, Quester I, et al. Transcriptome-Based Network Analysis Reveals a Spectrum Model of Human Macrophage Activation. Immunity. 2014;40(2):274-88.
20. Mass E. Delineating the origins, developmental programs and homeostatic functions of tissue-resident macrophages. Int Immunol. 2018;30(11):493-501.
21. Liu Z, Gu Y, Chakarov S, Bleriot C, Kwok I, Chen X, et al. Fate Mapping via Ms4a3-Expression History Traces Monocyte-Derived Cells. Cell. 2019;178(6):1509-25.e19.
22. Reynolds G, Haniffa M. Human and Mouse Mononuclear Phagocyte Networks: A Tale of Two Species? Front Immunol. 2015;6:330.
23. Lyadova I, Vasiliev A. Macrophages derived from pluripotent stem cells: prospective applications and research gaps. Cell Biosci. 2022;12(1):96.
24. Lyadova I, Gerasimova T, Nenasheva T. Macrophages Derived From Human Induced Pluripotent Stem Cells: The Diversity of Protocols, Future Prospects, and Outstanding Questions. Front Cell Dev Biol. 2021;9:640703.
25. Chen ST, Park MD, Del Valle DM, Buckup M, Tabachnikova A, Thompson RC, et al. A shift in lung macrophage composition is associated with COVID-19 severity and recovery. Sci Transl Med. 2022;14(662):eabn5168.
26. Park MD, Silvin A, Ginhoux F, Merad M. Macrophages in health and disease. Cell. 2022;185(23):4259-79.
27. Nowak WN, Deng J, Ruan XZ, Xu Q. Reactive Oxygen Species Generation and Atherosclerosis. Arterioscler Thromb Vasc Biol. 2017;37(5):e41-e52.

28. Kattoor AJ, Pothineni NVK, Palagiri D, Mehta JL. Oxidative Stress in Atherosclerosis. Curr Atheroscler Rep. 2017;19(11):42.
29. Slauch JM. How does the oxidative burst of macrophages kill bacteria? Still an open question. Mol Microbiol. 2011;80(3):580-3.
30. Schmölz L, Wallert M, Lorkowski S. Optimized incubation regime for nitric oxide measurements in murine macrophages using the Griess assay. J Immunol Methods. 2017;449:68-70.
31. Kojima Y, Weissman IL, Leeper NJ. The Role of Efferocytosis in Atherosclerosis. Circulation. 2017;135(5):476-89.
32. Doran AC, Yurdagul A, Tabas I. Efferocytosis in health and disease. Nat Rev Immunol. 2020;20(4):254-67.
33. Lagadic-Gossmann D, Huc L, Lecureur V. Alterations of intracellular pH homeostasis in apoptosis: origins and roles. Cell Death Differ. 2004;11(9):953-61.
34. Reutelingsperger CP, van Heerde WL. Annexin V, the regulator of phosphatidylserine-catalyzed inflammation and coagulation during apoptosis. Cell Mol Life Sci. 1997;53(6):527-32.
35. Eiz-Vesper B, Schmetzer HM. Antigen-Presenting Cells: Potential of Proven und New Players in Immune Therapies. Transfus Med Hemother. 2020;47(6):429-31.
36. Wigren M, Rattik S, Mattisson IY, Tomas L, Grönberg C, Söderberg I, et al. Lack of Ability to Present Antigens on Major Histocompatibility Complex Class II Molecules Aggravates Atherosclerosis in ApoE-/- Mice. Circulation. 2019;139(22):2554-66.
37. Gui Y, Zheng H, Cao RY. Foam Cells in Atherosclerosis: Novel Insights Into Its Origins, Consequences, and Molecular Mechanisms. Front Cardiovasc Med. 2022;9:845942.
38. Groenen AG, Halmos B, Tall AR, Westerterp M. Cholesterol efflux pathways, inflammation, and atherosclerosis. Crit Rev Biochem Mol Biol. 2021;56(4):426-39.
39. Sankaranarayanan S, Kellner-Weibel G, de la Llera-Moya M, Phillips MC, Asztalos BF, Bittman R, et al. A sensitive assay for ABCA1-mediated cholesterol efflux using BODIPY-cholesterol. J Lipid Res. 2011;52(12):2332-40.
40. Elkington PT, Green JA, Friedland JS. Analysis of matrix metalloproteinase secretion by macrophages. Methods Mol Biol. 2009;531:253-65.
41. Löffek S, Schilling O, Franzke C-W. Biological role of matrix metalloproteinases: a critical balance. European Respiratory Journal. 2011;38(1):191-208.
42. Newby AC. Metalloproteinase production from macrophages – a perfect storm leading to atherosclerotic plaque rupture and myocardial infarction. Exp Physiol. 2016;101(11):1327-37.
43. da Silva-Neto PV, do Valle VB, Fuzo CA, Fernandes TM, Toro DM, Fraga-Silva TFC, et al. Matrix Metalloproteinases on Severe COVID-19 Lung Disease Pathogenesis: Cooperative Actions of MMP-8/MMP-2 Axis on Immune Response through HLA-G Shedding and Oxidative Stress. Biomolecules. 2022;12(5):604.
44. van Kuijk K, Demandt JAF, Perales-Patón J, Theelen TL, Kuppe C, Marsch E, et al. Deficiency of myeloid PHD proteins aggravates atherogenesis via macrophage apoptosis and paracrine fibrotic signalling. Cardiovasc Res. 2021;118(5):1232-46.
45. Cougoule C, Le Cabec V, Poincloux R, Al Saati T, Mège JL, Tabouret G, et al. Three-dimensional migration of macrophages requires Hck for podosome organization and extracellular matrix proteolysis. Blood. 2010;115(7):1444-52.
46. Depuydt MAC, Prange KHM, Slenders L, Örd T, Elbersen D, Boltjes A, et al. Microanatomy of the Human Atherosclerotic Plaque by Single-Cell Transcriptomics. Circ Res. 2020;127(11):1437-55.
47. Willemsen L, de Winther MP. Macrophage subsets in atherosclerosis as defined by single-cell technologies. J Pathol. 2020;250(5):705-14.


9

Chapter 9

Summary
Samenvatting
Zusammenfassung

Cardiovascular disease weighs heavily on public health in nations at all economic levels as it is the leading cause of death worldwide. The most common cause of cardiovascular disease is atherosclerosis, an inflammatory disease that leads to the formation of atherosclerotic plaque in the artery wall. Atherosclerotic plaques can rupture, causing blood clots to form which can lead to myocardial infarction or stroke. Inflammation plays an important role in atherosclerosis and underlies its development. One of the main immune cells involved in the development of atherosclerosis is the macrophage (MΦ) which can exert a repertoire of functions in response to local factors. However, characterisation of the cells' function by laboratory experiments have been incomplete: so far, most studies considered a single factor, rather than the usual cocktail that MΦ encounter in the living body. Moreover, they often overlooked functional changes that may have been induced at the level of the MΦ precursor cell, the monocyte, or during the differentiation of monocyte into MΦ. In this thesis, we examined MΦ function and how it is affected by monocytic origin, growth factors, and complex (mixtures of) factors in the (direct) surrounding of the cell.

MΦ function may partly mirror the set of functional traits their monocytic precursors possess. In Chapter 2, we discussed the diversity of monocytes which is transcending the prevailing tripartite classification, considering recent technological advances to study single cells. Moreover, we discussed associations with cardiovascular disease, identifying the strongest association with one particular type of monocyte, so called "intermediate" monocytes. In Chapter 3, we studied the functional traits of MΦ derived from three known types of monocytes, namely "classical," "intermediate", and "non-classical" monocytes. We observed clear differences in cell size, shape, and function between MΦ that were stemming from these three monocyte classes, demonstrating that the monocyte origin is important for MΦ function.

MΦ function may also be influenced by the culture density in laboratory experiments. In Chapter 4, we investigated cell density as a modulator of human MΦ function. We observed a profound effect of culture density on a multitude of human MΦ functions, using two different types of experimental MΦ models. Moreover, we found evidence for growth pattern-associated functional adaptations in one of the models, namely THP-1 MΦ, and show substantial variability in the functional traits of MΦ isolated from different human donors. Given the bias that may be introduced by ignoring cell density differences, our findings demonstrate the need to account for differences in cell density in MΦ laboratory experiments.

MΦ function may be established during monocyte-to-MΦ differentiation. In Chapter 5, we used the growth factors macrophage colony-stimulating factor (M-CSF) or granulocyte-macrophage colony-stimulating factor (GM-CSF) to differentiate human monocytes to MΦ and studied their differentiation track. We identified changes in function and genetic information that we could relate to the differentiation trajectory itself or to the growth factor. We found these growth factor-induced changes to be established early in the differentiation process.

Next to differences, we also found common changes related to cell growth and differentiation induced by M-CSF or GM-CSF. In addition, we discovered M-CSF to be the main growth factor in atherosclerotic lesions. Plaque MΦ were more similar to M-CSF-grown MΦ than to GM-CSF-grown MΦ, especially later in the disease development. Moreover, newly recruited inflammatory MΦ and lipid-containing MΦ (also called foam cells) were mirroring the gene profile of M-CSF-derived MΦ.

MΦ respond to nanoparticles used as contrast agents in magnetic resonance imaging (MRI). In Chapter 6, we revealed a cell death-inducing effect of ferumoxide and ferumoxtran, two iron oxide nanoparticles, on lipid-containing MΦ. This effect was absent in MΦ not containing excess lipids, demonstrating foam cells to respond to environmental stimuli differently and to be more susceptible to stressors. Interestingly, a newer formulation of nanoparticles, ferumoxytol, did not induce cell death in foam cell MΦ, which was neither attributable to particle coating nor particle size.

MΦ respond to disease environment. In Chapter 7, we stimulated MΦ with serum of COVID-19 patients at hospitalisation or at 3-month follow-up, or serum of healthy subjects. We showed that MΦ react to the systemic COVID-19 disease environment reflected in the serum by adapting their functions to a higher activation status. Moreover, COVID-19 serum-stimulated MΦ instructed fibroblasts, cells which contribute to the formation of connective tissue, to multiply. Based on functional differences in the uptake of particles and lipids by MΦ, and the production of collagen by fibroblasts, we could predict the need for patients to be admitted to the intensive care unit (ICU) and/or determine which patients would be suffering from respiratory failure. Certain functional changes were found to persist even at 3-month follow-up, including increased particle uptake and cell death, and a more stretched appearance.

In Chapter 8, we summarised the main findings presented in thesis and discussed their implications for future research, their limitations, and the potential for drug screening and therapeutic approaches. Altogether, the findings presented in this thesis suggest that MΦ function is not only determined by environmental stimuli encountered locally, but also by the systemic environment as well as monocytic origin and the growth factors driving monocyte-to-MΦ differentiation.

Hart- en vaatziekten zijn wereldwijd de belangrijkste doodsoorzaak en wegen daarom zwaar op de volksgezondheid in landen van alle economische niveaus. De meest voorkomende oorzaak van hart- en vaatziekten is atherosclerose, een ontstekingsziekte die leidt tot de vorming van atherosclerotische plaque in de slagaderwand. Atherosclerotische plaques kunnen scheuren, waardoor zich bloedstolsels vormen die kunnen leiden tot een hartinfarct of een beroerte. Ontsteking speelt een belangrijke rol bij atherosclerose en ligt ten grondslag aan de ontwikkeling ervan. Een van de belangrijkste immuuncellen die bij de ontwikkeling van atherosclerose betrokken is, is de macrofaag (MΦ), die een breed repertoire van functies kunnen uitoefenen in reactie op lokale factoren. De karakterisering van de functie van deze cellen door middel van laboratoriumexperimenten is tot nu toe echter onvolledig: doorgaans keek men naar één enkele factor, in plaats van de gebruikelijke cocktail die MΦ in het levende lichaam tegenkomen. Daarenboven zijn functionele veranderingen over het hoofd gezien die al geïnduceerd kunnen zijn op het niveau van de MΦ voorlopercel, de monocyt, of tijdens de differentiatie van monocyt tot MΦ. In dit proefschrift onderzochten wij de MΦ functie en hoe deze wordt beïnvloed door monocytaire oorsprong, groeifactoren, en complexe (mengsels van) factoren in de (directe) omgeving van de cel.

MΦ-functie kan deels een afspiegeling zijn van de set van functionele eigenschappen die hun monocytische voorlopers bezitten. In hoofdstuk 2 bespraken wij de diversiteit van monocyten die de gangbare driedelige classificatie overstijgt, gezien de recente technologische vooruitgang die het mogelijk heeft gemaakt om individuele cellen te bestuderen. Bovendien bespraken wij de associaties met hart- en vaatziekten, waarbij wij de sterkste associatie met één bepaald type monocyt identificeerden, de zogenaamde "intermediaire" monocyten. In hoofdstuk 3 bestudeerden wij de functionele kenmerken van MΦ afkomstig van drie bekende typen monocyten, namelijk "klassieke", "intermediaire" en "niet-klassieke" monocyten. Wij zagen duidelijke verschillen in celgrootte, vorm en functie tussen MΦ die afkomstig waren van deze drie monocytensoorten, waaruit blijkt dat de monocytensoort van belang is voor de MΦ-functie.

De MΦ-functie kan ook worden beïnvloed door de kweekdichtheid in laboratoriumexperimenten. In hoofdstuk 4 onderzochten wij de celdichtheid als modulator van de menselijke MΦ-functie. Wij constateerden een duidelijk effect van de kweekdichtheid op verschillende menselijke MΦ-functies, met behulp van twee verschillende soorten experimentele MΦ-modellen. Bovendien vonden wij bewijs voor groeipatroon-geassocieerde functionele aanpassingen in een van de modellen, namelijk THP-1 MΦ, en tonen wij aanzienlijke variabiliteit in de functionele eigenschappen van MΦ geïsoleerd van verschillende menselijke donoren. Gezien de bias die kan ontstaan door het negeren van verschillen in celdichtheid, tonen onze bevindingen aan dat rekening moet worden gehouden met verschillen in celdichtheid in MΦ-laboratoriumexperimenten.

MΦ-functie kan worden vastgesteld tijdens de differentiatie van monocyt naar MΦ. In hoofdstuk 5 gebruikten wij de groeifactoren M-CSF of GM-CSF om menselijke monocyten te differentiëren tot MΦ en bestudeerden wij hun differentiatietraject. Wij identificeerden veranderingen in functie en in gen expressie die wij in verband konden brengen met het differentiatietraject zelf of met de groeifactor. Wij vonden dat deze door de groeifactor geïnduceerde veranderingen vroeg in het differentiatieproces tot stand kwamen. Naast verschillen vonden wij ook gelijkaardige veranderingen met betrekking tot celgroei en differentiatie geïnduceerd door M-CSF of GM-CSF. Bovendien ontdekten we dat M-CSF de belangrijkste groeifactor is in atherosclerotische laesies. Plaque MΦ leken meer op M-CSF-gegroeide MΦ dan op GM-CSF-gegroeide MΦ, vooral later in de ziekteontwikkeling. Bovendien spiegelden ook pas gerekruteerde inflammatoire MΦ en lipide bevattende MΦ (ook schuimcellen genoemd) het genprofiel van M-CSF-afgeleide MΦ.

MΦ reageren op nanodeeltjes die worden gebruikt als contrastmiddel bij MRI. In hoofdstuk 6 toonden we een celdood-inducerend effect aan van ferumoxide en ferumoxtran, twee ijzeroxide nanodeeltjes, op lipide-bevattende MΦ. Dit effect was afwezig in MΦ die geen overtollige lipiden bevatten, wat aantoont dat schuimcellen anders reageren op omgevingsstimuli en gevoeliger zijn voor stressoren. Interessant is dat een nieuwere formulering van nanodeeltjes, ferumoxytol, geen celdood induceerde in schuimcellen, hetgeen niet te wijten was aan de coating of de grootte van de deeltjes.

MΦ reageren op de ziekteomgeving. In hoofdstuk 7 hebben wij MΦ gestimuleerd met serum van COVID-19-patiënten bij opname in het ziekenhuis of bij 3 maanden follow-up, of met serum van gezonde proefpersonen. Wij toonden aan dat de MΦ reageren op de systemische COVID-19-ziekteomgeving die in het serum tot uiting komt, door hun functies aan te passen en actiever te worden. Bovendien vonden wij dat MΦ cellen die bijdragen tot de vorming van bindweefsel, fibroblasten genaamd, opdracht geven zich te vermenigvuldigen. Op basis van functionele verschillen in de opname van deeltjes en lipiden door MΦ, en de productie van collageen door fibroblasten, konden wij de noodzaak van opname op de IC en/of het risico op ademhalingsfalen voorspellen. Bepaalde functionele veranderingen bleken zelfs na 3 maanden follow-up te blijven bestaan, waaronder verhoogde deeltjesopname en celdood, en een meer uitgerekt uiterlijk.

In hoofdstuk 8 vatten we de belangrijkste bevindingen van dit proefschrift samen en bespraken we de implicaties ervan voor toekomstig onderzoek, alsook de beperkingen en het potentieel voor het screenen van geneesmiddelen en therapeutische benaderingen. Al met al suggereren de bevindingen in dit proefschrift dat de MΦ-functie niet alleen wordt bepaald door omgevingsstimuli die zich lokaal voordoen, maar ook door de systemische omgeving, de monocytaire oorsprong en de groeifactoren die de monocyt-naar-MΦ-differentiatie aansturen.

Herz-Kreislauf-Erkrankungen sind weltweit die häufigste Todesursache und belasten daher die Volksgesundheit in Ländern aller Wirtschaftsniveaus schwer. Die häufigste Ursache von Herz-Kreislauf-Erkrankungen ist Atherosklerose, eine entzündliche Erkrankung, die zur Bildung von atherosklerotischen Plaques in der Arterienwand führt. Atherosklerotische Plaques können reißen, wodurch sich Blutgerinnsel bilden, die zu einem Herzinfarkt oder Schlaganfall führen können. Entzündungen spielen bei der Atherosklerose eine wichtige Rolle und liegen ihrer Entstehung zugrunde. Eine der wichtigsten Immunzellen, die an der Entstehung von Atherosklerose beteiligt ist, ist der Makrophage (MΦ), der als Reaktion auf lokale Faktoren ein breites Repertoire an Funktionen ausüben kann. Die Charakterisierung der Funktionen von MΦ durch Laborexperimente ist bislang allerdings unvollständig: In den meisten Studien wurde bisher nur ein einziger Faktor anstelle einer Mischung aus Faktoren betrachtet, dem MΦ im lebenden Körper üblicherweise ausgesetzt sind. Darüber hinaus wurden funktionelle Veränderungen, die möglicherweise auf der Ebene der MΦ-Vorläuferzelle, dem Monozyten, oder während der Differenzierung von Monozyten zu MΦ ausgelöst wurden, nicht beachtet. In dieser Dissertation haben wir untersucht, wie die MΦ-Funktion durch den monozytären Ursprung, durch Wachstumsfaktoren sowie komplexe (Mischungen von) Faktoren in der (unmittelbaren) Umgebung der Zelle beeinflusst wird.

Die MΦ-Funktion kann teilweise die funktionellen Eigenschaften ihrer monozytären Vorläufer widerspiegeln. In Kapitel 2 haben wir, unter Berücksichtigung der jüngsten technologischen Fortschritte bei der Untersuchung einzelner Zellen, die Vielfalt der Monozyten erörtert, die über die aktuell geltende Dreiteilung hinausgeht. Des Weiteren haben wir Assoziationen mit Herz-Kreislauf-Erkrankungen dargelegt, wobei die stärkste Assoziation mit einem bestimmten Monozytentyp, den so genannten "intermediären" Monozyten, festgestellt wurde. In Kapitel 3 untersuchten wir die funktionellen Eigenschaften von MΦ, die von den drei geläufigen Typen von Monozyten, den "klassischen", "intermediären" und "nicht-klassischen" Monozyten, abstammen. Wir beobachteten deutliche Unterschiede in Zellgröße, -form und -funktion zwischen MΦ, die sich aus diesen drei Monozytentypen entwickelten, was die Bedeutung der Monozytenherkunft für die MΦ-Funktion zeigt.

Die MΦ-Funktion kann auch durch die Zelldichte in Laborexperimenten beeinflusst werden. In Kapitel 4 haben wir die Zelldichte als Modulator der menschlichen MΦ-Funktion untersucht. Wir beobachteten eine tiefgreifende Auswirkung der Zelldichte auf eine Vielzahl menschlicher MΦ-Funktionen, wobei wir zwei verschiedene Arten von experimentellen MΦ-Modellen verwendeten. Darüber hinaus fanden wir Hinweise auf wachstumsmusterbedingte funktionelle Anpassungen in einem der Modelle, nämlich THP-1 MΦ, und zeigen eine erhebliche Variabilität in den funktionellen Merkmalen von MΦ, die von verschiedenen menschlichen Spendern isoliert wurden. Angesichts der Verzerrung, die durch die Nichtberücksichtigung von Unterschieden in der Zelldichte entstehen kann, zeigen unsere Ergebnisse, dass Unterschiede in der Zelldichte bei MΦ-Laborversuchen berücksichtigt werden müssen.

Die MΦ-Funktion kann während der Differenzierung von Monozyten zu MΦ entstehen. In Kapitel 5 verwendeten wir die Wachstumsfaktoren M-CSF oder GM-CSF, um menschliche Monozyten zu MΦ zu differenzieren und untersuchten den Differenzierungsverlauf. Wir stellten Veränderungen in der Funktion und den genetischen Informationen fest, die wir mit dem Differenzierungsprozess selbst oder dem jeweiligen Wachstumsfaktor in Verbindung bringen konnten. Zudem stellten wir fest, dass diese wachstumsfaktorinduzierten Veränderungen bereits früh im Differenzierungsprozess auftreten. Neben Unterschieden fanden wir auch ähnliche Veränderungen im Zusammenhang mit Zellwachstum und -differenzierung, die durch M-CSF oder GM-CSF ausgelöst wurden. Darüber hinaus entdeckten wir, dass M-CSF der wichtigste Wachstumsfaktor in atherosklerotischen Läsionen ist. Plaque-MΦ ähnelten mehr den durch M-CSF differenzierten MΦ als den durch GM-CSF differenzierten MΦ, insbesondere im späteren Verlauf der Erkrankung. Außerdem spiegelten neu rekrutierte entzündliche MΦ und lipidhaltige MΦ (auch Schaumzellen genannt) das Genprofil von M-CSF-differenzierten MΦ wider.

MΦ reagieren auf Nanopartikel, die als Kontrastmittel in der Magnetresonanztomographie (MRT) verwendet werden. In Kapitel 6 zeigten wir eine zelltodauslösende Wirkung von Ferumoxid und Ferumoxtran, zwei Eisenoxid-Nanopartikeln, auf lipidhaltige MΦ. Dieser Effekt war bei MΦ, die keine überschüssigen Lipide enthielten, nicht vorhanden, was zeigt, dass Schaumzellen unterschiedlich auf Umweltreize reagieren und anfälliger für Stressfaktoren sind. Interessanterweise löste eine neuere Formulierung von Nanopartikeln, Ferumoxytol, keinen Zelltod in Schaumzellen-MΦ aus, was weder auf die Partikelbeschichtung noch auf die Partikelgröße zurückzuführen war.

MΦ reagieren auf das Krankheitsumfeld. In Kapitel 7 stimulierten wir MΦ mit dem Serum von COVID-19-Patienten, das bei der Aufnahme ins Krankenhaus oder bei der dreimonatigen Nachbeobachtung abgenommen wurde, oder mit dem Serum gesunder Personen. Wir konnten zeigen, dass MΦ auf das systemische COVID-19-Krankheitsumfeld, das sich im Serum widerspiegelt, reagieren, indem sie ihre Funktionen an einen höheren Aktivierungsstatus anpassen. Darüber hinaus veranlassten COVID-19-serumstimulierte MΦ wiederum Fibroblasten, Zellen, die zur Bildung von Bindegewebe beitragen, sich zu vermehren. Anhand der funktionellen Unterschiede bei der Aufnahme von Partikeln und Lipiden durch MΦ und der Produktion von Kollagen durch Fibroblasten konnten wir vorhersagen, ob Patienten auf die Intensivstation eingewiesen werden mussten und/oder welche Patienten an Atemversagen leiden würden. Bestimmte funktionelle Veränderungen blieben auch nach drei Monaten bestehen, darunter eine erhöhte Partikelaufnahme und ein vermehrter Zelltod sowie ein gestreckteres Erscheinungsbild der MΦ.

In Kapitel 8 fassten wir die wichtigsten Ergebnisse dieser Arbeit zusammen und erörterten ihre Bedeutung für die künftige Forschung, ihre Grenzen, und das Potenzial für Medikamenten-

Screening und therapeutische Ansätze. Insgesamt deuten die in dieser Arbeit vorgestellten Ergebnisse darauf hin, dass die MΦ-Funktion nicht nur durch lokal auftretende Umweltreize bestimmt wird, sondern auch durch die systemische Umgebung sowie die monozytäre Herkunft und die Wachstumsfaktoren, die die Differenzierung von Monozyten zu MΦ vorantreiben.

10

Chapter 10

Impact

Expanding the understanding of MΦ phenotype in CVD and beyond

The studies presented in this thesis have added to our understanding of macrophage (MΦ) phenotype by demonstrating that the functional response of MΦ is not only influenced by environmental stimuli (Chapters 6 and 7) but also by their monocytic origin (Chapter 2 and 3) and by the growth factors which are driving monocyte-to-MΦ differentiation (Chapter 5). In this way, the findings in this thesis could eventually contribute to the development of novel therapeutic strategies employing targeted phenotypic modulation of MΦ. Unlike conventional approaches that target the complete MΦ pool or MΦ with a specific disease-related phenotype, such therapy would aim at interfering with a specific context or (systemic) environment to modulate MΦ function. Next to cardiovascular disease (CVD), such thorough understanding of MΦ phenotype and its regulation may also benefit flanking fields and accelerate the development of therapies for other diseases, as MΦ are implicated in a wide range of immune-driven diseases, including multiple sclerosis, rheumatoid arthritis, fibrosis, or cancer (1). Chapter 7 illustrates the relevance of this approach for immune-driven diseases by showing the prognosis-dependent differences in functional response of MΦ to the coronavirus disease 2019 (COVID-19) disease context. This thesis also illustrates the potential of the MacroScreen for assessing effects of novel leads on MΦ, as it represents a robust and cost-effective platform that can streamline functional measurements by combining multiple functional assays in a high-throughput approach. Thus, we expect that the MacroScreen platform could also be used for immunotoxicity screening, and to facilitate the discovery of novel drugs and of new insights into MΦ function in the context of disease.

A methodology makeover to combat MΦ mayhem

Besides the pursuit of discovery and new theories based thereon, progress in science also relies on the verification, falsification or questioning, and if opportune, refinement of established concepts and models (2). While revisiting previous findings can lead to innovation, failure to replicate them may indicate that the model's or concept's robustness has been overestimated (3). The systematic approach to science, the "scientific method", is challenged by the increasing failure and perpetual inability to independently reproduce previous findings, the so-called replication crisis (4, 5). Whereas general factors contributing to the replication crisis, such as the incomplete description of the methods used or the bias towards publishing positive results (6) apply to any scientific discipline, we have, in this thesis, pinpointed some pitfalls in methodologies and taxonomies commonly used in the monocyte/MΦ research field. Our study presented in Chapter 4 demonstrated that disregarding density could introduce bias as it is unclear whether observed effects are induced by the tested compound or treatment condition or are indirectly caused by effects on cell density. We have stressed the importance of density for MΦ function *in vitro* and argue for better awareness of cell density as a confounding factor in *in vitro* testing. Chapter 2 calls for an update of monocyte taxonomy, as our outline clearly shows that the current nomenclature inadequately captures monocyte heterogeneity, and is,

on top, inconsistently used in publications, which complicates the drawing of conclusions. Incorporating these findings into methodological considerations for future studies can help ensure their reproducibility.

Sharing is caring: Disseminating scientific outcome

Scientific progress is directly or indirectly enabled via financial support by the community, and requires the publication of research outcomes in academic journals to be available to other researchers and to ensure return of investment for society (7). Out of the 6 articles that comprise this thesis, 3 have been published in international, peer-reviewed journals, all of them open access. The RNA-sequencing (RNA-Seq) data we present in Chapter 5 will be made available to other researchers in the public database repository Gene Expression Omnibus (GEO). This will enable other scientists to use our data for verification, validation, and deeper analyses or meta-analyses. The findings of this thesis have also been presented at various national and international meetings, such as the 28th annual conference of the Scandinavian Society for Atherosclerosis Research (SSAR).

Turning knowledge into benefit: Implications for therapeutic strategies

Science also aims at bringing a benefit to society. In Chapter 6, we showed that the second-generation superparamagnetic iron oxide nanoparticle ferumoxytol seems to be safe for application in patients with CVD, whereas ferumoxtran administration increased apoptosis in human atherosclerotic plaques, which can considerably affect disease progression. Despite that the manufacturing of ferumoxtran has been discontinued, several clinical studies are recruiting participants for trials on its use in prostate cancer, head and neck squamous cell carcinoma, and aortic dissection, which involves mostly elderly patients that will suffer from moderate to advanced atherosclerosis. Our results in Chapter 6 demonstrate that thorough safety testing regarding atherosclerosis progression and plaque destabilisation are necessary before ferumoxtran can be considered safe for use in these patients. In Chapter 5, our findings challenge the prevailing dogma of granulocyte-macrophage colony-stimulating factor (GM-CSF) as the driving growth factor of MΦ phenotype in chronic inflammation, as we found macrophage colony-stimulating factor (M-CSF) to be dominant in atherosclerotic plaque. This also raises concern about GM-CSF-targeted interventions, such as in cancer therapy or cancer vaccines (7), as a concealed side effect could be plaque destabilisation by an enhancement of the M-CSF-driven MΦ phenotype. In Chapter 7, we have investigated the functional response of MΦ to the COVID-19 systemic disease environment which may help the development of MΦ-based therapies for acute COVID-19. Moreover, we have found certain disease-associated stimuli reflected in serum to sustain even 3 months after hospitalisation which could potentially help understand the development of post-acute sequelae of COVID-19 (PASC), more commonly referred to as Long COVID. However, larger, independent cohort studies will be needed to confirm our findings and to draw firm conclusions. Moreover, we have found phagocytosis as

a predictor of the need to be transferred to the intensive care unit (ICU). As the overload of ICU posed a burden on society during the peaks of the pandemic, this finding could help better categorise patients. Although COVID-19 is likely to become endemic, our results keep its relevance because the course of disease may still be severe for patients at risk, and the emergence of new variants and/or a decline in herd immunity might again lead to infection of large populations.

Conclusion

In conclusion, the findings presented in this thesis have increased our understanding of the (functional) phenotype of MΦ, and its dependence on origin, differentiation trajectory, and local context (density, disease), which could facilitate the development of MΦ-targeted therapies for CVD, COVID-19, and other MΦ-driven diseases. Moreover, we have identified potential pitfalls for the reproducibility of studies using *in vitro* MΦ models and point out approaches for improvement. Lastly, the MacroScreen platform used in this thesis could be used to further characterise the functional phenotype of MΦ or other cell types and in other disease contexts in the future.

References

1. Poltavets AS, Vishnyakova PA, Elchaninov AV, Sukhikh GT, Fatkhudinov TK. Macrophage Modification Strategies for Efficient Cell Therapy. Cells. 2020;9(6):1535.
2. Popper KR. The logic of scientific discovery. Oxford, England: Basic Books; 1959.
3. Nosek BA, Errington TM. What is replication? PLoS Biol. 2020;18(3):e3000691.
4. Guttinger S, Love AC. Characterizing scientific failure. EMBO Rep. 2019;20(9):e48765.
5. Voit EO. Perspective: Dimensions of the scientific method. PLoS Comput Biol. 2019;15(9):e1007279.
6. Hunter P. The reproducibility "crisis": Reaction to replication crisis should not stifle innovation. EMBO Rep. 2017;18(9):1493-6.
7. Chiriboga L. The changing landscape of scientific publishing. J Histotechnol. 2019;42(3):95-7.

A

Addendum

Abbreviations

Ab	Antibody
ABTS	2,2'-azino-bis (3-ethylbenzthiazoline-6-sulfonic acid) diammonium salt
AC	Atherosclerotic core
ACE2	Angiotensin converting enzyme 2
acLDL	Acetylated low-density lipoprotein
AHR	Aryl hydrocarbon receptor
AMI	Acute myocardial infarction
ApoE	Apolipoprotein E
ApoE-/-	Apolipoprotein E-knockout
ARDS	Acute respiratory distress syndrome
ASC	Apoptosis-associated speck-like protein containing a CARD
Bax	BCL-2-associated X protein
BCA	Bicinchoninic acid
BMDM	Bone marrow-derived macrophages
BSA	Bovine serum albumin
CAD	Coronary artery disease
CANTOS	Canakinumab Anti-inflammatory Thrombosis Outcomes Study
CCL	Chemokine (C-C motif) ligand
CCR	Chemokine (C-C motif) receptor
CD	Cluster of differentiation
CEA	Carotid endarterectomy
CIRT	Cardiovascular Inflammation Reduction Trial
CM	Carboxymethyl
cMo	Classical monocytes
cMΦ	Macrophages derived of classical monocytes
COLCOT	Colchicine Cardiovascular Outcomes Trial
CON	Control
COVID-19	Coronavirus disease 2019
CRP	C-reactive protein
CSF	Colony-stimulating factor
CT	Computed tomography
CVD	Cardiovascular disease
CXCL	Chemokine (C-X-C motif) ligand
CXCR	Chemokine (C-X-C motif) receptor
CyTOF	Cytometry by time-of-flight
DAMPs	Danger-associated molecular patterns
DC	Dendritic cell
DEGs	Differentially expressed genes
Dh	Hydrodynamic diameter
DL_{CO}	Diffusion capacity of the lungs for carbon monoxide

DMEM	Dulbecco's Modified Eagle Medium
DMSO	Dimethyl sulfoxide
EC	Endothelial cells
ECM	Extracellular matrix
EDTA	Ethylenediaminetetraacetic acid
EdU	5’ethynyl-2’-deoxyuridine
eGFR	Estimated glomerular filtration rate
ER	Endoplasmic reticulum
FACS	Fluorescence-activated cell sorting
FBS	Foetal bovine serum
FITC	Fluorescein isothiocyanate
FOV	Field of view
GEO	Gene Expression Omnibus
GGO	Ground-glass opacities
GLI	Global Lung Function Initiative Network
GM-CSF	Granulocyte-macrophage colony-stimulating factor
GO	Gene Ontology
GSEA	Gene set enrichment analysis
GSOA	Gene set overrepresentation analysis
GTC	Guanidium isothiocyanate
HC	Healthy controls
HCA	High-content analysis
HDL	High-density lipoprotein
HF	Heart failure
HLA	Human leukocyte antigen
HPRT	Hypocanthine phospho-ribosyltransferase
HSCs	Haematopoietic stem cells
hVLDL	Human very-low-density lipoprotein
ICP-AES	Inductively coupled plasma atomic emission spectroscopy
ICU	Intensive care unit
IFN	Interferon
Ig	Immunoglobulin
IL	Interleukin
iMΦ	Macrophages from induced pluripotent stem cells
iNOS	Inducible nitric oxide synthase
intMo	Intermediate monocytes
intMΦ	Macrophages derived of intermediate monocytes
iPSCs	Induced pluripotent stem cells
LDL	Low-density lipoprotein
LDLR	Low-density lipoprotein receptor

LDLR-/-	Low-density lipoprotein receptor-knockout
LLN	Lower limit of normal
Lp(a)	Lipoprotein (a)
LPS	Lipopolysaccharide
LVEF	Left ventricular ejection fraction
MACE	Massive analysis of complimentary DNA ends
MAS	Macrophage activation syndrome
M-CSF	Macrophage colony-stimulating factor
MDM	Monocyte-derived macrophages
MGC	Multinucleated giant cells
MHC	Major histocompatibility complex
miR	microRNA
MMPs	Matrix metalloproteinases
MRI	Magnetic resonance imaging
MΦ	Macrophage
ncMo	Non-classical monocytes
ncMΦ	Macrophages derived of non-classical monocytes
NES	Normalised enrichment scores
NET	Neutrophil extracellular traps
NK	Natural killer
NLRP3	NLR family pyrin domain containing protein 3
NO	Nitric oxide
oxLDL	Oxidised low-density lipoprotein
P/F-ratio	pO2/FiO2-ratio
PA	Proximal adjacent
PAMPs	Pathogen-associated molecular patterns
PASC	Post-acute sequelae of COVID-19
PBMCs	Peripheral blood mononuclear cells
PBS	Phosphate-buffered saline
PC	Principal component
PCA	Principal component analysis
PDCD4	Programmed cell death 4
PDI	Polydispersity index
PET-CT	Positron emission tomography-computed tomography
PFA	Paraformaldehyde
PHAMOS	Prospective Halle Monocyte Study
PMA	Phorbol 12-myristate 13-acetate
PPARγ1	Peroxisome proliferator-activated receptor-γ1
PRRs	Pattern-recognition receptors
PS	Phosphatidylserine

RCT	Randomised control trial
RF	Respiratory failure
RMA	Robust multichip average
RNA-Seq	RNA sequencing
ROC	Receiver operating characteristic
ROS	Reactive oxygen species
RPMI	Roswell Park Memorial Institute
SARS-CoV-2	Severe acute respiratory syndrome coronavirus 2
scRNA-Seq	Single-cell RNA sequencing
SD	Standard deviation
SEM	Standard error of mean
SHP-1	Src homology region 2 domain-containing phosphatase 1
siRNA	Small interfering RNA
SIRPα	Signal regulatory protein α
slan	6-sulfo LacNAc
SMC	Smooth muscle cell
SPIO	Small superparamagnetic iron oxide nanoparticles
SSAR	Scandinavian Society for Atherosclerosis Research
ssGSEA	Single-sample gene set enrichment analysis
STEMI	ST-elevation myocardial infarction
TCA	Trichloroacetic acid
TEAC	Trolox equivalent antioxidant capacity
TGF-β	Transforming growth factor-beta
T_H	T helper
TLR	Toll-like receptor
TNF	Tumour necrosis factor
TOM	Topological overlap matrix
TRITC	Tetramethyl rhodamine isothicyanate
t-SNE	t-Distributed Stochastic Neighbour Embedding
UMAP	Uniform manifold approximation and projection
USPIO	Small superparamagnetic iron oxide nanoparticles
VCAN	Versican
VLDL	Very-low-density lipoprotein
VST	Variance stabilising transformation
WGCNA	Weighted gene co-expression network analysis
WTD	Western-type diet
XIAP	X-linked inhibitor of apoptosis

A

Addendum

Acknowledgements
Danksagung

With a mixture of gratitude, humility, and a touch of sadness, I write these words as I realise that this marks the end of a significant chapter in my academic career and in my life. Throughout my PhD journey, I have been fortunate to receive invaluable support and contributions from many remarkable individuals.

First of all, I would like to express my deep appreciation and gratitude to my supervisory team - Prof. Erik Biessen, Dr. Lieve Temmerman, and Prof. Judith Sluimer.

Erik, thank you for your unwavering guidance and encouragement throughout my PhD studies. You have been the most enthusiastic, compassionate, and encouraging supervisor I could have asked for. Your belief in my abilities, regardless of my unusual educational background and limited laboratory experience, allowed me to pursue a PhD in your group. One statement that you once made in a lab meeting stuck with me and lifted me up when I was doubting myself: "Even with a derailed career track, you can still perform satisfactory science". Four and a half years later, it seems that the science is even good enough to fill an entire PhD thesis. Your ideas and insightful suggestions have been critical to my thesis. I am deeply grateful for the time you have spent providing feedback, reviewing drafts, and offering constructive criticism. Your guidance has been instrumental in shaping my thinking, refining my research questions, and improving the quality of my work. During my PhD, I encountered at least as many personal as scientific obstacles which would have been much more difficult to overcome without your support and kindness. Your willingness to listen, offer advice, and show empathy made all the difference. The lessons I am taking away extend far beyond experimental techniques or scientific knowledge. Thank you! Lieve, you played a crucial role in my journey towards becoming a scientist. Without you, I would have never even found my way into science. What started as an email looking for an internship resulted in this thesis, thanks to you taking me on and teaching me everything I know about working in the lab. Your expertise, patience and guidance have been invaluable to my development as a researcher. No matter how serious a problem seemed in my mind, you were always so supportive and helped me find a solution. You were always understanding of my struggles and always made sure I was alright. I truly cannot imagine having done this PhD without you. I admire your curiosity, your openness and how you manage to balance the demands of being a devoted mother and brilliant scientist. I am so grateful for the opportunity to work with you and to be a part of the HCA team. Thank you for your mentorship, your guidance, and your support. You have had a lasting impact on my professional and personal life for which I will be forever grateful. Judith, you became an invaluable member of my supervisory team. Your expertise always brought a fresh and insightful viewpoint to the table, and your comments on my manuscript drafts never failed to highlight crucial points that I had overlooked before. Your input was always purposeful, structured, and helped me look at the big-picture perspective of my research. I believe modern keyboards simply cannot keep up with the lightning-fast speed of your thoughts which is why typos sneak their way into your emails. They never detracted from the immense value of your

feedback anyways. Your commitment to science and your high standards have set a powerful example for me to follow, and I aspire to be as driven and confident as you are. Thank you for all your help and encouragement!

I would like to thank the members of my assessment committee, Prof. Monika Stoll, Prof. Sabine Steffens, Dr. Marit Westerterp, and Dr. Kristiaan Wouters, for dedicating their time to carefully read and evaluate my thesis.

Prof. Axel zur Hausen, vielen Dank für die Möglichkeit, in der Abteilung Pathologie forschen und promovieren zu dürfen.

Thank you to all tissue and blood donors who have made this research possible.

My wonderful paranymphs and office roommates, Renée and Valeria, thank you for being by my side during my PhD defence and the journey leading up to it. Renée, from our humble beginnings as interns sitting in the lab to becoming senior PhD students, you have been outstanding. Your thoughtfulness, organisational skills, and structured approach to everything you do are impeccable. Thank you for your kindness and compassion which always made me feel heard and understood when talking to you. Valeria, especially in the latter stages of our PhD, we faced many similar struggles. One of them was to encourage the other PhD students to join us for lunch… Sharing our challenges and supporting one another has been a source of comfort. Beyond our shared difficulties, our light-hearted conversations and funny anecdotes brightened the long days in the office. Thank you for that!

Pia, ich bin absolut begeistert vom Cover meiner Doktorarbeit und möchte mich herzlich für deine Arbeit und dein großartiges Design bedanken!

Thank you to all my colleagues in the Experimental Vascular Pathology group and beyond, to all co-authors and to all collaborators who contributed to this work with their ideas and expertise. Pieter, although you were not officially a member of my supervisory team, I consider you an important member of my scientific support system. Your input to my projects, particularly the review on monocyte heterogeneity and our study on the functional effects of culture density, was critical to their success, and I appreciate your expertise in these areas. Thank you! I am also grateful for your willingness to share your extensive and diverse knowledge on… well, any topic remotely related to macrophages, with me. I have no doubt that your dedication and passion for science will lead to many more successes in the future. Marjo, you were always so approachable and willing to help. I appreciate your friendly and collaborative attitude, and that you always asked me how I was doing and showed genuine interest. I still vividly recall the conversation we had during my internship about pursuing a career in science, which was so helpful and encouraging. I thoroughly enjoyed our plaque

classification session, and you made it so easy for me to find interest in plaque features and morphology. Mat, I am so grateful for your help in solving many issues I encountered in the lab. You and your extensive knowledge of the lab's workings are irreplaceable. Thank you for everything! Make sure to take care of yourself and I hope to see you soon! Gregorio and Erwin, thank you for all your help and the countless hours you spent sorting cells! Elias, du einmalig heiterer Zeitgenosse! Vielen Dank für die tolle Zeit in Dänemark, bei unseren Bandito-Mittagspausen (die ich gerne schon viel früher entdeckt hätte), beim Squash und unserem Abenteuer im Adidas-Anzug im Labor. Sebastiaan, while running a successful burger restaurant and conducting research may seem worlds apart, you have enough dedication and boldness for both. Keep living life in the fast lane! Baixue, your kind and sweet nature is such a delight to be around. Best of luck with completing your PhD! Laura, Lele, Zhenyu, Dlzar, Marion, Clairy, Audrey, Monique, Jacques, Jack, Dietbert, Andy, and Emiel, thank you for your help and all the fun times we shared! Marjo, thank you for helping me and teaching me how to perform multiplex ELISAs! Joep and Michele, thank you for your hard work and good luck with your future endeavours!

Thank you to all my former colleagues who have already left the lab but have made a lasting impression on me. Jan, it was an absolute pleasure to work with you and to continue the projects we started together. I hope I did them justice! I learned so much from you and I am forever grateful for the opportunity to collaborate with such a talented scientist. I hope we will meet again soon, in Cologne or elsewhere! Han, I cannot thank you enough for the invaluable contribution you have made to this thesis, with your brilliance and determination. It was truly an honour to be your paranymph, and I have no doubt that your future will be bright and filled with great success. Let's keep in touch! Suzan, from the moment we both started at the Pathology department, I could tell that we would work well together, and the experiments we conducted together proved that to be true. It is amazing to think that what could have been a mere lockdown pastime ended up becoming a publication. Thank you for optimising the HCA for 384-well format, for your support, and our little tea breaks! Chang, I am grateful for the time we spent together. We shared many struggles and I appreciate how easy it was for me to trust and confide in you. I miss my companion for late night bike rides home, my decaf coffee buddy, and friend. I hope you are taking good care of yourself in Heidelberg! Olivia, I cherish the fun moments we shared in the lab, laughing about the smallest things together. Please know that you are always welcome to visit my island to catch up and catch some fish! Margaux, you have been a role model for me since the day I had the interview for my internship. Thank you for introducing me to the lab and for everything I learned from you! Kim, Jenny, Jasper, Danielle, Ruud, and Anke, thank you for the fun memories and your help during the early stages of my PhD journey.

Thank you to all members of the EPC and of I'MCARIM for allowing me to serve as a PhD representative and for the wonderful time I had with the group.

A heartfelt thank you goes out to my old roommates who welcomed me into their home without hesitation when I first came to Maastricht. Nokhez, thank you for your kindness and generosity. I will never forget the fun times we had living at Koningsplein, and I am so grateful for the fun memories we created together. Thank you so much for your support! Elian, der am fleißigsten schaffende Häuslebauer jenseits des Schwabenlandes! Vielen Dank für all die wundervollen Erinnerungen, die wir miteinander teilen, sei es von unserer Fahrradtour durch das Heuvelland, oder von deinem Besuch in Gunningen. Vielen Dank, dass du in Höhen und Tiefen für mich da warst. Pass gut auf dich auf!

I am incredibly fortunate to have amazing friends who have been by my side throughout this journey. Alwine und Wlad, ich wünschte, ich könnte Bahlingen näher an Maastricht schieben, um mehr Zeit mit euch verbringen zu können! Mit euch habe ich einfach immer eine Menge zu lachen und eine großartige Zeit. Vielen Dank für eure Hilfe bei der deutschen Zusammenfassung meiner Doktorarbeit! Gabriel, welch glücklicher Zufall, dass wir uns in Konstanz noch einmal begegnet sind. Ohne dich wären die Prüfungsphasen definitiv viel schauriger und trauriger gewesen. Mit dir kann man sowohl witzige als auch tiefgründige Gespräche führen, und ich bin mir sicher, dass du ein toller Vater sein wirst. Für dich und deine kleine Familie, die du mit der lieben Evelyn gründest, nur das Beste! Daniela, vielen Dank für deine Freundschaft, die seit der ersten Woche im ersten Semester andauert. Danke für deinen Besuch in Maastricht und die schöne Zeit! Stefan, so gut wie jeden Tag rufe ich Unsinn über das Mikrophon direkt in dein Ohr. Unsere kleinen Interaktionen haben mir oft die Pausen von der Arbeit an meiner These erheitert. Vielen Dank! Renate und Rainer, vielen Dank, dass ich mit euch hin und wieder eine Auszeit vom PhD nehmen konnte.

I am deeply indebted to my family for their unwavering love and support throughout my academic journey. Mama und Papa, ich danke euch von Herzen für eure bedingungslose und unermüdliche Unterstützung. Ich kann mich in allen Lebenslagen auf eure Hilfe verlassen und weiß, dass eure Tür mir immer offensteht. Dank eurer harten Arbeit und Aufopferung war es mir möglich, meine akademischen Ziele zu verfolgen. Живите долго, будьте здоровы и оставайтесь такими же веселыми. Спасибо вам, мама и папа! Saskia und Simon, meine lieben Geschwister. Euch mit gutem Beispiel voranzugehen, war mir immer besonders wichtig und hat mich motiviert. Heute weiß ich, dass ihr kein Vorbild braucht, denn ihr seid selbst groß, klug und wunderbar. Ihr geht mutig euren eigenen Lebensweg und meistert Herausforderungen mit Bravour. Danke, dass es euch gibt! Oma Irene und Opa Alexander, danke, dass ihr euch immer erkundigt, wie es mir im weit entfernten Maastricht geht und für euer Interesse an meinen Fortschritten. Oma Amalia, vielen Dank, dass du mir bei jedem Schritt zur Verwirklichung meiner (süßen) Träume (von sauren Gurken) die Daumen drückst! Opa Jakob, wie sehr wünsche ich mir, du wärst hier, um diesen Meilenstein mit mir zu feiern. Jedes Mal, wenn ein Bienchen an mir vorbeischwirrt, denke ich an dich.

Matthias, Worte reichen nicht aus, um auszudrücken, wie dankbar ich dir bin. Du hast mich dazu ermutigt, über meine selbstgesteckten Grenzen hinauszuwachsen und mir meinen Wert immer wieder vor Augen geführt. Mit dir an meiner Seite habe ich Vertrauen in mich selbst gefunden und mich neuen Herausforderungen gestellt. So oft hast du mir neue Perspektiven auf meine Forschung eröffnet und mir geholfen, komplizierte Probleme zu lösen. Du bist nicht nur mein größter Unterstützer, sondern auch mein Sonnenschein und bester Freund, dafür danke ich dir aus tiefstem Herzen. Ich freue mich darauf, mit dir zu wachsen, zu lachen und das Leben zu meistern.

Thank you to the parts of me that carried me this far but can no longer be a part of me as I continue moving forward.

“I’m going to be my own kind of princess” – Sailor Moon

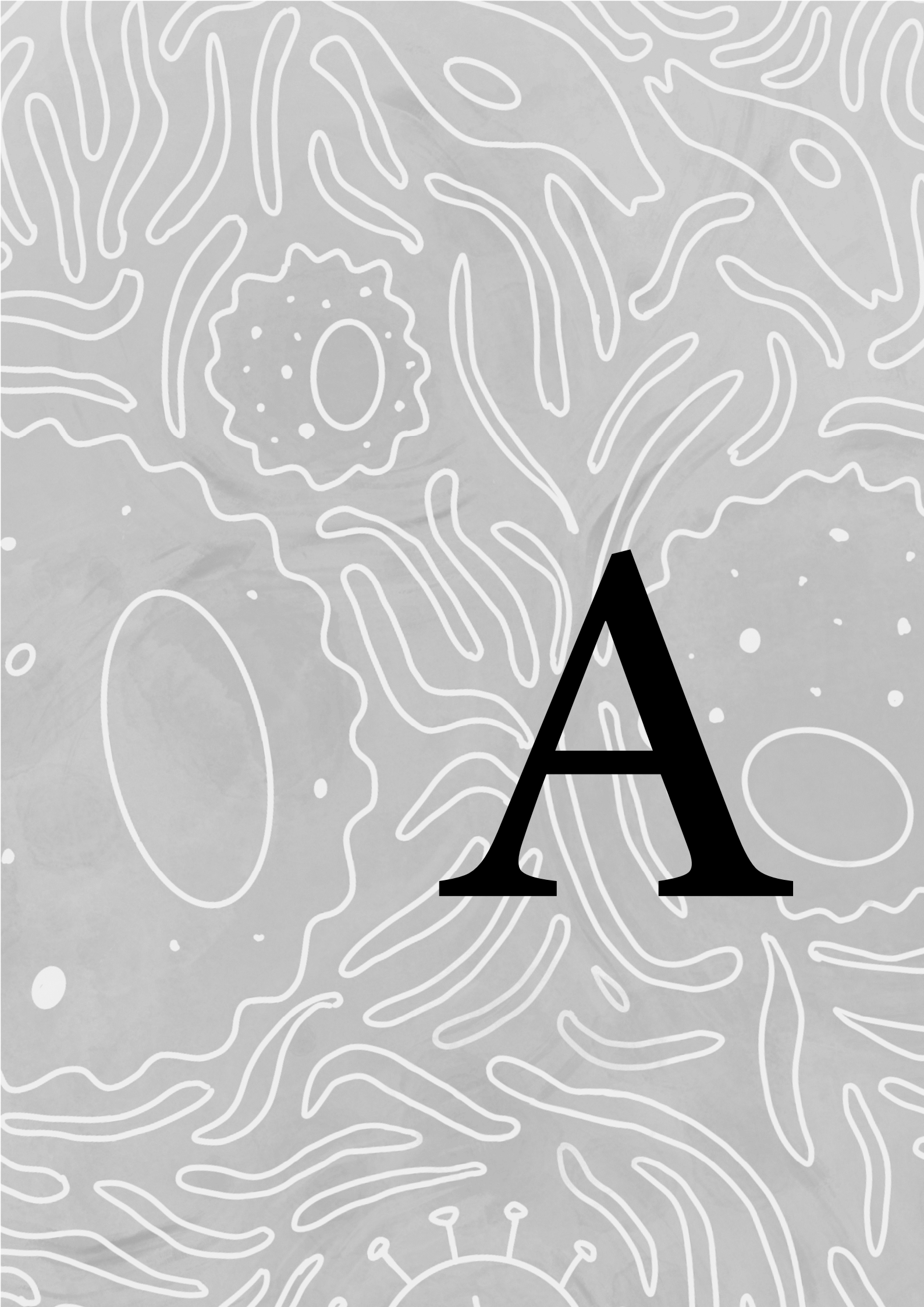
A

Addendum

Curriculum vitae

Personal information

Name:	Adele Veronika Ruder
Date of birth:	23 July 1994
Place of birth:	Spaichingen (Germany)

Education

Sep 2018 – Mar 2023	**PhD training in Biomedical Sciences** Department of Pathology Maastricht University Medical Center+ (The Netherlands)
Oct 2012 – Nov 2017	**Erstes Staatsexamen (First State Examination) Biology and English** University of Konstanz (Germany)

Experience

Sep 2018 – Mar 2023	**PhD training in Biomedical Sciences** Department of Pathology Maastricht University Medical Center+ (The Netherlands) Supervisors: Prof. Erik Biessen, Prof. Judith Sluimer Co-supervisor: Dr. Lieve Temmerman *Origin versus Context: Defining Key Determinants of Human Macrophage Function in Health and Disease*
Mar 2018 – Jul 2018	**Research laboratory internship** Department of Pathology Maastricht University Medical Center+ (The Netherlands) Supervisor: Dr. Lieve Temmerman *The Role of PCSK9 in Human Macrophages*
May 2017	**Clinical laboratory internship** Schwarzwald-Baar-Klinikum Villingen-Schwenningen (Germany) Klinikum Landkreis Tuttlingen (Germany)
Sep 2014 – Dec 2014	**Trainee teacher Biology and English** Gymnasium Spaichingen (Germany)

Courses & Certificates

Sep 2021	**Performing Venipuncture** Maastricht University Medical Center+
Aug 2020	**Principles of Problem-Based Learning and Tutoring/Teaching Skills** Maastricht University
Jun 2021	**Heart Failure Research** Cardiovascular Research Institute Maastricht (CARIM)
Mar 2021	**Statistics I** Maastricht University

Jun 2019	**Advanced Optical Microscopy** Maastricht University
Oct 2018	**Vascular Biology** Dutch Heart Foundation
Jun 2018	**Translational Medicine** Technical University of Munich

Other activities

Aug 2020 – Feb 2023	**PhD representative I'MCARIM** Cardiovascular Research Institute Maastricht (CARIM)
Aug 2020 – Oct 2020 & Aug 2021 – Oct 2021	**Tutor** *Threats and Defence Mechanisms* Maastricht University

Conferences & Seminars

Dutch Atherosclerosis Society Symposium 2023 Amersfoort (The Netherlands)	Poster presentation *M-CSF and GM-CSF induce distinct changes in functional phenotype during monocyte-to-macrophage differentiation*
28th Annual Conference of the Scandinavian Society for Atherosclerosis Research 2022 Humlebæk (Denmark)	Poster presentation *A Trojan horse in contrast-enhanced MRI? Superparamagnetic iron oxide nanoparticles enhance apoptosis in human and murine atherosclerosis*
Department of Pathology Science Day 2022 Valkenburg (The Netherlands)	Poster presentation *M-CSF and GM-CSF induce distinct changes in functional phenotype during monocyte-to-macrophage differentiation*
Department of Pathology Science Day 2019 Valkenburg (The Netherlands)	Poster presentation *Dissecting the impact of macrophage origin (and disease context) on its functional profile*
EVOluTION Conference 2019 Seeon Abbey (Germany)	Poster presentation *Dissecting the impact of macrophage origin (and disease context) on its functional profile*

Awards & Prizes

Commitment Award 2022	Cardiovascular Research Institute Maastricht
First Poster Prize	Department of Pathology Science Day 2022
Second Poster Prize	Department of Pathology Science Day 2019

Publications

Monocyte heterogeneity in cardiovascular disease
Ruder AV, Wetzels SMW, Temmerman L, Biessen EAL* and Goossens P*
Cardiovasc Res. 2023;cvad069

Culture density influences the functional phenotype of human macrophages
Ruder AV, Temmerman L, van Dommelen JMA, Nagenborg J, Lu C, Sluimer JC, Goossens P* and Biessen EAL*
Front Immunol. 2023;14:1078591

Magnetic resonance imaging contrast-enhancement with superparamagnetic iron oxide nanoparticles amplifies macrophage foam cell apoptosis in human and murine atherosclerosis
Segers FME, Ruder AV, Westra MM, Lammers T, Dadfar SM, Roemhild K, Lam TS, Kooi ME, Cleutjens KBJM, Verheyen FK, Schurink GWH, Haenen GR, van Berkel TJC, Bot I, Halvorsen B, Sluimer JC* and Biessen EAL*
Cardiovasc Res. 2022;118(17):3346-3359

M-CSF and GM-CSF induce distinct changes in functional phenotype during monocyte-to-macrophage differentiation
Ruder AV, Jin H, Nagenborg J, Temmerman L, Bonaguro L, De-Domenico E, Ulas T, Schalkwijk CG, Donners MMCP, Sluimer JC, Goossens P, and Biessen EAL
Submitted

GM-CSF-activated STAT5A but not STAT5B regulates macrophage functions and inflammation in atherosclerosis
Nagenborg J, Jin H, Ruder AV, Temmerman L, Mees BME, Müller-Klieser D, Berg T, Goossens P, Donners MMPC, and Biessen EAL
Submitted

Genome-scale metabolic network of human carotid plaque reveals the pivotal role of glutamine/glutamate metabolism in macrophage modulating plaque inflammation and vulnerability
Jin H, Zhang C*, Nagenborg J*, Juhasz P, Ruder AV, Sikkink CJJM, Mees BME, Waring O, Sluimer JC, Neumann D, Goossens P, Donners MMPC, Mardinoglu A and Biessen EAL
Submitted

Reprogramming of human macrophages by the blood milieu of SARS-CoV-2-infected patients is predictive of respiratory function decline
Ruder AV, Ueland T, Temmerman L, Dyrhol-Riise AM, Barratt-Due A, Lerum TV, Aukrust P, Dahl TB, Biessen EAL* and Halvorsen B*
In preparation

Monocyte subsets give rise to functionally distinct macrophages
Ruder AV, Fazzi GE, Wijnands E, Hoeft K, Schalkwijk CG, Sluimer JC, Temmerman L, Biessen EAL
In preparation

Macrophage-specific CDK5 knockdown reduces calcification in atherosclerotic plaques
Waring OJ, Saar-Kovrov V, Jin H, Lu C, Ruder AV, Gijbels M, Nagenborg J, Giacca M, Vettorazzi S, Jaminon AMG, Stoll M, Goossens P, Donners MMPC, and Biessen EAL
In preparation

** Authors contributed equally*